Theoretical Studies on Heterogeneous Catalysis Based on Reaction Route Network and Kinetic Analysis

（反応経路ネットワークと速度論解析を用いた不均一系触媒反応の理論研究）

Kanami Sugiyama

（杉山　佳奈美）

Hokkaido University

2022

Contents

Chapter 1. General introduction

1.1 Heterogeneous catalysis and its development

A catalyst is a material that promotes reactions and utilized in many chemical reactions. Chemical reactions involving catalysts can be classified into several types depending on the environment in which the catalyst works. One is a heterogeneous reaction which proceeds in substrates consists of two or more phases, e.g., a reaction of gas molecules on solid catalysts. Another is a homogeneous reaction in which the catalyst and reactants have the same phase. In addition, a reaction occurring in the body by enzymes are called bioreaction. In this study, we focused on heterogeneous reactions.

Heterogeneous catalysts can be easily separated from the catalyst and reactants or products, and can be used continuously and repeatedly. This is a great advantage for industrial manufacturing processes that require mass production with lower costs. In fact, Haber-Bosch process caused innovative changes to industry. The Haber-Bosch process is the process which synthesizing ammonia from nitrogen and water ($N_2 + 3\ H_2 \rightarrow 2\ NH_3$) using a catalyst containing Fe, and established at the beginning of the 1900s. Ammonia is a useful compound that can be used as a fertilizer and a raw material for chemical products such as nylon. For this work, the developers Haber and Bosch were awarded the Nobel Prize in Chemistry in 1918 and 1931, respectively [1,2].

On the other hand, environmental pollution has become a problem with the rapid development of industry. Therefore, catalysts for the removal of environmental pollutants have been developed and used. For example, a three-way catalyst is a catalyst to purify the exhaust gas of automobiles. The catalyst is consisting of platinum (Pt), palladium (Pd), and rhodium (Rh), and converts toxic carbon monoxide, hydrocarbons, and nitrogen oxides into harmless carbon dioxide, water, and nitrogen [3]. In addition, use of hydrogen energy instead of fossil fuels has

been encouraged to reduce greenhouse gas emissions. A fuel cell is an example of the topic. Besides, direct methanol fuel cells (DMFCs) taking out electricity by using methanol are also attracted [4,5]. Furthermore, in recent years, the manufacturing process of chemical products with less environmental impact has also been paid attention as green chemistry. One example is reactions of titanium silicalite-1 (TS-1), a porous material and a kind of zeolite. TS-1 is used industrially as a catalyst for the oxidation of olefins, especially with using hydrogen peroxide as an oxidant [6,7]. It is said that the byproduct of this reaction is harmless water only.

In summary, heterogeneous catalysts have been essential materials in modern society. It is important to understand the mechanism of reactions on heterogeneous catalysts and surface reactions in order to design new catalysts having outstanding high performance.

1.2 Kinds of catalyst surfaces and reaction mechanisms

There are various heterogeneous catalysts. The size of catalysts is existing like small nano clusters, and large surfaces or bulks. Metals, oxides like SiO_2 and TiO_2, or a combination of them can compose surfaces. Therefore, the reaction mechanism on surface becomes very complicated because of the variety of the surfaces.

It can be thought that the complexity of reactions on heterogeneous catalysts was caused by many kinds of elementary steps as well as complex surface structures. First, not only bond rearrangement steps such as dissociation and association but also adsorption, desorption, and surface diffusion (migration) are involved to reactions. Thus, all kinds of the elementary steps have to be considered. Next, atoms which located the interface of solid surfaces, especially metal surface, usually shows the different properties and/or reactivities from atoms in bulks since surface atoms have dangling (unsatisfied) bonds. Defects and adatoms induce structural the changes of surfaces and catalytic activities. In addition, oxygen atoms included in oxides can be

reacts with substrates. It is required to consider all these factors for discussing reaction mechanisms.

1.3 Methods to understanding surface reactions

The previous experiments have been conducted to analyze surface reaction at the atomic and molecular levels, with the development of surface observation techniques. The surface structures and adsorbed species can be studied by X-ray photoelectron spectroscopy (XPS) [8,9], electron energy loss spectroscopy (EELS) [10], and XRD [11], and so on. The temperature programmed desorption (TPD) is a method to measure the products desorbed on the surface [12,13]. By these methods, the states of surfaces before, after, and during the reaction were investigated. In particular, Ertl was awarded the Nobel Prize in Chemistry for his study of chemical processes on solid surfaces [14,15]. However, it is difficult to track all the elementary reaction steps experimentally. Therefore, analysis using theoretical method is expected.

In most previous theoretical studies, calculations using density functional theory (DFT) have been conducted. Structural optimization was performed for reactants, products, and intermediates that seems to be important [16]. Then the elementary reaction paths connecting them were determined by the nudged elastic band (NEB) method [17,18] and the dimer method [19,20] etc. The transition states were optimized, then the reaction barriers and the rate constants were estimated. In addition, simulation methods such as microkinetic modeling were applied to the obtained reaction barriers and rate constants to discuss reaction kinetics [21,22]. However, these analyses may have overlooked important but unexpected paths. Besides, simulations using ab initio molecular dynamics (AIMD) [23-25], meta-dynamics simulations [26,27], and stochastic simulations such as the blue moon ensemble (BME) method [28,29] have also been performed. However, comprehensive discussion of surface reactions is still challenging topic since it is

difficult to treat with wide range timescale from $10^{-15} \sim 10^{10}$ seconds, or need to select appropriate reaction coordinates and biases in advance.

On the other hand, automatic reaction path search methods have been developed in ourselves [30-40] and other groups [41-54] to clarify unknown mechanisms. The artificial force induced reaction (AFIR) method developed by our group is one of them and implemented in global reaction route mapping (GRRM) program. In the AFIR method, structural deformation was induced by adding artificial force between the fragments in the system. This force is called AFIR function. When using the single component (SC-) AFIR method, the targeted fragment pair is determined automatically and applied the AFIR method to the fragment pair. By repeating the determining of fragment pairs and applying AFIR function, many structures and connection paths were searched automatically and systematically from the one initial structure. Namely, researchers have to prepare one initial structure and some parameters to search paths, whereas any knowledge of the reaction mechanism is not required. Then the obtained structures and paths can be represented as a reaction route network where nodes and edges correspond structures and connecting elementary steps, respectively. At first, the application of the AFIR method was limited to the search of non-periodic systems like organic reactions, but it has become available for that of periodic systems such as crystal structures in recent years [55]. However, the applications to surface reaction was limited [56-59].

1.4 Purpose of the thesis

From the introduction above, understanding reaction mechanism of surfaces reactions are very important task while it is difficult to analyze unknown process without missing unexpected important paths. Therefore, we aimed to establish a theoretical method that can analyze surface reactions comprehensively. Specifically, the reaction path search by the AFIR method was applied

to surface reactions and reaction route networks of surface reactions were created. Then the network was kinetically analyzed with considering side reactions and their kinetic contributions.

1.5 Overview of the thesis

Chapter 1 gives the general introduction for reactions on heterogeneous catalysts. The importance of the reactions and difficulty and/or complexity of the reaction mechanism were explained. In addition, some experimental techniques and theoretical analyzes were introduced.

In Chapter 2, a reaction of H_2O molecule on a Cu(111) surface was focused. This is the case study for the reaction path search on simple metal surfaces. The efficient path search procedure for surface reactions, a reaction route network including both migration paths of adsorbates and bond rearrangement paths between them, were showed. In addition, time hierarchical description of the reaction and the bottleneck step were discussed by kinetic analysis.

In Chapter 3, applying the developed procedure to CO oxidation on a Pt(111) surface is represented. The reaction is simple but very important as the model case of surface reactions. The reaction mechanism from a reaction route network and its kinetic analysis were compared to previous experimental and theoretical studies. Furthermore, the influence of entropic contributions arising from existing many stable structure and transition states in the network to the overall rate constant were discussed.

In Chapter 4, the procedure was applied to methanol decomposition reaction on a Pt(111) surface. In this study, kinetic-based navigation option is introduced to get kinetically important paths more efficiently. Then the most kinetically favorable decomposition route was extracted from the network. Furthermore, paths to generate byproducts and their kinetic influence were investigated by using time hierarchy of the reaction and time evolution of the structures.

In Chapter 5, an application to reaction on a porous material was described. Epoxidation

reaction of propylene on titanium silicalite-1 (TS-1) with hydrogen peroxides were targeted in this chapter. The reaction mechanism including various epoxidation steps, catalytic cycles and byproducts were discussed.

Finally, in Chapter 6, concluding remarks are shown.

References (Chapter 1)

[1] https://www.nobelprize.org/prizes/chemistry/1918/haber/facts/

[2] https://www.nobelprize.org/prizes/chemistry/1931/bosch/facts/

[3] H. Hirata, *Catal. Surv. Asia*, **2014**, *18*, 128–133.

[4] S. S. Munjewar, S. B. Thombre, and R. K. Mallick, *Renew. Sust. Energ. Rev.*, **2017**, *67*, 1087–1104.

[5] M. S. Alias, S. K. Kamarudin, A. M. Zainoodin, and M. S. Masdar, *Int. J. Hydrog. Energy*, **2020**, *45*, 19620–19641.

[6] H. Xu and P. Wu, *Chin. J. Chem.*, **2017**, *35*, 836–844.

[7] R. Bai, Y. Song, R. Bai, and J. Yu, *Adv. Mater. Interfaces*, **2021**, *8*, 2001095 (13 pages).

[8] C. Hardacre, R. M. Ormerod and R. M. Lambert, *Chem. Phys. Lett.*, 1993, **206**, 171–174.

[9] A. V. Miller, V. V. Kaichev, I. P. Prosvirin and V. I. Bukhtiyarov, *J. Phys. Chem. C*, 2013, **117**, 8189–8197.

[10] H. Steininger, S. Lehwald and H. Ibach, *Surf. Sci.*, 1982, **123**, 1–17.

[11] A. Farkas, K. Zalewska-Wierzbicka, C. Bachmann, J. Goritzka, D. Langsdorf, O. Balmes, J. Janek and H. Over, *J. Phys. Chem. C*, 2013, **117**, 9932–9942.

[12] G. Ertl, M. Newmann and K. M. Streit, *Surf. Sci.*, 1977, **64**, 393.

[13] L. Diekhöner, D. A. Butler, A. Baurichter and A. C. Luntz, *Surf. Sci.*, 1998, **409**, 384–391.

[14] https://www.nobelprize.org/prizes/chemistry/2007/ertl/facts/

[15] G. Ertl, *Angew. Chem. Int. Ed.*, 2008, **47**, 3524–3535.

[16] J. K. Nørskov, T. Bligaard, J. Rossmeisl and C. H. Christensen, *Nat. Chem.*, 2009, **1**, 37–46.

[17] G. Henkelman, B. P. Uberuaga and H. Jónsson, *J. Chem. Phys.*, **2000**, *113*, 9901−9904.

[18] G. Henkelman and H. Jónsson, *J. Chem. Phys.*, **2000**, *113*, 9978−9985.

[19] G. Henkelman and H. Jónsson, *J. Chem. Phys.*, 1999, **111**, 7010−7022.

[20] A. Heyden, A. T. Bell and F. J. Keil, *J. Phys. Chem.*, 2005, **123**, 224101 (14 pages).

[21] A. Ishikawa and Y. Tateyama, *J. Phys. Chem. C*, 2018, **122**, 17378−17388.

[22] A. H. Motagamwala and J. A. Dumesic, *Chem. Rev.*, 2021, **121**, 1049−1076.

[23] L. Agosta, E. G. Brandt and A. P. Lyubartsev, *J. Chem. Phys.*, 2017, **147**, 024704 (16 pages).

[24] L. Zhou, X. Zhou, M. Alducin, L. Zhang, B. Jiang and H. Guo, *J. Chem. Phys.*, 2018, **148**, 014702 (8 pages).

[25] B. C. Bukowski, W. N. Delgass and J. Greely, *J. Phys. Chem.*, 2021, **125**, 4519−4531.

[26] T. Cheng, H. Xiao and W. A. Goddard, III, *J. Phys. Chem. Lett.*, 2015, **6**, 4767–4773.

[27] T. Cheng, W. A. Goddard, III, Q. An, H. Xiao, B. Merinov and S. Morozov, *Phys. Chem. Chem. Phys.*, 2017, **19**, 2666–2673.

[28] A. Tilocca and A. Selloni, *J. Chem. Phys.*, 2003, **119**, 7445–7450.

[29] K. Koizumi, K. Nobusada and M. Boero, *Chem. −Eur. J.*, 2016, **22**, 5181–5188.

[30] K. Ohno and S. Maeda, A Scaled Hypersphere Search Method for the Topography of Reaction Pathways on the Potential Energy Surface, *Chem. Phys. Lett.*, 2004, **384**, 277–282.

[31] S. Maeda and K. Ohno, *J. Phys. Chem. A*, 2005, **109**, 5742–5753.

[32] K. Ohno and S. Maeda, *J. Phys. Chem. A*, 2006, **110**, 8933–8941.

[33] K. Ohno and S. Maeda, *Phys. Scr.*, 2008, **78**, 058122 (8 pages).

[34] S. Maeda and K. Morokuma, *J. Chem. Phys.*, 2010, **132**, 241102 (4 pages).

[35] S. Maeda and K. Morokuma, *J. Chem. Theory Comput.*, 2011, **7**, 2335–2345.

[36] S. Maeda, K. Ohno and K. Morokuma, *Phys. Chem. Chem. Phys.*, 2013, **15**, 3683–3701.

[37] S. Maeda, T. Taketsugu and K. Morokuma, *J. Comput. Chem.*, 2014, **35**, 166–173.

[38] S. Maeda, T. Taketsugu, K. Morokuma and K.Ohno, *Bull. Chem. Soc. Jpn.*, 2014, **87**, 1315–1334.

[39] W. M. C. Sameera, S. Maeda and K. Morokuma, *Acc. Chem. Res.*, 2016, **49**, 763–773.

[40] S. Maeda, Y. Harabuchi, M. Takagi, K. Saita, K. Suzuki, T. Ichino, Y. Sumiya, K. Sugiyama and Y. Ono, *J. Comput. Chem.*, 2018, **39**, 233–250.

[41] D. Rappoport, C. J. Galvin, D. Y. Zubarev and A. Aspuru-Guzik, *J. Chem. Theory Comput.*, 2014, **10**, 897–907.

[42] D. J. Wales, J. P. K. Doye, M. A. Miller, P. N. Mortenson and T. R. Walsh, *Adv. Chem. Phys.*, 2000, **115**, 1–111.

[43] M. Dallos, H. Lischka, E. V. D. Monte, M. Hirsch and W. Quapp, *J. Comput. Chem.*, 2002, **23**, 576–583.

[44] J. Baker and K. Wolinski, *J. Comput. Chem.*, 2011, **32**, 43–53.

[45] P. M. Zimmerman, *J. Comput. Chem.*, 2013, **34**, 1385–1392.

[46] D. Rappoport, C. J. Galvin, D. Y. Zubarev and A. Aspuru-Guzik, *J. Chem. Theory Comput.*, 2014, **10**, 897–907.

[47] B. Schaefer, S. Mohr, M. Amsler and S. Goedecker, *J. Chem. Phys.*, 2014, **140**, 214102 (13 pages).

[48] D. J. Wales, *J. Chem. Phys.*, 2015, **142**, 130901 (12 pages).

[49] S. Habershon, *J. Chem. Phys.*, 2015, **143**, 094106 (14 pages).

[50] E. Martínez-Núñez, *J. Comput. Chem.*, 2015, **36**, 222–234.

[51] M. Bergeler, G. N. Simm, J. Proppe and M. Reuher, *J. Chem. Theory Comput.*, 2015, **11**, 5712–5722.

[52] X.-J. Zhang and Z.-P. Liu, *Phys. Chem. Chem. Phys.*, 2015, **17**, 2757–2769.

[53] L.-P. Wang, R. T. McGibbon, V. S. Pande and T. J. Martinez, *Chem. Theory Comput.*, 2016, **12**, 638–649.

[54] M. Yang, J. Zou, G. Wang and S. Li, *J. Phys. Chem. A*, 2017, **121**, 1351–1361.

[55] M. Takagi, T. Taketsugu, H. Kino, Y. Tateyama, K. Terakura, and S. Maeda, *Phys. Rev. B*, **2017**, *95*, 184110 (11 pages).

[56] S. Ohno, K. Shudo, M. Tanaka, S. Maeda and K. Ohno, *J. Phys. Chem. C*, 2010, **114**, 15671–15677.

[57] X.-J. Zhang, C. Shang and Z.-P. Liu, *J. Chem. Phys.*, 2017, **147**, 152706 (9 pages).

[58] Z. W. Ulissi, A. J. Medford, T. Bligaard and J. K. Nørskov, *Nat. Commun.*, 2017, **8**, 14621 (7 pages).

[59] S.-D. Huang, C. Shang, X.-J. Zhang and Z.-P. Liu, *Chem. Sci.*, 2017, **8**, 6327–6337.

Chapter 2. Making reaction route network of surface reaction and its kinetic analysis: a case study for the reaction of H_2O molecule on Cu(111) surface

2.1 Introduction

Metals have been utilized for one of the heterogeneous catalysts which show great catalytic activities to various reactions. It is an important task to understand the reaction mechanism which occurs the interface of metal surfaces and molecules. In surface reactions, bond rearrangement steps between reactant molecules as well as adsorption, desorption and surface migration steps are involved. Therefore, systematic reaction path searches and comprehensive analyses are required.

We have developed the artificial force induced reaction (AFIR) method [1] which is one of the automatic reaction path search methods. The AFIR method has been applied to the non-periodic systems such as reactions of organic molecules [2]. In recent years, it was extended to crystal structures such as carbons (periodic systems) [3].

In this study, I applied the AFIR method to the simple surface reaction, the reaction of H_2O molecule on Cu(111) surface, and revealed that the AFIR method can search paths of surface reactions with considering various kinds of elementary processes[4].

2.2 Method

2.2.1 DFT calculations

The potential energies and gradients were calculated by using the SIESTA 4.0 program [5,6]. The Perdrew-Burke-Ernzerhof (PBE) functional and DZP basis set were selected. The pseudopotentials were prepared from GGA potential database [7]. The relativistic effect including nonlinear core correction (NLCC) was applied to the cupper atom, and nonrelativistic pseudopotential without NLCC was applied to the other hydrogen and oxygen atoms. The

smearing parameter was set to 10000 K with the occupation function of the Methfessel–Paxton scheme [8]. The Monkhorst-Pack grid which determines k-point sampling was changed depending on the calculation as described below.

2.2.2 Preparation of a Cu(111) surface

A periodic model of Cu(111) surface was prepared by following procedures. First, the lattice constant of Cu crystal having face-centered cubic (fcc) structure was optimized with k-point sampling 8 × 8 × 8 and mesh cur off 200 Ry. The initial parameter was set to 3.6149 Å refer to the experimental lattice constant value. The optimized value 3.7065 Å was slightly longer than the experimental value. Then, the periodic slab model composed of two Cu(111) surface layer was created from the optimized Cu crystal. The surface has *p*(4×4) surface area (16 atoms per layer) and vacuum region about 15 Å. In the following calculations, all surface atoms and translational vectors were fixed at the initial positions.

2.2.3 The artificial force induced reaction method

The AFIR method can search reaction paths automatically and systematically. The Idea of the AFIR method is adding the artificial force between the two fragments (reactants) and inducing reactions. Figure 2-1 and Eq. (1) shows the potential energy curves for the case of the simple reaction from atom A and atom B to molecule AB.

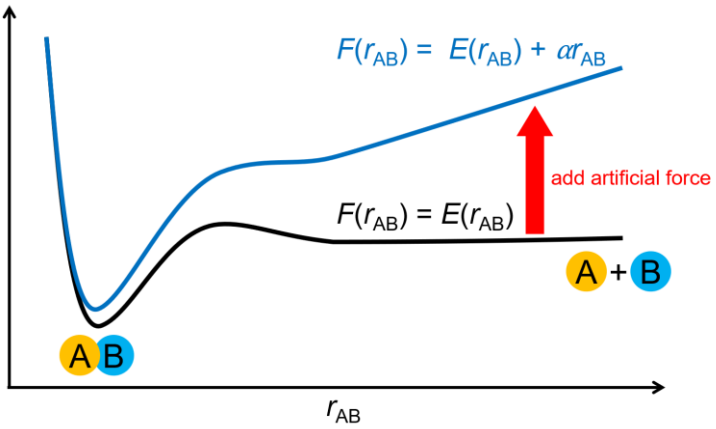

Figure 2-1. Potential energy curves for a reaction between two atoms.

$$F(r_{AB}) = E(r_{AB}) + \alpha r_{AB} \tag{1}$$

The second term on the right side of Eq. (1) is called artificial force term which is adding the "force" proportional to the distance between atoms (r_{AB}). Then, the product AB is found quickly by optimizing on the AFIR function $F(r_{AB})$. The obtained potential energy $E(r_{AB})$ corresponds to the approximate reaction pathway (AFIR path). The further optimization was required to get the actual transition state (TS).

The AFIR function $F(\mathbf{Q})$ for the coordinates $\mathbf{Q}$ including multiple atoms are defined as Eq. (2) [1]:

$$F(\mathbf{Q}) = \mathrm{E}(\mathbf{Q}) + \rho\alpha \frac{\sum_{i\in A}\sum_{j\in B}\omega_{ij}r_{ij}}{\sum_{i\in A}\sum_{j\in B}\omega_{ij}} \tag{2}$$

ρ is a constant that is set to 1.0 for attractive force and -1.0 for repulsive force. α is represented the magnitude of the added force between two fragments as described below.

$$\alpha = \frac{\gamma}{\left[2^{-\frac{1}{6}} - \left(1 + \sqrt{1 + \frac{\gamma}{\varepsilon}}\right)^{-\frac{1}{6}}\right] R_0} \tag{3}$$

R_0 and ε correspond to the Ar-Ar interaction of the Lennard-Jones potential, and are set to 3.8164

Å and 1.0061 kJ/mol, respectively. The α in Eq. (3) represents the average force felt when Ar-Ar pair moves from minimum to a turning point and directly collides with each other at collision energy γ. γ is the model collision parameter that gives approximate upper bound of the considering barrier. The second term on the right side of Eq. (2) are consisted of the weighted sum of the distance (r_{ij}) between atom i and atom j. The weight term ω_{ij} is defined as shown in Eq. (4).

$$\omega_{ij} = \left[\frac{(R_i + R_j)}{r_{ij}}\right]^6 \tag{4}$$

R_i and R_j correspond to the covalent radius of atom i of atom j. For the thermal reaction, γ is estimated by the following equation:

$$\gamma = -RT\ln\left(\frac{h}{tk_B T}\right) \tag{5}$$

R, T, h, t and k_B means gas constant, reaction temperature, Planck constant, reaction timescale and Boltzmann constant, respectively. t and T are changed depending on the reaction conditions. t is set to 10 times to the actual reaction temperature.

In the single-component (SC-) AFIR method [1], which is a kind of the AFIR method, fragments i and j are determined automatically determined among the atoms in the system. Then the optimization on the AFIR function is applied to the selected atom pairs. By repeatedly redefining fragments and applying the AFIR method to the obtained structures, many structures and connecting paths are systematically calculated from the one initial structure.

2.2.4 Making a reaction route network of H_2O molecule on a Cu(111) surface

The reaction path search was done by using the single component SC-AFIR method implemented to the developer version of global reaction route mapping (GRRM) program. The initial structure is a H_2O molecule adsorbed on Cu(111) surface. The model collision parameter γ of the AFIR function was set to γ = 500.0 kJ/mol. Target atoms generating the fragment pairs during the search

are each atom of H_2O and the Cu central dimer. In addition, to prevent adsorbates go away from the center of the surface, weak biases of γ_{add} = 25.0 kJ/mol were applied to each atom of H_2O and the Cu central dimer by using the AFIR function. The weak biases were finally removed as described below.

The obtained force-induced paths were optimized by using the locally updated plane (LUP) method [9,10]. The LUP method optimized discrete path points along the path to the perpendicular to path tangent direction. The obtained LUP paths were good approximation of the corresponding intrinsic reaction coordinate (IRC) [11,12]. Then the network composed of the LUP paths were obtained. Monkhorst-Pack grind was set to 1 × 1 × 1 during this calculation.

Next, further LUP optimization was carried to remove weak biases which were applied during the search. In this step, Monkhorst-Pack grid was set to 2 × 2 × 2. Furthermore, normal mode frequency analyses were done for the obtained local minima (MINs) and the highest energy points along the LUP paths in the second LUP calculation. Finally, the reaction route network consisting 26 local minima and 291 LUP paths were obtained.

2.2.5 Kinetic analysis of the reaction route network by using the rate constant matrix contraction method

The bottleneck steps were automatically extracted by applying the RCMC method [13,14]. Then IRC calculation was applied to the extracted paths. The RCMC method is kinetic analysis method for the reaction route network. For a reaction route network including N MINs, $N \times N$ rate constant matrix was obtained. The element of the rate constant matrix was calculated by using Eq. (6).

$$k_{XY} = \Gamma \frac{k_B T}{h} e^{-(\Delta\Delta G)/RT} \quad (6)$$

$\Delta\Delta G$ is the corresponding free energy of the LUP path from the state X to the state Y. Γ is the

Wigner modification which is used when considering the one-dimensional tunneling effect defined as the equation below:

$$\Gamma = 1 + \frac{1}{24}\left(\frac{h\nu^{\ddagger}}{k_{\mathrm{B}}T}\right)^{2} \tag{7}$$

$\nu^{\ddagger}$ is the value represents the magnitude of virtual vibration modes of TS (or path top). k_{B} is the Boltzmann constant. T is reaction temperature and was set to T = 300 K. R is gas constant.

RCMC reduces the original $N \times N$ rate constant matrix to $n \times n$ rate constant matrix by applying contraction procedure M times, where $n + M = N$. The resultant $n \times n$ rate constant matrix means transitions between n superstates. In other words, the MINs contracted to the same superstates can reach a thermal equiribrium within the applied timescale. In addition, the paths connecting superstates correspond to the bottleneck paths. The time hierarchy of the reaction can be understood by applying the RCMC method at various timescales.

Thus, the bottleneck steps which were extracted when applying the RCMC method at reaction temperature T = 300 K and timescale $t = 10^{-3}$ s, and calculated IRC paths after optimizing the highest energy points to TS. Monkhorst-Pack grid was set to 2 × 2 × 2. Finally, the reaction route network including 13 IRC paths and 291 LUP paths were obtained.

2.3 Results and Discussion

2.3.1 Reaction route network

Figure 2-2 shows the reaction route network of H_2O molecule on Cu(111) at reaction temperature T = 300 K. This network includes 27 local minima (MINs), 13 transition states (TSs) and 291 LUP paths (PTs). However, 27 nodes and 86 edges were shown in Figure 2-2 because the LUP paths connecting the same MIN and duplicated edges which connects same combination of MINs were omitted. Bold and thick edges correspond to IRC paths and LUP paths, respectively.

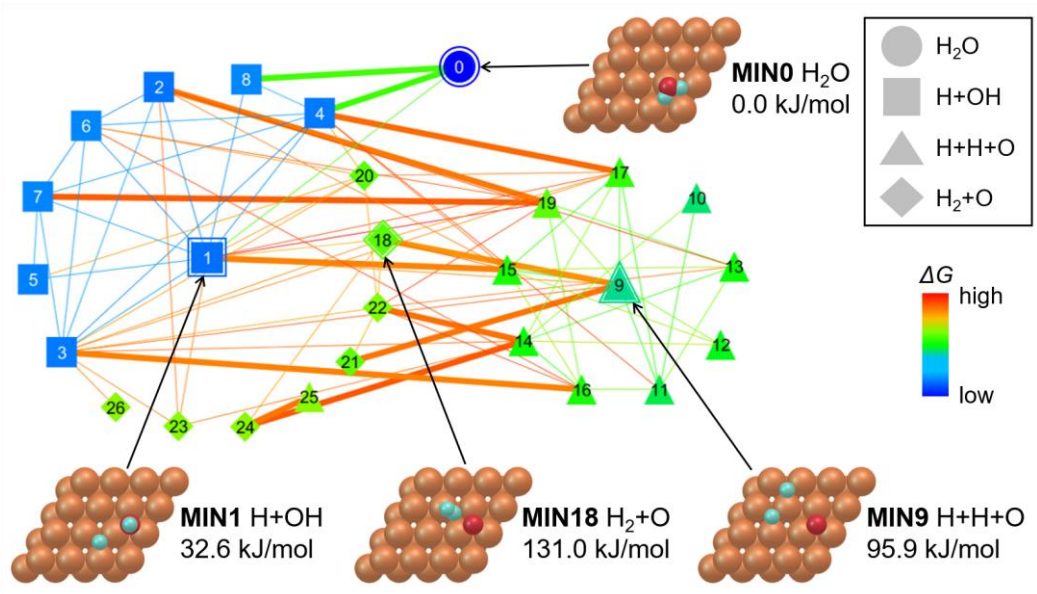

Figure 2-2. A reaction route network for reaction of H_2O on a Cu(111) surface at T = 300 K.

The network includes four kinds of adsorption states: H_2O, H+OH, H+H+O and H_2+O. These structures were distinguished by the shape of nodes. The structures having the lowest energies among the corresponding adsorption state were represented in Figure 2-2. The light blue, red, and brown atoms correspond to H, O and Cu atoms. MIN0 means the initial structure of the search and the most stable structure. The energies are relative free energies refer to MIN0. The colors of nodes and edges correspond to the energies of structures. The nodes are labeled from the lower energy structures. The network includes not only bond rearrangement paths between the paths connecting different adsorptions states but also migration paths between the paths connecting same adsorption states. Therefore, the obtained network was more complicated as expected although this is the simple system.

2.3.2 Time hierarchy of the reaction route network

The RCMC method was applied to the obtained network at reaction temperature T = 300 K and three reaction timescales; t = 10^{-3}, 1.0, 10^{3} s. The obtained time hierarchy was summarized in Figure 2-3 and superstates at each timescale was represented in Figure 2-4. In Figure 2-4, the values between superstates were activation free energies (kJ/mol) calculated by logarithm of n × n rate constant matrix obtained from the RCMC method.

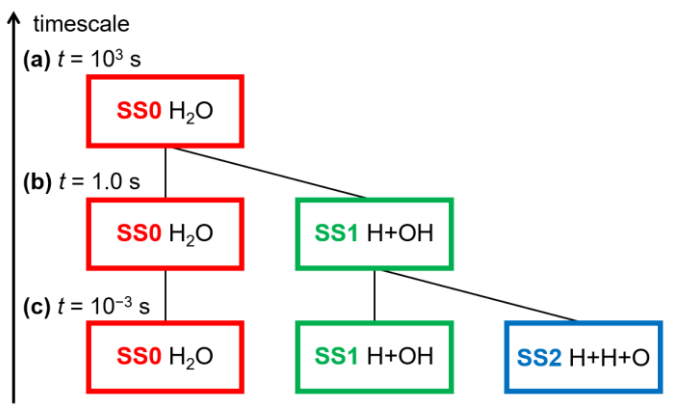

Figure 2-3. Time hierarchy of reaction of H_2O on a Cu(111) surface at T = 300 K.

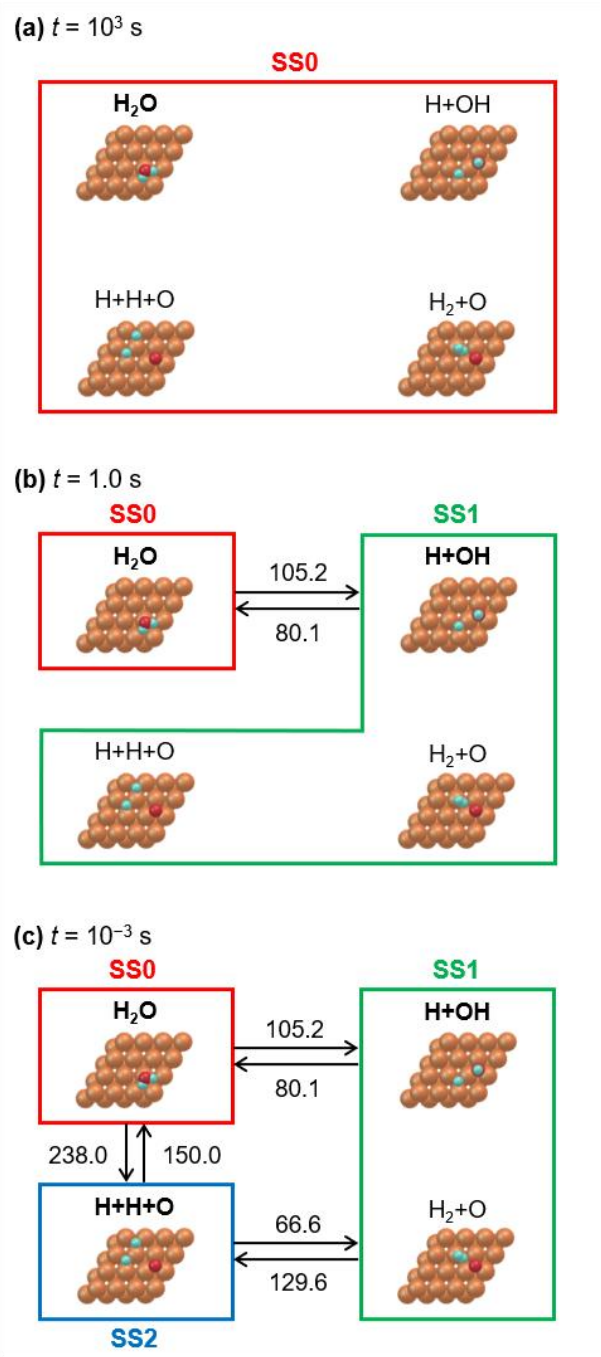

Figure 2-4. Superstates at T = 300 K and various timescale t.

First, when the timescale (a) t = 10^3 s, all MINs were contracted to the one superstate. In other words, all elementary processes in the network can proceed within 10^3 seconds. The

representative structure of the superstate, thus, the MIN which has the largest population among the structures in the superstate is H_2O. Next, in the case of (b) t = 1.0 s, the two superstates were obtained. At this timescale, H+OH and H_2O are contracted to the same superstate. This means the reaction step H+OH $\rightarrow$ H_2O can proceed > 1.0 s and within 10^3 s. Note that the IRC path between H+OH and H_2O shows good agreement with the previous study [15] for the structures and energies. Finally, when the timescale is set to (c) $t = 10^{-3}$ s, the three superstates were found. At this timescale, H_2O belongs to SS0, H+OH and H_2+O mainly belong to SS1, and H+H+O belongs to SS2, respectively. The result corresponds to the network of Figure 2-2. SS1 includes two kinds of adsorption states. This is because H_2+O is kinetically less favorable and the reaction H_2+O $\rightarrow$ H+OH occurs within 10^{-3} s.

By applying the RCMC method at different timescale t, the time hierarchy of the reaction route network was elucidated. Similar time hierarchy analysis was done for the organic reaction in the previous study [16]. In addition, the reaction route network in this study was created by calculating IRC paths only for bottleneck steps but others were LUP paths. The long-time kinetics can understand enough for the hybrid network (see Appendix of ref. 4).

2.4. Conclusion

In this study, the reaction route network for a H_2O molecule on Cu(111) surface was constructed by using the SC-AFIR method. The migration paths of adsorbed molecules or atoms on the surface as well as bond rearrangement paths were included in the obtained network. Furthermore, time hierarchy was elucidated by applying the RCMC method to the network. From these results, it was revealed that the bottleneck step of the network is H_2O $\rightarrow$ H+OH, dissociation of H_2O molecule on the surface and generating H+OH. This strategy, combination of the AFIR method and the RCMC method can be other heterogeneous reactions.

References (Chapter 2)

[1] S. Maeda, Y. Harabuchi, M. Takagi, K. Saita, K. Suzuki, T. Ichino, Y. Sumiya, K. Sugiyama and Y. Ono, *J. Comput. Chem.*, 2018, **39**, 233–250.

[2] T. MIta, Y. Harabuchi and S. Maeda, *Chem. Sci.*, 2020, **11**, 7569–7577.

[3] M. Takagi, T. Taketsugu, H. Kino, Y. Tateyama, K. Terakura, and S. Maeda, *Phys. Rev. B*, 2017, **95**, 184110 (11 pages).

[4] S. Maeda, K. Sugiyama, Y. Sumiya, M. Takagi and K. Saita, *Chem. Lett.*, 2018, **47**, 396–399.

[5] J. M. Soler, E. Artacho, J. D. Gale, A. García, J. Junquera, P. Ordejón and D. Sánchez-Portal, *J. Phys.: Condens. Matter*, 2002, **14**, 2745–2779.

[6] E. Artacho, J. M. Cela, J. D. Gale, A. García, J. Junquera, R. M. Martin, P. Ordejón, D. Sánchez-Portal and J. M. Soler, *SIESTA 4.0 (Revision 530)*, The Siesta Group, 2016, see http://www.uam.es/siesta

[7] Translation of Abinit's GGA Pseudo Database to Siesta Format: https://departments.icmab.es/leem/SIESTA_MATERIAL/Databases/Pseudopotentials/periodictable-gga-abinit.html

[8] M. Methfessel and A. T. Paxton, *Phys. Rev. B*, 1989, **40**, 3616–3621.

[9] C. Choi and R. Elber, *J. Chem. Phys.*, 1991, **94**, 751–760.

[10] P. Y. Ayala and H. B. Schlegel, *J. Chem. Phys.*, 1997, **107**, 375–384.

[11] K. Fukui, *Acc. Chem. Res.*, 1981, **14**, 363–367.

[12] S. Maeda, Y. Harabuchi, Y. Ono, T. Taketsugu and K. Morokuma, *Int. J. Quantum Chem*, 2015, **115**, 258–269.

[13] Y. Sumiya, Y. Nagahata, T. Komatsuzaki, T. Taketsugu and S. Maeda, *J. Phys. Chem. A*, 2015, **119**, 11641–11649.

[14] Y. Sumiya and S. Maeda, *Chem. Lett.*, 2020, **49**, 553–564.

[15] T. Liu, Z. Zhang, B. Fu, X. Yang and D. H. Zhang, *Chem. Sci.*, **2016**, *7*, 1840–1845.

[16] Y. Nagahata, S. Maeda, H. Teramoto, T. Horiyama, T, Taketsugu and T. Komatsuzaki, *J. Phys. Chem. B*, 2016, **120**, 1961–1971.

Chapter 3. Theoretical analysis of CO oxidation on Pt(111) surface: reaction route network and its entropic contributions to the kinetics

3.1 Introduction

Platinum (Pt) catalyst has been utilized for many surface reactions because it shows high catalytic activities even if low temperatures. One of the major applications of Pt catalysts is an automotive catalytic converter in which oxidation of carbon monoxide to carbon dioxide, $2CO + O_2 \rightarrow 2CO_2$. This reaction proceeds with the help of metal particles the platinum group such as platinum (Pt), palladium (Pd), and rhodium (Rh) [1,2]. Thus, CO oxidation reaction on the Pt(111) surface which generates a carbon dioxide (CO_2) from a carbon monoxide (CO) and an oxygen (O_2) have been treated as a model system of surface reactions and widely studied [2-23]. The Pt(111) surface is not considered to be reconstructed because it is fcc close-packed surface [24]. It is known that O_2 molecule prefers dissociative adsorption on the Pt(111) surface rather than molecular adsorption except at low temperature [17, 25-28]. Therefore the paths to form CO_2 from an adsorbed CO molecule and an adsorbed O atom have been discussed not only on the Pt(111) surface but on the other various surfaces [2-16,18,19,21,22,29-31]. In addition, CO_2 generation path via OC-OO complex was also reported on poisoned surfaces by toxic CO molecules [18,23], or on metal nano particles [31].

In this study, the systematic reaction path search by the artificial force induced reaction (AFIR) method [32] was applied to CO oxidation on a Pt(111) surface, and a reaction route network including many bond rearrangement paths and migration paths was obtained [33]. Furthermore, two kinds of CO_2 generation paths, byproducts and their lifetimes, and temperature dependence of the entropic contributions, which is caused by a lot of transition paths among the same adsorption states (migration paths) and bond rearrangement paths between them, were discussed by applying the RCMC method [34] to the network.

3.2 Method

3.2.1 DFT calculations

The potential energies and gradients were calculated by using the SIESTA 4.0 program [35,36]. The Perdrew-Burke-Ernzerhof (PBE) functional and DZP basis set were selected. The pseudopotentials were prepared from GGA potential database [37]. The relativistic effect including nonlinear core correction (NLCC) was applied to the platinum atom, and nonrelativistic pseudopotential without NLCC was applied to the other carbon and oxygen atoms. The smearing parameter was set to 10000 K with the occupation function of the Methfessel–Paxton scheme [38]. The Monkhorst-Pack grid which determines k-point sampling and the mesh cut off were changed depending on the calculation stage as described below.

3.2.2 Preparation of a Pt(111) surface

A periodic model of Pt(111) surface was prepared using same procedure as the Cu(111) surface described in 2.2.2. First, the lattice constant of Pt crystal having face-centered cubic (fcc) structure was optimized with k-point sampling 8 × 8 × 8 and mesh cur off 200 Ry. The initial parameter was set to 3.9242 Å refer to the experimental lattice constant value [39]. The optimized value 4.0319 Å was slightly longer than the experimental value. Then, the periodic slab model composed of two Pt(111) surface layer was created from the optimized Pt crystal. The surface has *p*(4×4) surface area (16 atoms per layer) and vacuum region about 15 Å. In the following calculations, all surface atoms and translational vectors were kept fixed at the initial positions.

3.2.3 Making a reaction route network of CO oxidation on a Pt(111) surface

A reaction route network for CO oxidation on a Pt(111) surface was created by using almost same

procedure as the H_2O reaction on a Cu(111) surface described in 2.2.4. The reaction path search was done by using the single component (SC-) AFIR method [32] implemented in the developer version of global reaction route mapping (GRRM) program developing in our laboratory. Figure 3-1 shows the initial structure of the search. A CO molecule and an O_2 molecule adsorb on atop site and bridge (t-b-t) site, respectively. This structure is also represented in the network (Figure 3-2) as MIN 127. The energy value is adsorption free energy ΔG_{ads} at T = 300 K defined as equation below:

$$\Delta G_{\mathrm{ads}} = G_{\mathrm{mol+slab}} - \left(G_{\mathrm{CO}} + G_{\mathrm{O_2}} + G_{\mathrm{slab}}\right)$$

$G_{\mathrm{mol+slab}}$ means the free energy of the total system consisting of a CO molecule, an O_2 molecule and a Pt(111) surface. G_{CO} and $G_{\mathrm{O_2}}$ correspond to the free energy of a CO(gas) molecule and an O_2(gas) molecule. G_{slab} represents the free energy of the Pt(111) surface, but the value is equal to the electronic energy because all surface atoms were fixed in this study. The model collision parameter γ of the AFIR function was set to γ = 500.0 kJ/mol. Target atoms generating the fragment pairs during the search are set to each atom of CO, O_2 and the Pt central dimer. In addition, to prevent adsorbates go away from the center of the surface, weak biases of γ_{add} = 25.0 kJ/mol were applied between each atom of CO, O_2 and the Pt central dimer by the AFIR function. The weak biases were finally removed as described below. The obtained force-induced paths (AFIR paths) were minimized by using the locally updated plane (LUP) method [40,41]. Then the network composed of LUP paths was obtained. The Monkhorst-Pack grid and the mech cur off were set to 1 × 1 × 1 and 150 Ry during the search.

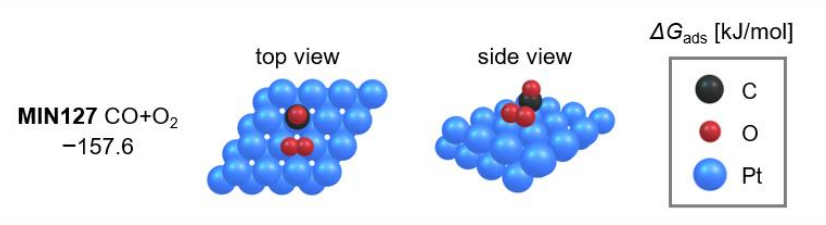

Figure 3-1. Initial structure of a reaction path search.

Next, further LUP calculations were done to remove weak biases which were added during the search. In this calculation, The Monkhorst-Pack grid and the mech cur off were set to 2 × 2 × 1 and 150 Ry during the search. Furthermore, normal mode vibration analysis was applied to all the obtained local minima (MINs) and highest energy points along the LUP paths. Finally, a reaction route network including 139 local minima and 545 LUP paths were created.

3.2.4 Kinetic analysis of the reaction route network by using the rate constant matrix contraction method

The bottleneck steps were extracted by applying the RCMC method to the obtained network using almost same procedure as the H_2O reaction on a Cu(111) surface described in 2.2.5. In other words, LUP paths that are behaved as the bottleneck step were extracted by applying the RCMC method at reaction temperature T = 300, 500, 1000 K and timescale $t = 1.0 \times 10^{-1}$ s. Then the highest energy point along the extracted LUP paths were optimized to the actual transition states (TSs). The Monkhorst-Pack grid was set to 2 × 2 × 1. 26 TSs were obtained by this operation. After that, the kinetic analysis by the RCMC method was applied again to this TS/PT hybrid network.

3.3 Results and Discussion

3.3.1 Reaction route network

139 MINs and 573 LUP paths (including 545 PTs and 27 TSs) were obtained by the search. The reaction route network at T = 300 K is shown in Figure 3-2. The network is composed on 133 nodes and 298 edges where these values correspond to the number of MINs and that of LUP paths (272 PTs and 26 TSs). 6 nodes of 139 MINs obtained by the search were deleted because these nodes were disconnected due to the numerical problems during the LUP calculations. This problem is caused if changing the Monkhorst-Pack grid depending on the calculation stage. However, the entire picture of the network is not changed. The number of edges is less than that of LUP paths because the LUP path that connecting the same MIN and the multiple LUP paths between the same pair of MINs were omitted. The thick and the thin lines represent the bottleneck edges and the other edges, respectively. The nodes were labeled based on the relative free energy of the structure from the most stable structure MIN0. The shape of nodes was classified into six groups based on the adsorption states; $CO+O_2$, CO+2O, CO_2+O, CO_2(g) + O, OC-OO and CO_3. The most stable structure of each adsorption state was shown in Figure 3-3.

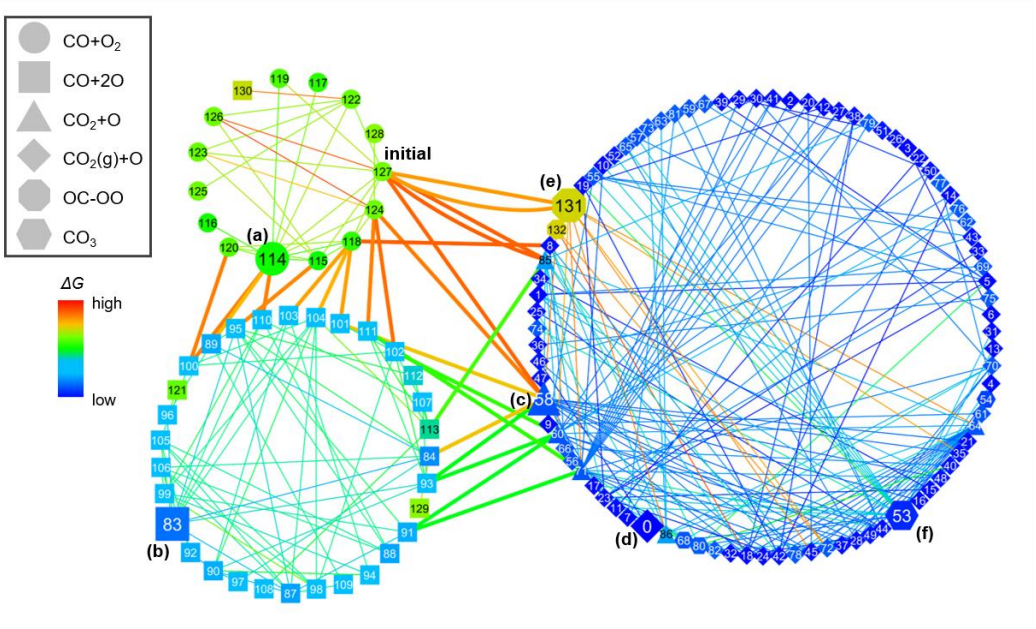

Figure 3-2. A reaction route network for CO oxidation on a Pt(111) surface at T = 300 K.

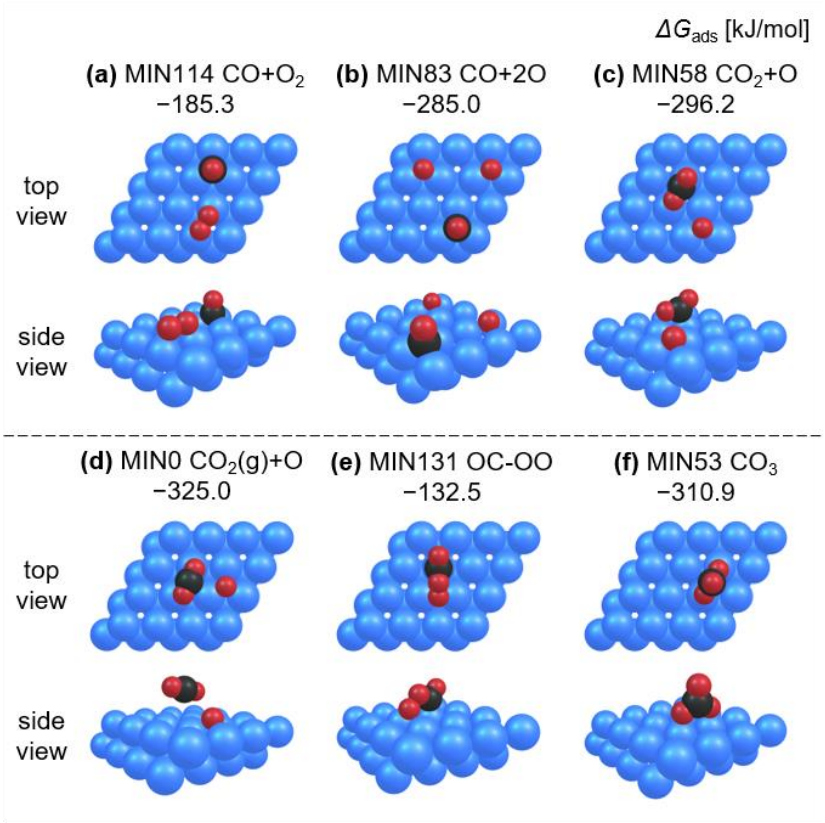

Figure 3-3. Adsorption states included in the reaction route network.

The energy value of the structures was adsorption free energy ΔG_{ads} at $T = 300$ K. The stability of the adsorbed structure depends on the adsorption states of each species and their relative positions. MIN 114, shown in Figure 3-3(a), is the most stable structure among the reactant region where CO molecule is adsorbed on fcc hollow site and O_2 molecule is adsorbed on bridge (t-b-t) site. The most stable adsorption state of CO molecule in this study (fcc hollow site) was inconsistent with the previous experimental studies that mentioned that of CO molecule is atop site [42-46]. This problem was known as CO puzzle, although this study does not aim to give the fundamental solution of the task (see Appendix of ref. 33). Figure 3-3(b) is the O_2 dissociated intermediate where CO molecule and two O atoms were adsorbed on fcc hollow sites. In the case of (c), CO_2 adsorbs on the surface with the bended form and O atom adsorbs on fcc hollow site.

In this study, two kinds of CO_2 are distinguished: chemisorbed and bended CO_2 is depicted as CO_2 and desorbed and linear CO_2 is depicted as CO_2(g). (e) is the intermediate OC-OO complex was formed on the surface for (e), and (f) is the byproduct CO_3 was formed on the surface.

3.3.2 Time hierarchy of the reaction route network

The results obtained by applying the RCMC method at T = 300 K and three kinds of timescale t = 1.0×10^3, 1.0, 1.0×10^{-1} s was summarized in Figure 3-4 and Figure 3-5. The values in Figure 3-5 means activation free energy (kJ/mol) for transitions between the superstates. These values were obtained by calculating logarithm of the overall rate constant which is the non-diagonal term of the $n \times n$ rate constant matrix acquired after applying RCMC to the original 133 × 133 rate constant matrix. n = 1, 2, 3 correspond to the result of RCMC at t = 1.0×10^3, 1.0, 1.0×10^{-1} s, respectively. The result at t = 1.0×10^2, 1.0×10^1 s was same as the result at t = 1.0 s.

First, in the case of (a) t = 1.0×10^3 s, all structures were contracted into the one superstate. This means all structures in the network can reach thermal equilibrium within this timescale. Next, if the timescale is set to (b) t = 1.0 s, two superstates were obtained. The reactant CO+O_2 and O_2 dissociated intermediate CO+2O belong to the same superstate SS1, but to the different the product CO_2(g)+O which belongs to the superstate SS0. This indicates that the path between MIN of SS1 and MIN of SS0, i.e. CO_2 formation step from an adsorbed CO molecule and an adsorbed O atom, is the bottleneck path of CO oxidation on a Pt(111) surface. The result is consistent with the previous studies that proposed the CO_2 formation proceeds with LH (Langmuir-Hinshelwood) mechanism. Finally, in the case of (c) t = 1.0×10^{-1} s, the network was contracted into the three superstates. The representative structure of each superstate is CO_2(g)+O (SS0), CO+2O (SS1) and CO+O_2 (SS2). Although SS0 also includes the other three adsorption states CO_3, OC-OO and CO_2+O, these states immediately convert into CO_2(g)+O shorter within

1.0×10^{-1} s due to having the short lifetime 10^{-12}, 10^{-9} and 10^{-4} seconds.

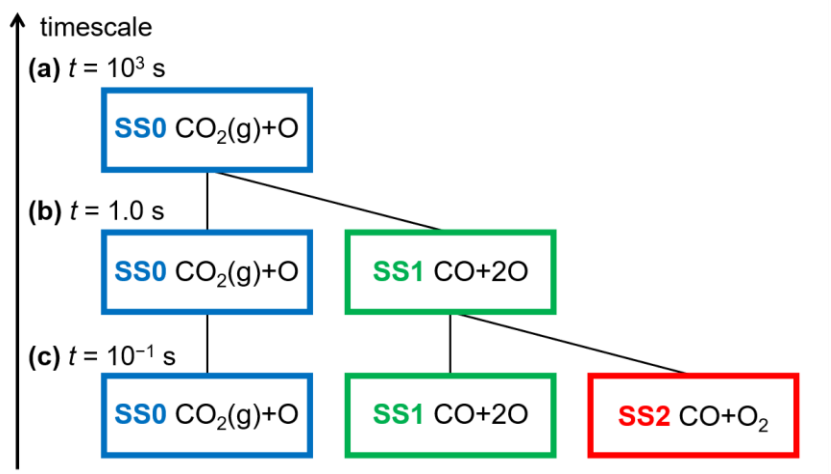

Figure 3-4. Time hierarchy of the reaction route network at $T = 300$ K.

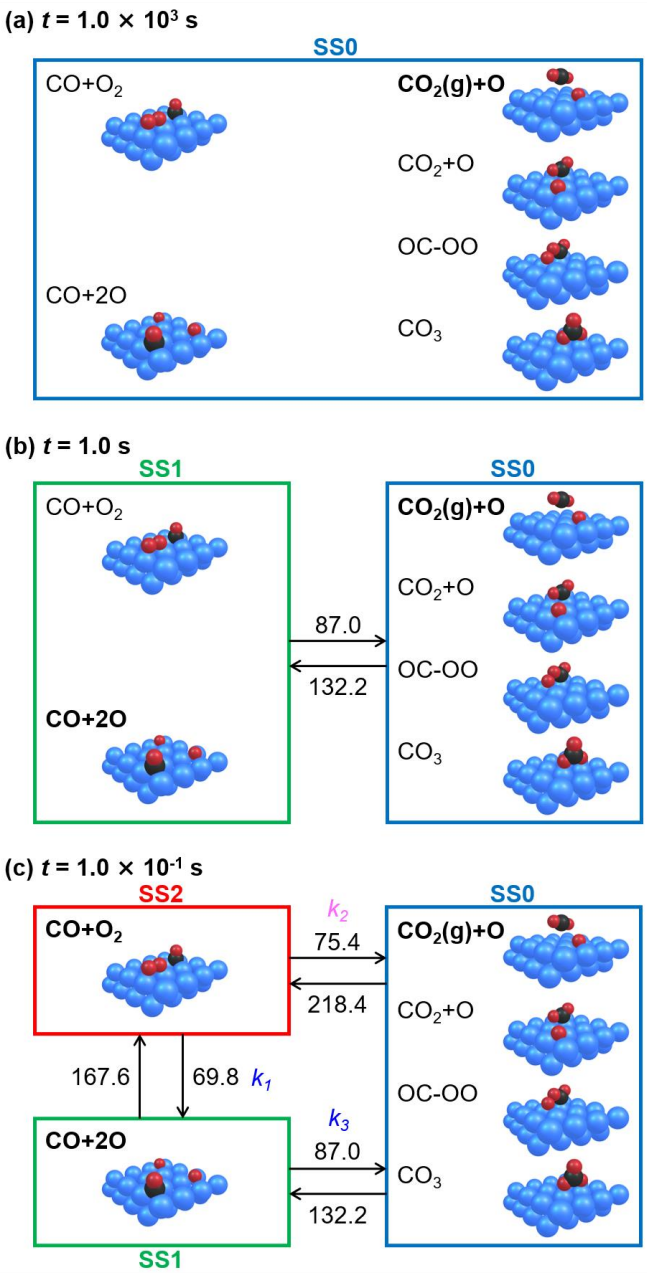

Figure 3-5. Superstates at T = 300 K and various timescale t.

Furthermore, the values of the overall rate constants k_1 and k_2 shown in Figure 3-5(c) were compared as shown in Table 3-1. k_1 is the overall rate constant from SS2 to SS1 and corresponds to the O_2 dissociation step, while k_2 is the overall rate constant from SS2 to SS0 and corresponds to direct CO_2 generation step through the MIN or TS having the shape of OC-OO.

From Table 3-1, it can be understood that the CO_2 formation path via O_2 dissociation is more favorable at the all temperatures because the contribution of minor path k_2 becomes at most 10%.

Table 3-1. Rate constant k_1, k_2, and contribution of minor path $k_2 / (k_1 + k_2)$

T [K]	300	500	1000
k_1 [s^{-1}]	4.39×10^{0}	5.37×10^{5}	4.10×10^{9}
k_2 [s^{-1}]	4.59×10^{-1}	4.95×10^{4}	5.03×10^{8}
$k_2 / (k_1 + k_2)$	0.0947	0.0844	0.1093

3.3.3 Detailed mechanism of CO oxidation

As described above, two different CO_2 formation paths are known to the previous studies. The energy profile for two kinds of CO_2 formation paths at $T = 300$ is shown in Figure 3-6. The energy values are adsorption free energy ΔG_{ads} at $T = 300$ K. In addition, this energy profile consists of the most stable conformer of the adsorption states and the corresponding LUP path having the lowest energy of TS/PT. This simplified model is called as the lowest conformer to single transition state (LC-TS) model [34].

The blue line in Figure 3-6 shows (i) via O_2 dissociation route. The rate determining step is the second step $CO+2O \rightarrow CO_2(g)+O$, corresponds to the step that CO_2 formed and desorbed on the surface. On the other hand, the pink line shows (ii) via OC-OO complex route. The rate determining step is the first step $CO+O_2 \rightarrow OC\text{-}OO$, corresponds to the step generating OC-OO complex. Note that the last step $CO_2+O \rightarrow CO_2(g)+O$ (CO_2 desorption step) is omitted in Figure 3-6 because its reaction barrier is very small (about 2.3 kJ/mol). In the case of (i) via O_2 dissociation route, the reaction barrier of the first step ($CO+O_2 \rightarrow CO+2O$) is 69.7 kJ/mol (73.5 kJ/mol in electronic energy), and that of the second step ($CO+2O \rightarrow CO_2(g)+O$) is 89.2 kJ mol/1

(90.5 kJ/mol in electronic energy). This indicates our result is in the range of previous theoretical studies, 27.0– 74.3 kJ/mol (in ref. 14 and 17) and 37.6–111.9 kJ/mol (in ref. 9–12, 14–16 and 29), respectively. Although route (ii) via the OC–OO complex on the clean Pt(111) surface has not been calculated to our knowledge, a similar route was suggested from both experimental and theoretical studies [18,23].

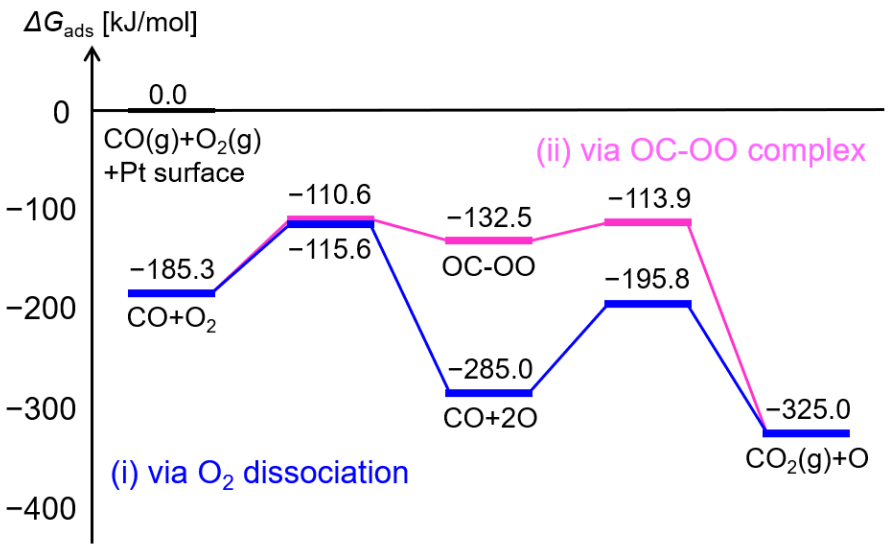

Figure 3-6. The energy profile of the two kinds of CO_2 generation paths at $T = 300$ K.

3.3.4 Impact of the reaction route network

To discuss the influence of the reaction route network on the overall kinetics, the result of RCMC was compared to that of LC-TS model. The rate constant calculated by using the RCMC method is different from the rate constant calculated by using the LC-TS model because the rate constant by RCMC includes the entropic contribution of transitions among many structures having the same adsorption state but different relative positions (migration paths) as well as bond rearrangement paths connecting them. This effect is called as conformation entropy [34]. There are two kinds of conformation entropies. One is the conformation entropy of MINs that decreases

the rate constant due to having various MINs. The other is the conformation entropy of TSs that increases the rate constant due to having various configurations of bond rearrangement TSs.

The influence of the conformation entropy of MINs and TSs were investigated by comparing the overall rate constant by RCMC with the rate constants excluding these entropic contributions. k_1, k_2 and k_3 in Figure 3-5 (c) are represented as k_x(RCMC), and corresponding the rate constants by LC-TS model and LC-mTS (lowest conformer to multiple transition states) model are k_x(LC-TS) and k_x(LC-mTS), respectively. k_x(LC-TS) is calculated from the energy difference between the most stable conformer of the reactant region and the bottleneck TS having the lowest energy, regarded as the energy barrier $\Delta\Delta G$. k_x(LC-mTS) is the sum of the rate constants, where the energy differences between the most stable conformer of the reactant region and all bottleneck TSs are regarded as the energy barrier $\Delta\Delta G$. The difference between k_x(LC-TS) and k_x(LC-mTS) corresponds to the conformation entropy of TSs, while the difference between k_x(LC-mTS) and k_x(RCMC) corresponds to the conformation entropy of MINs.

k_1, k_2 and k_3 calculated by the three different RCMC, LC-TS, LC-mTS model at T = 300, 500, 1000 K is summarized in Table 3-2. Furthermore, the ratio of k_x(LC-TS) and k_x(LC-mTS) refer to k_x(RCMC) is shown in Figure 3-7 to show the differences clearly. In Figure 3-7, some trends can be understood although the dependency is not simple because the most stable conformer and the bottleneck TS is changed by the temperature. First, the conformation entropy of TSs affects to all the k_x (x = 1–3) and k_x(LC-mTS) becomes twice or three times bigger than k_x(LC-TS). This indicates that multiple TSs having the various configurations are important to the bond rearrangement step. In other words, it is shown that the conformation entropy of TSs is important for CO oxidation on a Pt(111) surface. The importance of multiple TSs was discussed for the selectivity and/or reactivity of the other chemical reactions [47-55].

Focusing on k_x(LC-mTS), the conformation entropy of MINs is small especially the case

of k_3 at low temperature. It is supposed that migrations on the surface in SS1 are inhibited because all chemical species in SS1, i.e., O atoms and a CO molecule strongly adsorb (chemical adsorption) on the surface. On the other hand, the conformation entropy of MINs for k_1 and k_2 are relatively large because of the smaller adsorption energy of O_2 molecule on a Pt(111) surface. Furthermore, the overall trends is that the k_x(LC-TS) of k_1 and k_2 are consistent as a result of the cancelling two types of conformation entropy, but this does not always occur. The elementary rate constants considering both the conformation entropy of MINs and TSs can be evaluated to compare k_x(RCMC) and the other models as described above.

Table 3-2. k_1, k_2 and k_3 calculated by RCMC, LC-TS and LC-TS model and the temperature dependency

T [K]	300	500	1000
k_1 (RCMC) [s^{-1}]	4.39×10^{0}	5.37×10^{5}	4.10×10^{9}
k_1 (LC-TS) [s^{-1}]	5.03×10^{0}	4.55×10^{5}	2.73×10^{9}
k_1 (LC-mTS) [s^{-1}]	9.70×10^{0}	9.96×10^{5}	7.80×10^{9}
k_2 (RCMC) [s^{-1}]	4.59×10^{-1}	4.95×10^{4}	5.03×10^{8}
k_2 (LC-TS) [s^{-1}]	6.28×10^{-1}	8.01×10^{4}	5.35×10^{8}
k_2 (LC-mTS) [s^{-1}]	1.24×10^{0}	1.59×10^{5}	1.60×10^{9}
k_3 (RCMC) [s^{-1}]	4.41×10^{-3}	1.11×10^{4}	4.23×10^{8}
k_3 (LC-TS) [s^{-1}]	2.04×10^{-3}	5.19×10^{3}	3.25×10^{8}
k_3 (LC-mTS) [s^{-1}]	4.48×10^{-3}	1.21×10^{4}	8.51×10^{8}

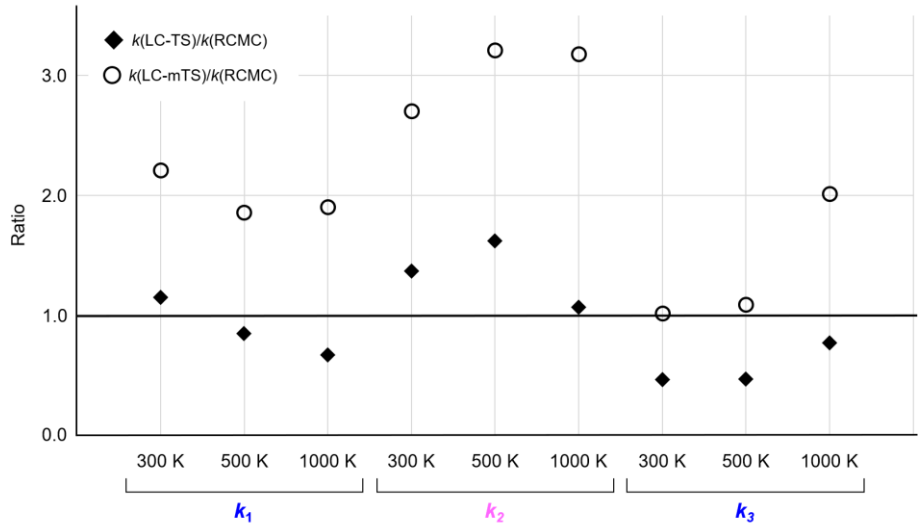

Figure 3-7. The ratio and temperature dependency of *k*(LC-TS) and *k*(LC-mTS) refer to *k*(RCMC)

3.4 Conclusion

In this study, the reaction path search by the AFIR method was applied to CO oxidation on a Pt(111) surface. A reaction route network consists of 133 structures and connecting paths was obtained. The network includes not only bond rearrangement paths but also short-range migration paths. Furthermore, the time hierarchy of the network was elucidated by using kinetic analysis of the RCMC method. From the results, it is elucidated that bottleneck step of the entire reaction is CO_2 formation step occurring between adsorbed a CO molecule and an O atom. This is consistent with the previous results that proposed CO oxidation is LH mechanism accompanied by the dissociation of O_2 molecule.

In addition, short-lived intermediates such as CO_2+O, OC-OO and CO_3 were included in the network. Then the kinetic influence of two kinds of CO_2 formation paths, via O_2 dissociation and via OC-OO complex, were discussed. Furthermore, temperature dependency of the entropic contributions caused by the many transitions among the same adsorption states (migration paths)

and the connecting bond rearrangement paths were studied [60].

References (Chapter 3)

[1] J. Kašpar, P. Fornasiero and N. Hickey, *Catal. Today*, 2003, **77**, 419–449.

[2] G. Ertl, *Angew. Chem. Int. Ed.*, 2008, **47**, 3524–3535.

[3] R. L. Palmer and J. N. Smith, Jr., *J. Chem. Phys.*, 1974, **60**, 1453–1463.

[4] C. T. Campbell, G. Ertl, H. Kuipers and J. Segner, *J. Chem. Phys.*, 1980, **73**, 5862–5873.

[5] J. L. Gland and E. B. Kollin, *J. Chem. Phys.*, 1983, **78**, 963–974.

[6] C. Hardacre, R. M. Ormerod and R. M. Lambert, *Chem. Phys. Lett.*, 1993, **206**, 171–174.

[7] G. Ertl, *Surf. Sci.*, 1994, **299–300**, 742–754.

[8] J. Wintterlin, S. Volkening, T. V. W. Janssens, T. Zambelli, and G. Ertl, *Science*, 1997, **278**, 1931–1934.

[9] A. Eichler and J. Hafner, *Phys. Rev. B: Condens. Matter Mater. Phys.*, 1999, **59**, 5960–5967.

[10] R. J. Baxter and P. Hu, *J. Chem. Phys.*, 2002, **116**, 4379–4381.

[11] A. Eichler, *Surf. Sci.*, 2002, **498**, 314–320.

[12] X.-Q. Gong, Z.-P. Liu, R. Raval and P. Hu, *J. Am. Chem. Soc.*, 2004, **126**, 8–9.

[13] S. Kandoi, A. A. Gokhale, L. C. Grabow, J. A. Dumesic, and M. Mavrikakis, *Catal. Lett*, 2004, **93**, 93–100.

[14] L. Grabow, Y. Xu and M. Mavrikakis, *Phys. Chem. Chem. Phys.*, 2006, **8**, 3369–3374.

[15] M. Nagasaka, H. Kondoh, I. Nakai and T. Ohta, *J. Chem. Phys.*, 2007, **126**, 044704 (7 pages).

[16] H. Falsig, B. Hvoæk, I. S. Kristensen, T. Jiang, T. Bligaard, C. H. Christensen and J. K. Nørskov, *Angew. Chem. Int. Ed.*, 2008, **47**, 4835–4839.

[17] B. Shan, N. Kapur, J. Hyn, L. Wang, J. B. Nicholas and K. Cho, *J. Phys. Chem. C*, 2009, **113**, 710–715.

[18] A. D. Allian, K. Takanabe, K. L. Fujdala, X. Hao, T. J. Truex, J. Cai, C. Buda, M. Neurock and E. Iglesia, *J. Am. Chem. Soc.*, 2011, **133**, 4498–4517.

[19] A. Farkas, K. Zalewska-Wierzbicka, C. Bachmann, J. Goritzka, D. Langsdorf, O. Balmes, J. Janek and H. Over, *J. Phys. Chem. C*, 2013, **117**, 9932–9942.

[20] S. K. Calderón, M. Grabau, L. Óvári, B. Kress, H.-P. Steinrück and C. Papp, *J. Chem. Phys.*, 2016, **144**, 044706 (9 pages).

[21] M. A. van Spronsen, J. W. M. Frenken and I. M. N. Groot, *Chem. Soc. Rev.*, 2017, **46**, 4347–4374.

[22] H. Ueta and M. Kurahashi, *J. Chem. Phys.*, 2017, **147**, 194705 (4 pages).

[23] J. Kim, M. C. Noh, W. H. Doh and J. Y. Park, *J. Phys. Chem. C*, 2018, **122**, 6246–6254.

[24] A. R. Sandy, S. G. J. Mochrie, D. M. Zehner, G. Grübel, K. G. Huang and D. Gibbs, *Phys. Rev. Lett.*, 1992, **68**, 2192–2195.

[25] H. Steininger, S. Lehwald and H. Ibach, *Surf. Sci.*, 1982, **123**, 1–17.

[26] A. Eichler and J. Hafner, *Phys. Rev. Lett.*, 1997, **79**, 4481–4484.

[27] A. Groß, A. Eichler, J. Hafner, M. J. Mehl and D. A. Papaconstantopoulos, *Surf. Sci.*, 2003, **539**, L542–L548.

[28] A. Eichler, F. Mittendorfer and J. Hafner, *Phys. Rev. B*, 2000, **62**, 4744–4755.

[29] K. Koizumi, K. Nobusada and M. Boero, *Chem. —Eur. J.*, 2016, **22**, 5181–5188.

[30] S. Piccinin and M. Stamatakis, *Top Catal*, 2017, **60**, 141–151.

[31] N. Lopez and J. K. Nørskov, *J. Am. Chem. Soc.*, 2002, **124**, 11262–11263.

[32] S. Maeda, Y. Harabuchi, M. Takagi, K. Saita, K. Suzuki, T. Ichino, Y. Sumiya, K. Sugiyama and Y. Ono, *J. Comput. Chem.*, 2018, **39**, 233–250.

[33] K. Sugiyama, Y. Sumiya, M. Takagi, K. Saita and S. Maeda, *Phys. Chem. Chem. Phys.*, 2019, **21**, 14366–14375.

[34] Y. Sumiya, Y. Nagahata, T. Komatsuzaki, T. Taketsugu and S. Maeda, *J. Phys. Chem. A*, 2015,

119, 11641–11649.

[35] J. M. Soler, E. Artacho, J. D. Gale, A. García, J. Junquera, P. Ordejón and D. Sánchez-Portal, *J. Phys.: Condens. Matter*, 2002, **14**, 2745–2779.

[36] E. Artacho, J. M. Cela, J. D. Gale, A. García, J. Junquera, R. M. Martin, P. Ordejón, D. Sánchez-Portal and J. M. Soler, *SIESTA 4.0 (Revision 530)*, The Siesta Group, 2016, see http://www.uam.es/siesta

[37] Translation of Abinit's GGA Pseudo Database to Siesta Format: https://departments.icmab.es/leem/SIESTA_MATERIAL/Databases/Pseudopotentials/periodictable-gga-abinit.html

[38] M. Methfessel and A. T. Paxton, *Phys. Rev. B*, 1989, **40**, 3616–3621.

[39] Y. Waseda, K. Hirata and M. Ohtani, *High Temp. － High Pressures*, 1975, **7**, 221–226.

[40] C. Choi and R. Elber, *J. Chem. Phys.*, 1991, **94**, 751–760.

[41] P. Y. Ayala and H. B. Schlegel, *J. Chem. Phys.*, 1997, **107**, 375–384.

[42] H. Froitzheim, H. Hopster, H. Ibach and S. Lehwald, *Appl. Phys.*, 1977, **13**, 147–151.

[43] G. Ertl, M. Newmann and K. M. Streit, *Surf. Sci.*, 1977, **64**, 393–410.

[44] P. J. Feibelman, B. Hammer, J. K. Nørskov, F. Wagner, M. Scheffler, R. Stumpf, R. Watwe and J. Dumesic, *J. Phys. Chem. B*, 2001, **105**, 4018–4025.

[45] Y. Wang, S. de Gironcoli, N. S. Hush and J. R. Reimers, *J. Am. Chem. Soc.*, 2007, **129**, 10402–10407.

[46] P. Janthon, F. Viñes, J. Sirijaraensre, J. Limtrakl and F. Illas, *J. Phys. Chem. C*, 2017, **121**, 3970–3977.

[47] S. Maeda and K. Ohno, *J. Am. Chem. Soc.*, 2008, **130**, 17228–17229.

[48] P. J. Donoghue, P. Helquist, P. O. Norrby and O. Wiest, *J. Am. Chem. Soc.*, 2009, **131**, 410–411.

[49] P. Seal, E. Papajak and D. G. Truhlar, *J. Phys. Chem. Lett.*, 2012, **3**, 264–271.

[50] M. Hatanaka, S. Maeda and K. Morokuma, *J. Chem. Theory. Comput.*, 2013, **9**, 2882–2886.

[51] E. Lime, M. D. Lundholm, A. Forbes, O. Wiest, P. Helquist and P. O. Norrby, *J. Chem. Theory. Comput.*, 2014, **10**, 2427–2435.

[52] M. Gao, A. Lyalin, S. Maeda and T. Taketsugu, *J. Chem. Theory Comput.*, 2014, **10**, 1623–1630.

[53] M. Gao, A. Lyalin, M. Takagi, S. Maeda and T. Taketsugu, *J. Phys. Chem. C*, 2015, **119**, 11120–11130.

[54] E. T. Baxter, M.-A. Ha, A. C. Cass, A. N. Alexandrova and S. L. Anderson, *ACS Catal.*, 2017, **7**, 3322–3335.

[55] G. Sun and P. Sautet, *J. Am. Chem. Soc.*, 2018, **140**, 2812–2820.

Chapter 4. Theoretical analysis of decomposition reaction on Pt(111) surface: kinetic importance of the major and minor reaction routes

4.1 Introduction

Platinum is a useful catalyst to generate syngas of carbon monoxide and hydrogen by decomposition reaction of a methanol [1,2]. It is important to understand the reaction mechanism since hydrogen is also paid attention to be energy resources. From previous experimental studies, products and/or intermediates were elucidated by using the measurement techniques such as X-ray photoelectron spectroscopy (XPS), electron energy loss spectroscopy (EELS), temperature programmed desorption (TPD) [3-11]. It was pointed out that CO and H_2 are major product of methanol decomposition reaction on a Pt(111) surface while CO_2 and H_2O are generated on a pre-oxidized Pt(111) surface or in oxygen gas [4,7,9,10]. In addition, temperature dependency [5] and surface structure [6,11] were investigated. To see the results, reactions likely to occur at defect sits of O_2 treated surface with low temperature, and using Pt−Re alloy prevents the surface from being covered with carbons.

The detailed decomposition mechanism of a methanol on Pt clusters and surfaces has been studied by theoretical methods. Some promising elementary steps and reaction intermediates were investigated by density functional theory (DFT) calculations [8,11-25]. In addition to the reactant CH_3OH and the product CO and H_2, various adsorbed species such as CH_3O, CH_2OH, CH_2O, HCOH, CH_3, HCO, COH, and OH and paths connecting them have been discussed. From these theoretical studies, the major path was specified to be $CH_3OH \rightarrow CH_2OH \rightarrow HCOH \rightarrow HCO \rightarrow CO$ [17,22]. Besides this, the path via COH is supposed to be a competitive path [17]. Then the reaction kinetics by using the rate constants of bond rearrangement steps between adsorbed species were discussed [17,22]. Furthermore, microkinetic modeling was done using the calculated reaction barriers for the elementary steps. Then the change of coverage of intermediates

and turnover frequencies for H_2 generation were simulated [22,25]. The reaction mechanisms and kinetics of methanol decomposition reaction on Pt surfaces were clarified from these previous studies.

In this study, a reaction route network for methanol decomposition reaction on a Pt(111) network was represented [26]. Systematic reaction path search was done by using the artificial force induced reaction (AFIR) method [27]. The calculated network consists of 292 nodes and 430 edges. Nodes and edges correspond to local minimum (MIN) structures and the connecting paths, respectively. Then the time hierarchy of the network, the time evolution of the population from reactant nodes to products nodes, the kinetically most favorable route was calculated by kinetic analyzed of the RCMC method [28,29].

4.2 Computational method

4.2.1 DFT calculations

The potential energies and gradients were calculated by using the SIESTA 4.0 program [30,31]. The Perdrew-Burke-Ernzerhof (PBE) functional and DZP basis set were selected. The pseudopotentials were prepared from GGA potential database [32]. The relativistic effect including nonlinear core correction (NLCC) was applied to the platinum atom, and nonrelativistic pseudopotential without NLCC was applied to the other hydrogen, carbon and oxygen atoms. The smearing parameter was set to 10000 K with the occupation function of the Methfessel–Paxton scheme [33]. The Monkhorst-Pack grid which determines k-point sampling and the mesh cut off were changed depending on the calculation stage as described below.

4.2.2 Preparation of a Pt(111) surface

A periodic model of Pt(111) surface was prepared using same procedure as described in section

3.2.2. First, the lattice constant of Pt crystal having face-centered cubic (fcc) structure was optimized with k-point sampling 8 × 8 × 8 and mesh cur off 200 Ry. Then, the periodic slab model composed of three Pt(111) surface layer was created from the optimized Pt crystal. The surface has *p*(4×4) surface area (16 atoms per layer) and vacuum region about 15 Å. During the AFIR calculations, a slab model created by the upper two layers of three-layered Pt(111) surface and all surface atoms and translational vectors were fixed at the initial positions was used. Further refinement calculations using three-layered and fixed the bottom layer and the translational vectors were applied to the kinetically import elementary paths extracted from the network by the RCMC method.

4.2.3 Making a reaction route network of CH_3OH decomposition reaction on a Pt(111) surface

A reaction route network for methanol decomposition reaction on a Pt(111) surface was created by using almost same procedure as the H_2O reaction on a Cu(111) surface (see 2.2.4) and CO oxidation on a Pt(111) surface (see 3.2.3). The reaction path search was done by using the single component (SC-) AFIR method [27] implemented in the developer version of global reaction route mapping (GRRM) program developing in our laboratory, and this version has almost same function as GRRM20. The model collision parameter γ of the AFIR function was set to γ = 300.0 kJ/mol. Target atoms generating the fragment pairs during the search are set to atoms in CH_3OH and the Pt central dimer. In addition, to prevent adsorbates go away from the center of the surface, weak biases of γ_{add} = 25.0 kJ/mol were applied by the AFIR function between six atoms in CH_3OH and the Pt central dimer. Figure 3-1 shows the initial structure of the search, that is, an adsorbed methanol molecule on a Pt(111) surface. The kinetics-based navigation option, which ranks MINs based on their kinetic importance and avoids to search from those of low rank, was

used [29]. The obtained force-induced paths (AFIR paths) were minimized by using the locally updated plane (LUP) method [34, 35]. The LUP calculation was held twice, where the weak additional bias was reduced to γ_{add} = 8.3 kJ/mol at the second time. The Monkhorst-Pack grid and the mech cur off were set to 1 × 1 × 1 and 75.0 Ry during this calculation.

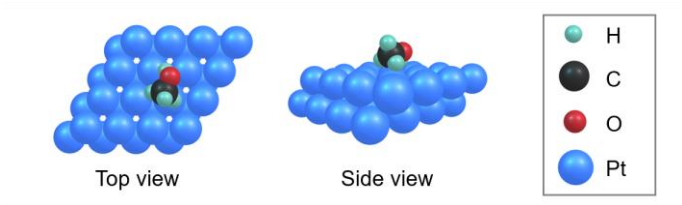

Figure 4-1. Initial structure for methanol decomposition reaction on a Pt(111) surface. CH_3OH weakly adsorbs on the surface.

Finally, a reaction route network consisting of 292 structures and 430 LUP paths were found. The calculation took 70.2 hours by using 200 CPU-cores of Xeon Gold 6248 (2.50GHz). Note that our purpose is obtaining a reaction route network with a moderate accuracy to gain the overview of entire reaction mechanism. The kinetically important steps in the network were treated with more accurate levels. Namely, the highest energy point of the corresponding LUP paths were optimized to the actual transition states (TSs). In this calculation, three-layered surface with fixing Pt atoms of the bottom layer was used, and the Monkhorst-Pack grid and the mech cur off were set to 2 × 2 × 1 and 100.0 Ry.

4.2.4 Kinetic analysis by rate constant matrix contraction (RCMC) method

The bottleneck steps can be extracted by applying the RCMC method [28,29] to the network as described in section 2.2.5. However, each element of the original $N \times N$ rate constant matrix for a reaction route network including N MINs were estimated by using the following equation.

$$k_{X\to Y} = \frac{k_B T}{h} e^{-\frac{\Delta\Delta E}{RT}}$$

$\Delta\Delta E$ is a reaction barrier from state X to state Y along the corresponding LUP path, and represented in electronic energy. T is reaction temperature and set to T = 500 K. k_B, h, R correspond to the Boltzmann constant, the Planck constant, and gas constant, respectively. In general transition state theory (TST), the free energy is used instead of $\Delta\Delta E$. However, we used electronic energy assuming that the contribution of vibration is not significant. In other words, no entopic contribution was considered.

In addition, MINs were grouped by the bond-connectivity of the adsorbed atoms. The distance which is shorter than 1.25 times of the sum of covalent radius was regarded as "bonded". Then the MINs in the same group are assumed to interconvert each other easily. Namely, if the energy of MIN*I* is higher than that of MIN*J* which belongs to the same group, the reaction barrier from MIN*I* to MIN*J* was set to $\Delta\Delta E = 0$ (no barrier). On the other hand, if the energy of MIN*I* is lower than that of MIN*J*, the reaction barrier from MIN*I* to MIN*J* was set to $\Delta\Delta E = (\Delta E_J - \Delta E_I)$ (energy difference between MIN*I* and MIN*J*).

In RCMC, the original $N \times N$ rate constant matrix is reduced to $n \times n$ rate constant matrix by applying the contraction procedure M times, where $n + M = N$. The contraction was applied to state having shorter lifetimes than given threshold timescale t. To apply RCMC procedure aa various timescale, the time hierarchy of the network and the time evolution that the initial population was set to MIN(s) can be calculated.

4.3. Results and discussion

4.3.1 Reaction route network

The resultant reaction route network for CH_3OH decomposition reaction on a Pt(111) surface is represented in Figure 4-2. In this study, the search from kinetically less important MINs were note

done because of using the kinetic-based navigation option [29]. Therefore, the high-lying part of the network is less meaningful. It was elucidated that 290 MINs of 292 nodes can be accessible from the most stable CH_3OH within 10^{-3} seconds at T = 500 K. This means 290 MINs and the connecting 640 paths (384 LUP paths and 256 added paths by grouping based on the bond connectivity of the adsorbates as explained in 4.2.4) are kinetically important. Figure 4-2 shows this kinetically important network consists of 290 odes and 640 edges (loop paths and multiple edges connecting the same node pair were omitted). In Figure 4-2(a), color of nodes and edges represents relative electronic energy.

CH_2OH, CH_3O, CH_2O, HCOH, HCO, COH, adsorbed C atom, hydrocarbons (CH_2, CH) and H_2O were obtained from the network. Then the various decomposition paths including byproduct generation paths can be discussed. Furthermore, the number of paths in the network is much more than expected for the simple species like CH_3OH. This is because the network includes migration paths between structures having the same adsorption states but different relative positions as well as bond rearrangement paths between structures having different adsorption states. In Figure 4-2(b), 13 kinds of adsorptions stated are distinguished by the color of nodes ($CH+H_2O+H$ was omitted because it cannot access from reactant CH_3OH within 10^{-3} s).

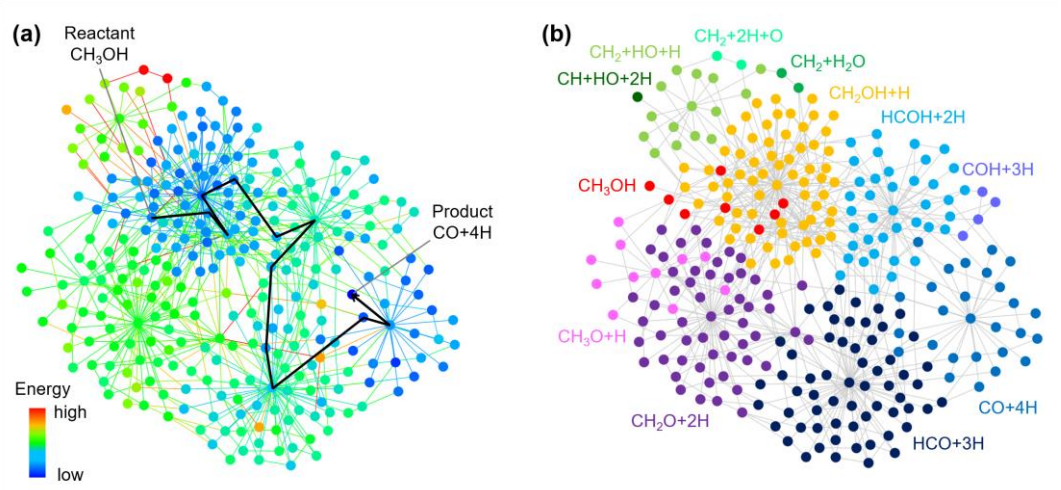

Figure 4-2. Reaction route network for methanol decomposition reaction on a Pt(111) surface. Nodes and edges represent obtained MINs and paths connecting them, respectively. 290 MINs which can be accessible from reactant CH_3OH within 10^{-3} s were depicted. (a) Nodes and edges are colored based on their electronic energies. Bold black line represents kinetically favorable decomposition route (see Figure 4-6). (b) Color of Nodes represents adsorption states.

4.3.2 Time hierarchy of the reaction route network

Next, the reaction mechanism was extracted from the complex network by the RCMC method. Figure 4-3 shows a time hierarchy diagram of the entire reaction. Namely, obtained superstates by applying the RCMC method at $T = 500$ K and various timescale were represented. The vertical axis means the applied timescale t. Each frame corresponds to the representative (energetically dominant) adsorption state. As shown in the top layer of Figure 4-3, all 292 original states are contracted to one superstate at $t = 10^6$ s. This means all MINs in the network can reach thermal equilibrium within this timescale. The representative structure, the structure having the maximum population among the structures belong to the superstate, is not $CO+2H_2$ but CO+4H. This corresponds that H_2 favors dissociative adsorption energetically on platinum surfaces, and is released into gas phase by entropic contributions. Assuming to moving hydrogen freely, it would

be required to additionally consider the entropic contribution of their motion to the H_2 dissociation.

Next, the superstate of CO+4H obtained at $t = 10^6$ s was divided into two superstates at $t = 10^{-3}$ s (The second layer of the hierarchical diagram). The composition of superstates at $t = 10^3$ and 1.0 s were same as the case of $t = 10^{-3}$ s. One is main product CO+4H and the other is byproduct CH+H_2O+H. This means it takes $>10^3$ s to convert to CO+4H from CH+H_2O+H. The reactant CH_3OH is mainly contracted to the superstate of CO+4H. The result shows CO generation is completed within this timescale.

The third layer of the hierarchical diagram is superstates obtained by RCMC at $t = 10^{-6}$ s. The reactant CH_3OH is contracted to the superstates of intermediate CH_2OH+H. This means decomposition reaction takes longer than 10^{-6} s in this reaction route network. At this timescale, tiny component of CH_3OH is contracted to the superstates of hydrocarbons (CH and CH_2) and water, and it means these species are minor byproducts having small yields. These byproducts have possibilities to generate at the actual experiment under the other experimental conditions [9]. The fourth layer show the result of RCMC at $t = 10^{-9}$ s. The state of reactant CH_3OH, intermediate CH_2OH+H, HCO+3H and product CO+4H can be distinguished at this timescale. This means the most stable dissociation steps takes longer than 10^{-9} s.

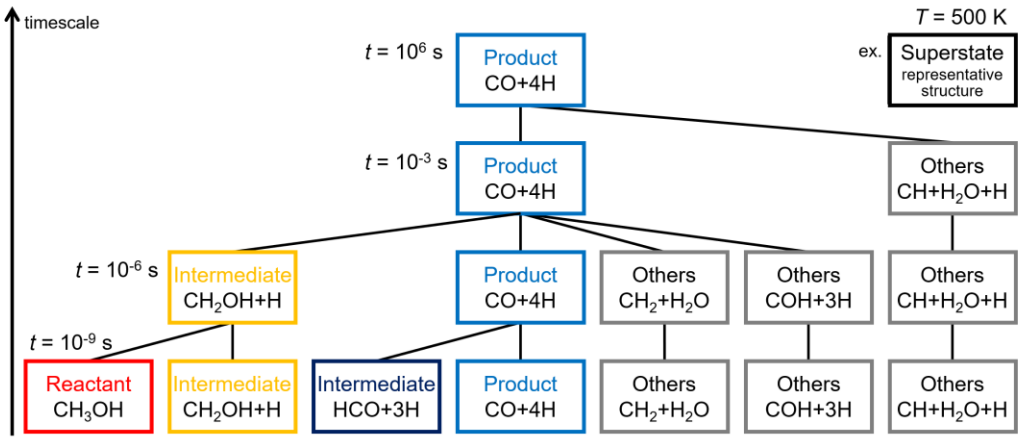

Figure 4-3. Time hierarchy diagram of methanol decomposition reaction on a Pt(111) surface. The vertical axis represents timescale when applying RCMC. The representative adsorption state of each superstate is given in each frame. The reaction temperature T was set to 500 K.

Figure 4-4 shows to which superstates each adsorption state belongs at each layer of Figure 4-3. For example, methoxy (CH_3O+H) belongs to the superstate which representative structure is CH_3OH at $t = 10^{-9}$ s. This means CH_3O+H can convert to CH_3OH within 10^{-9} s. The column "n_{str}" represents the number of corresponding MINs in the reaction route network. Each adsorption state has a lot of MINs having different relative positions of adsorbates. Note that not all considerable structures for each adsorption state were obtained because of using the kinetic-based navigation option.

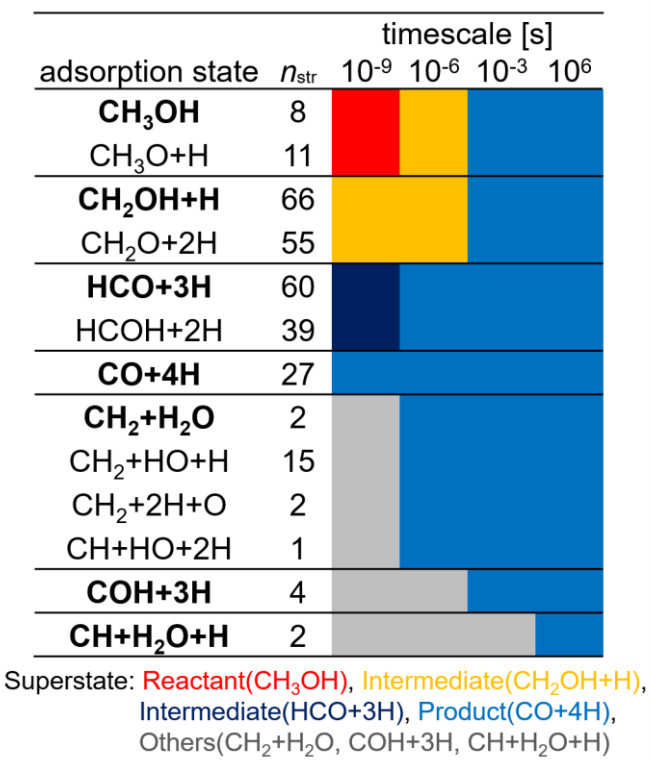

Figure 4-4. Superstates for each adsorption state at reaction temperature T = 500 K. "n_{str}" means the number of corresponding structures in the reaction route network. Color of cells corresponds to the superstate of reactant (red), product (blue), intermediate (orange or dark blue) and others (gray). The seven structures written in bold are representative adsorption states at timescale $t = 10^{-9}$ s (see the bottom layer of the hierarchy diagram of Figure 4-3).

4.3.3 Population change in adsorption states

The time evolution was investigated by using the kinetic simulation of the RCMC method where the initial population was set to CH_3OH in the reaction route network [29]. The population change of each adsorption state at T = 500 K was plotted in Figure 4-5. Sum of the population for all states is unity at each timescale. Figure 4-5(a) shows the population change of reactant CH_3OH (red), intermediate CH_2OH+H (orange) and main product CO+4H (blue). The population of CH_3OH is almost 1.0 at $t < 10^{-6}$ s, while CO+4H becomes main product at $t > 10^{-6}$ s. The population of intermediate CH_2OH+H is increased at $t = 10^{-6}$ s. From the result, it is clarified that

methanol decomposition reaction on a Pt(111) surface was occurred via CH_2OH+H and completed within ~10^{-5} s. The estimated overall reaction time from the reaction route network is 6.54×10^{-6} s. The value is slightly bigger than 3.98×10^{-8} s which was estimated by Kramer et al [20]. The slightly overestimation was thought to occur by overestimation of the barriers in the network. As shown in 4.3.4, the barriers are lowered if using the better calculation model like partially fixed three-layered model.

Figure 4-5(b) shows the population change of minor adsorption states having the maximum population over 10^{-4}. HCOH+2H (light blue) and HCO+3H (dark blue) are intermediate to form CO+4H. The population of these adsorption states are increased at $t = 10^{-6} \sim 10^{-5}$ s, but becomes not so high because these structures can convert to CO+4H within very short timescale. In addition, the yield of byproduct CH_2+H_2O (green) is also small. As described above, various elementary steps of the reaction were seen by kinetic analyses of the entire reaction route network.

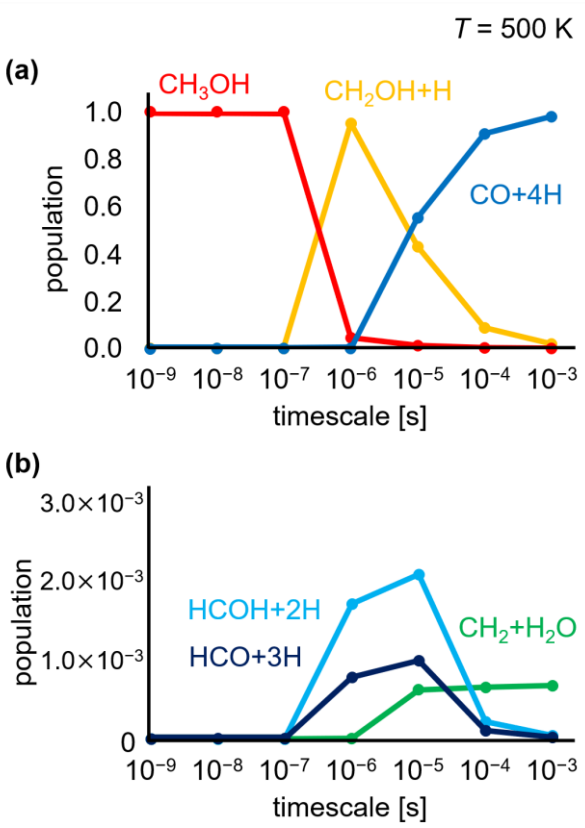

Figure 4-5. Population change at reaction temperature T = 500 K, (a) for reactant CH_3OH, main product CO+4H and intermediate CH_2OH+H, and (b) for minor adsorption states. The horizontal axis represents logarithm of timescale t when applying the RCMC method and the vertical axis corresponds to population of each adsorption state.

4.3.4 Detailed decomposition route of the methanol

To understand the detailed decomposition route, the energy profile for the most kinetically favorable path was extracted by following procedure. First, the RCMC method was recursively applied at $t = 10^{-3}$ s to $t = 10^{-13}$ s, and found important MINs as a representative structure of a superstate. The calculated MINs were connected to the minimum energy path by using the Dijkstra method. The obtained path $CH_3OH \rightarrow CH_2OH+H \rightarrow HCOH+2H \rightarrow HCO+3H \rightarrow CO+4H$ is consistent to the previous DFT calculation studies [17,22]. Then the MINs and TSs along the extracted path were further optimized with three-layered Pt(111) surface which the

bottom layer was kept fixed and the other two layers were relaxed. Monkhorst-Pack grid and mesh cut off were set to 2 × 2 × 1 and 100.0 Ry. The resultant energy profile was shown in Figure 4-6 and the reaction barriers were summarized in Table 4-1. Furthermore, the number of surface layers and their relaxations were discussed in Supplementary information S1 of ref. 26, and the structures along the path were summarized in S5 of ref. 26.

There are three possible paths for the first decomposition step of adsorbed methanol molecule: C-H dissociation ($CH_3OH \rightarrow CH_2OH+H$), O-H dissociation ($CH_3OH \rightarrow CH_3O+H$) and C-O dissociation ($CH_3OH \rightarrow CH_3+OH$). The most favorable path obtained from the network is C-H dissociation path which proceeds exothermically with the reaction barrier 58.4 kJ/mol. The other paths are not favorable (see Supplementary Information S2 of ref. 26). O-H dissociation step was also obtained with the reaction barrier 78.9 kJ/mol and exothermic process. C-O dissociation was not obtained during the search of this study focused on kinetically favorable paths because its reaction barrier was high (190.5 kJ/mol).

Table 4-1. Reaction barriers $\Delta\Delta E$ [kJ/mol] along the methanol decomposition route.

	$CH_3OH\rightarrow$ CH_2OH+H	$CH_2OH+H\rightarrow$ $HCOH+2H$	$HCOH+2H\rightarrow$ $HCO+3H$	$HCO+3H\rightarrow$ $CO+4H$
$\boldsymbol{\Delta\Delta E}$ [kJ/mol][a]	58.4	53.5	12.9	9.9
previous study[b]	59.8-74.3	56.9-60.8	14.5-52.1	22.2-34.7

[a] Values computed using the three-layered surface where the upper two layer were relaxed and the bottom layer was fixed.

[b] Corresponding values in the previous theoretical studies.[15,17,19,22]

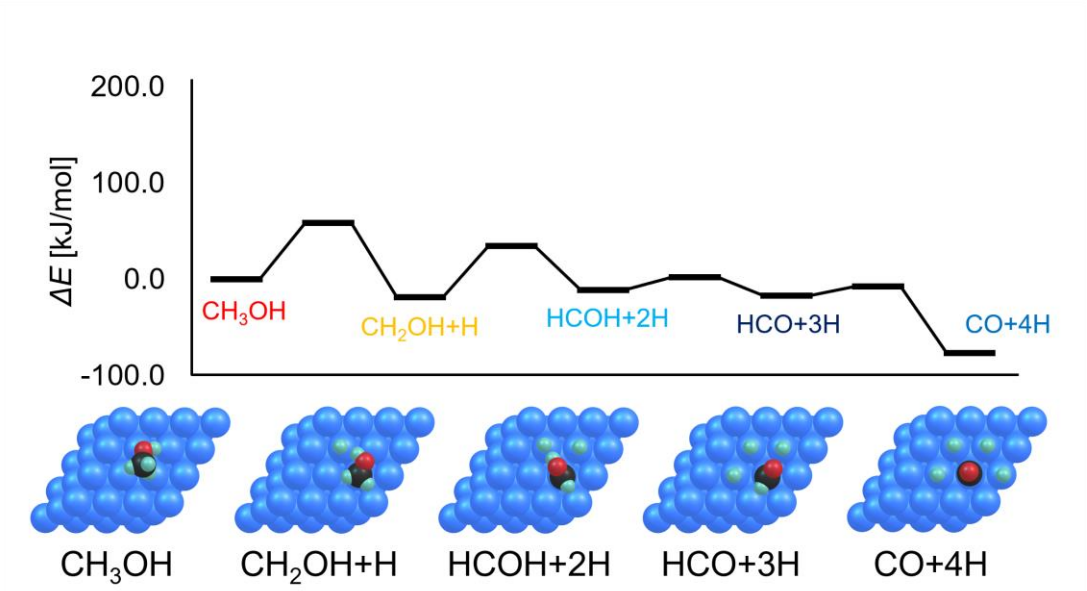

Figure 4-6. Energy profile of decomposition of methanol on a Pt(111) surface. The most kinetically favorable path is extracted from the network by the RCMC method and the Dijkstra algorithm. The energy values are electronic energies relative to the adsorbed CH_3OH. The structures shown at the bottom correspond to those further optimized using the partially fixed three-layer surface model. The reaction barrier for each step is summarized in Table 4-1. Color of the labels in the profile correspond to that of nodes in the network (see Figure 4-2(b)).

Furthermore, byproducts generation processes were also studied, i.e., $CH_2OH+H \rightarrow CH_2+H_2O$, $HCOH+2H \rightarrow CH+H_2O+H$, and $COH+3H \rightarrow CO+4H$. The energy profiles and the reaction barriers were shown in Figure 4-7 and Table 4-2. These paths were unfavorable compared to the main path although CH_2 and H_2O can be energetically generated at $T = 500$ K. $COH+3H \rightarrow CO+4H$ is also accessible but unfavorable compared to the main path. The structures along the paths were summarized in S5 and S6 of ref. 26.

Table 4-2. Reaction barriers $\Delta\Delta E$ [kJ/mol] of formation of byproducts.

	$CH_2OH+H\rightarrow$ CH_2+H_2O	$HCOH+2H\rightarrow$ $CH+H_2O+H$	$COH+3H\rightarrow$ $CO+4H$
$\boldsymbol{\Delta\Delta E}$ [kJ/mol][a]	88.9	124.3	79.7
previous study[b]			81.0-93.6

[a] Values computed using the three-layered surface where the upper two layer were relaxed and the bottom layer was fixed.

[b] Corresponding values in the previous theoretical studies.[15,17,19,22]

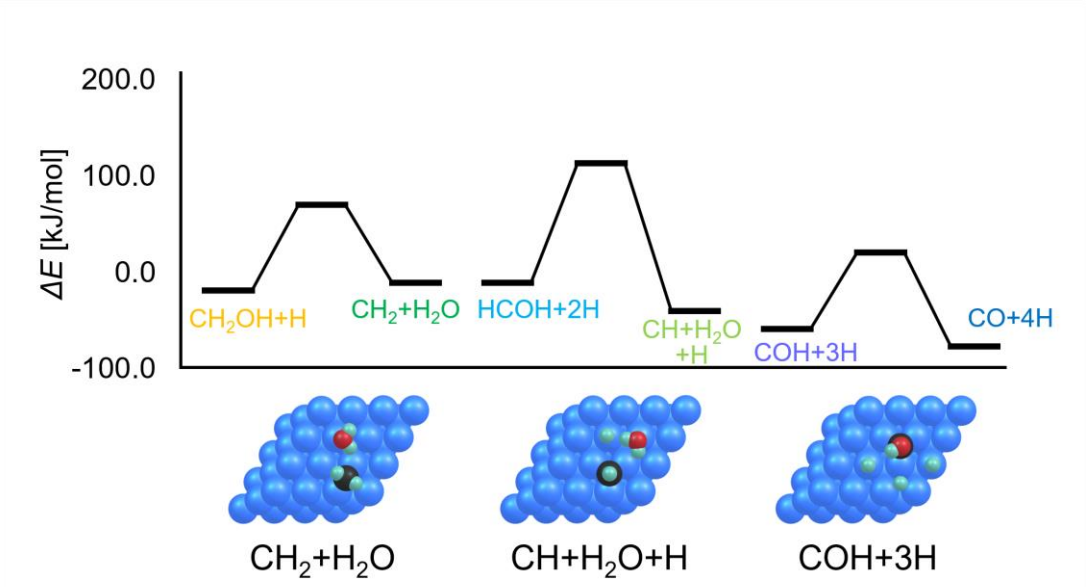

Figure 4-7. Energy profile of formation of byproducts on a Pt(111) surface. The energy values are electronic energy relative to the adsorbed CH_3OH. The structures shown at the bottom correspond to those further optimized using the partially fixed three-layer surface model. The reaction barrier for each step is summarized in Table 4-2. Color of the labels in the profile correspond to that of nodes in the network (see Figure 4-2 (b)).

4.4 Conclusion

In this study, a reaction route network for methanol decomposition reaction on a Pt(111) surface was created by reaction path search of the AFIR method. The time hierarchy of the reaction was elucidated from the kinetic analysis using the RCMC method at various timescale. Furthermore, the population change over 10^{-3} second was simulated. It was indicated that the path from reactant CH_3OH to carbon monoxides and four hydrogen atoms via intermediate CH_2OH+H is the most favorable. In addition, it was also clarified that the paths to generate byproducts like hydrocarbons and water can be ignored. We succeeded in explaining the reaction without any prior information about the products and reaction mechanism by the combined procedure of the AFIR method and the RCMC method.

References (Chapter 4)

[1] J. J. Spivey, *Catal. Today*, 2005, **100**, 171–180.

[2] Z. Bai, T. Liu, Q. Liu, J. Lei, L. Gong and H. Jin, *Energy Procedia*, 2017, **142**, 1582–1588.

[3] B. A. Sexton, *Surf. Sci.*, 1981, **102**, 271–281.

[4] S. Akhter and J. M. White, *Surf. Sci.*, 1986, **167**, 101–126.

[5] K. D. Gibson and L. H. Dubois, *Surf. Sci.*, 1990, **233**, 59–64.

[6] L. Diekhöner, D. A. Butler, A. Baurichter and A. C. Luntz, *Surf. Sci.*, 1998, **409**, 384–391.

[7] Z. Liu, T. Sawada, N. Takagi, K. Watanabe and Y. Matsumoto, *J. Chem. Phys.*, 2003, **119**, 4879–4886.

[8] S. Kandoi, J. Greely, M. A. Sanchez-Castillo, S. T. Evans, A. A. Gokhale, J. A. Dumesic and M. Mavrikakis, *Top. Catal.*, 2006, **37**, 17–28.

[9] A. V. Miller, V. V. Kaichev, I. P. Prosvirin and V. I. Bukhtiyarov, *J. Phys. Chem. C*, 2013, **117**, 8189–8197.

[10] V. V. Kaichev, I. P. Prosvirin and V. I. Buktiyarov, *Kinetics and Catalysis*, 2014, **55**, 509–519.

[11] A. S. Duke, R. P. Galhenage, S. A. Tenney, S. C. Ammal, A. Heyden, P. Sutter and A. Chen, *J. Phys. Chem. C*, 2015, **119**, 23082–23093.

[12] J. Kua, and W. A. Goddard III, *J. Am. Chem. Soc.*, 1999, **121**, 10928–10941.

[13] Y. Ishikawa, M.-S. Liao and C. R. Cabrera, *Surf. Sci.*, 2000, **463**, 66–80.

[14] J. R. B. Gomes and J. A. N. F. Gomes, *Electronanal. Chem.*, 2000, **483**, 180–187.

[15] J. Greely and M. Mavrikakis, *J. Am. Chem. Soc.*, 2002, **124**, 7193–7201.

[16] S. K. Desai, M. Neurock and K. Kourtakis, *J. Phys. Chem. B*, 2002, **106**, 2559–2568.

[17] J. Greely and M. Mavrikakis, *J. Am. Chem. Soc.*, 2004, **126**, 3910–3919.

[18] M. Neurock, M. Janik and A. Wieckowski, *Faraday Discuss.*, 2008, **140**, 363–378.

[19] Y. Chen and D. G. Vlachos, *Ind. Eng. Chem. Res.*, 2012, **51**, 12244–12252.

[20] Z. C. Kramer, X.-K. Gu, D. D. Y. Zhou, W.-X. Li and R. T. Skodje, *J. Phys. Chem. C*, 2014, **118**, 12364–12383.

[21] P. Du, P. Wu and C. Cai, *J. Phys. Chem. C*, 2017, **121**, 9348–9360.

[22] R. H. Wells, X.-K. Gu, W.-X. Li and R. T. Skodje, *J. Phys. Chem. C*, 2018, **122**, 28158–28172.

[23] L. Ou, *ACS Omega*, 2018, **3**, 886–897.

[24] T. L. M. Pham, D.-V. N. Vo, H. N. T. Nguen and N.-N. Phan-Tran, *Surf. Sci.*, 2019, **481**, 1327–1334.

[25] A. A. Gokhale, S. Kandoi, J. P. Greeley, M. Mavrikakis and J. A. Dumesic, *Chem. Eng. Sci.*, 2004, **59**, 4679–4691.

[26] K. Sugiyama, K. Saita and S. Maeda, *J. Comput. Chem.*, 2021, **42**, 2163–2169.

[27] S. Maeda, Y. Harabuchi, M. Takagi, K. Saita, K. Suzuki, T. Ichino, Y. Sumiya, K. Sugiyama and Y. Ono, *J. Comput. Chem.*, 2018, **39**, 233–250.

[28] Y. Sumiya, Y. Nagahata, T. Komatsuzaki, T. Taketsugu and S. Maeda, *J. Phys. Chem. A*, 2015,

119, 11641–11649.

[29] Y. Sumiya and S. Maeda, *Chem. Lett.*, 2020, **49**, 553–564.

[30] J. M. Soler, E. Artacho, J. D. Gale, A. García, J. Junquera, P. Ordejón and D. Sánchez-Portal, *J. Phys.: Condens. Matter*, 2002, **14**, 2745–2779.

[31] E. Artacho, J. M. Cela, J. D. Gale, A. García, J. Junquera, R. M. Martin, P. Ordejón, D. Sánchez-Portal and J. M. Soler, *SIESTA 4.0 (Revision 530)*, The Siesta Group, 2016, see http://www.uam.es/siesta

[32] Translation of Abinit's GGA Pseudo Database to Siesta Format: https://departments.icmab.es/leem/SIESTA_MATERIAL/Databases/Pseudopotentials/periodictable-gga-abinit.html

[33] M. Methfessel and A. T. Paxton, *Phys. Rev. B*, 1989, **40**, 3616–3621.

[34] C. Choi and R. Elber, *J. Chem. Phys.*, 1991, **94**, 751–760.

[35] P. Y. Ayala and H. B. Schlegel, *J. Chem. Phys.*, 1997, **107**, 375–384.

Chapter 5. Application to reaction on porous materials: propylene oxidation reaction with hydrogen peroxides on titanium silicalite-1

5.1 Introduction

Porous materials have holes of various sizes, and are widely used as heterogeneous catalysts because of large surface area and/or being selective reaction fields as the size of holes. Titanium silicalite-1 (TS-1) having MFI zeolite framework is one of useful catalysts industrially [1,2]. Especially, oxidation of olefins with hydrogen peroxides as oxidants have been studied both experimentally and theoretically [3-14].

TS-1 contains 2 ~ 3 wt% of Ti atoms in the unit cell [15]. Therefore, many experimental and theoretical studies investigated the detailed reaction mechanism on TS-1 having one Ti site. It is elucidated that a hydroperoxide reacts with the tetrahedral Ti site that one of the four sites was terminated by -OH to form η^2-(OOH) structure and catalyze epoxidation reaction [16-18]. On the other hand, the experimental result that selective propylene epoxidation was occurred at low temperature (0℃) was recently reported [19]. It is indicated from the measurement of ^{17}O-NMR that TS-1 in the study had a partial structure having two Ti sites, and reaction occurred at the sites. In addition, the proposed epoxidation mechanism by DFT calculation was showed: a catalytic cycle includes TS1-$(OOH)_2$ as a precursor of epoxidation where TS1-$(OOH)_2$ was generated from the TS-1 and two hydrogen peroxides. However, the detailed mechanisms and reaction barriers are still unclear. For the mechanism of catalytic reaction on oxide catalysts such as TS-1, it is required to consider the structural changes of the catalyst, i.e., reactions between lattice oxygen and reactants and/or generation of defected catalyst structures. Therefore, it is difficult to assume the complicated reaction mechanism.

As described in the previous sections, we enabled systematic reaction path search by the artificial force induced reaction (AFIR) method [20] for surface reactions, a kind of heterogeneous

reactions, without any prior knowledge of the reaction mechanism [21-23]. The search of the AFIR method can treat structural changes of catalysts by relaxing and considering both atoms in reactants and atoms in catalysts as “target atoms”. Thus, in this study, the search using the AFIR method was applied to epoxidation reaction of propylene on TS-1 having two adjacent Ti sites with hydrogen peroxides. Then the resultant reaction networks were kinetically analyzed by applying the rate constant matrix contraction (RCMC) method [24,25] to extract favorable paths and/or paths to byproducts.

5.2 Method

5.2.1 Preparation of TS-1 cluster model

In this study, two types of TS-1 catalyst model structures, i.e., periodic PBC model and non-periodic cluster model, were used. The created two TS-1 models are shown in Figure 5-1. First, a zeolite structure which has MFI framework was obtained from the database [26]. Next, two adjacent Si sites, T7 and T11 site were substituted into Ti atoms to get TS-1 unit cell. Then all atoms in the unit cell was optimized. In this calculation, potential energies and gradients were calculated by using VASP 5.4.4 software [27-29]. The functional is RPBE and Grimme’s dispersion D3 is considered. The k-point sampling was set to 2 × 2 × 2, and all translational vectors were fixed. The created TS-1 PBC model is represented in Figure 5-1(a).

The TS-1 PBC model is the system including 288 atoms ($Ti_2Si_{94}O_{192}$). It takes too long time to search by the AFIR method using such a large system. So, a smaller and non-periodic TS-1 cluster model is prepared from TS-1 PBC model (Figure 5-1(b), (c)). Assuming that reaction occurs near Ti atoms, the TS-1 model structure can be considered the simplified model like Figure 5-1(b). The all ends of the extracted cluster are O atoms. Then the edges of the cluster were terminated by adding H atoms and optimized. In this step, energies and gradients were calculated

by B3LYP-D3/def2-SV(P) implemented in Gaussian16 [30]. The cluster atoms consisting of Ti, Si and O were fixed in the calculation. Finally, TS-1 cluster model containing 90 atoms ($Ti_2Si_{16}O_{48}$ with 24 terminating H atoms) was obtained (Figure 5-1(c)). Note that two Ti atoms, seven O atoms and six Ti atoms to the nearest to Ti were relaxed while the other atoms in TS-1 cluster were fixed in the subsequent calculations.

As explained below, the semiempirical GFN2-xTB [31] was used during the search to reduce computational costs. The important structures and paths were further optimized by using Gaussian16, In this calculation, more accurate DFT level like BP86 functional was applied with Grimme's dispersion function (D3) [32]. The Los Alamos LANL2DZ [33,34] effective core pseudopotentials were applied to titanium, and a basis set of 6-31G(d) was applied for others. Finally, the structures will be reoptimized by B3LYP-D3/def2-SV(P) to see the dependence of functionals.

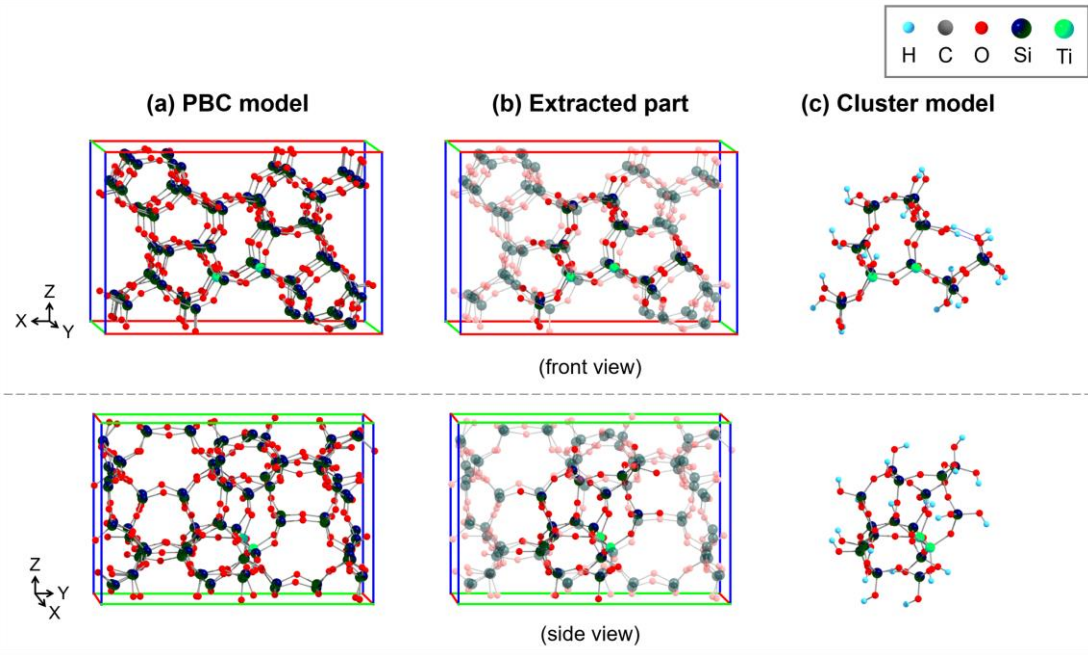

Figure 5-1. TS-1 model structures. (a) TS-1 PBC model. (b) The extracted part for TS-1 cluster model. Remaining transparent atoms were not used. (c) TS-1 cluster model.

5.2.2 Making reaction route networks using TS-1 cluster model

Reaction route networks for epoxidation reaction of propylene on TS-1 with H_2O_2 were created by using almost same procedure as surface reactions described above, especially for the case of methanol decomposition reaction on a Pt(111) surface (see 4.2.3). However, the reaction paths were searched step-by-step because it was thought that the reaction is a multi-step reaction and the reaction mechanism is very complicated. The considering steps were summarized in Table 5-1. First, the reactions between the original TS-1 catalyst (represented as TS1-O) and reactants were considered by (1) TS1-O+H_2O_2, (2) TS1-O+H_2O, (3) TS1-O+propylene, (4) TS1-O+2H_2O_2, and (5) TS1-O+H_2O_2+H_2O. Then epoxidation steps from various precursors were searched by (6) TS1-(OOH)(OH)+propylene, (7) TS1-O_2-OH+propylene, (8) TS1-O_2+propylene, and (9) TS1-O+H_2O+propylene. These precursors were mainly selected from the result of (1) TS1-O+H_2O_2. The search of (10) TS1-$(OH)_2$+H_2O_2 targeted to find regeneration path of the catalyst structure toward the next epoxidation steps. Finally, the paths proposed by the previous study [19] were considered by (11) TS1-O_2+H_2O_2 and (12) TS1-$(OOH)_2$+propylene.

Table 5-1. Initial structures and the number of obtained nodes/edges.

	Initial structure	nodes	edges
(1)	TS1-O+H_2O_2	617	1944
(2)	TS1-O+H_2O	176	758
(3)	TS1-O+propylene	175	247
(4)	TS1-O+2H_2O_2	2868	4901
(5)	TS1-O+H_2O_2+H_2O	1669	3064
(6)	TS1-(OOH)(OH)+propylene	1942	4410
(7)	TS1-O_2-OH+propylene	1775	4191
(8)	TS1-O_2+propylene	610	1375
(9)	TS1-O_2+H_2O+propylene	2422	4959
(10)	TS1-$(OH)_2$+H_2O_2	1990	3739
(11)	TS1-O_2+H_2O_2	1346	2652
(12)	TS1-$(OOH)_2$+propylene	1385	2373

Each reaction path search was done by using the SC-AFIR method [20] implemented in the developer version of GRRM program which is almost same as GRRM20. The model collision parameter γ of the AFIR function was set to γ = 300.0 kJ/mol. Target atoms generating the fragment pairs during the search are atoms in reactants, two Ti atoms, and O atoms next to Ti. In addition, to prevent adsorbates go away from the center of the catalyst, weak biases γ_{add} was applied by the AFIR function between reactants, two Ti atoms, and O atoms next to Ti, where sum of the biases were set to 100.0 kJ/mol. The kinetics-based navigation option, which ranks MINs based on their kinetic importance and avoids to search from those of low rank, was used [25]. The obtained force-induced paths (AFIR paths) were minimized by using the locally updated plane (LUP) method [35,36]. The energies and gradients were calculated by GFN2-xTB implemented in xTB6.4.0 program [31].

5.2.3 Kinetic analysis

Each reaction route network obtained by the search is very complicated because of including hundreds of thousands of structures and connecting paths. To extract the kinetically important bottleneck paths, the RCMC method [24,25] was used as the same procedure as described in 4.2.4. Note that a reaction barrier $\Delta\Delta E$ by an electronic energy was used to calculate the rate constant (see 4.2.4 in details). The extracted structures and paths will be further optimized using more accurate DFT levels as explained in 5.2.1.

5.3 Results and Discussion

As explained above, the reaction mechanism of propylene epoxidation by TS-1 with H_2O_2 were discussed from the twelve reaction route networks. First, the result of (1) TS1-O+H_2O_2 is shown in the section 5.3.1. The other results of the searches were summarized in Supporting information

(see the section 5.5). A reaction network, population change to the reaction timescales, and kinetically favorable paths are represented. Then the overview of the reaction mechanism was discussed in 5.3.2. As a result, four types of epoxidation steps via the different TS-1 precursor structures, were found and included in the mechanism. By comparing energy profiles, the most kinetically favorable epoxidation path was determined. In the following sections, the energy values are the relative electronic energies ΔE compared to the energy of the "total system" E_{tot}, estimated by Eq (1).

$$E_{tot} = E(\text{TS1-O}) + 2 \times E(H_2O_2) + E(H_2O) + E(\text{propylene}) \quad (1)$$

E(X) corresponds to the electronic energy of X in gas phase.

5.3.1 Reaction path search of (1) TS1-O+H_2O_2

In this section, reaction of the original TS-1 catalyst (TS1-O) and one H_2O_2 molecule were systematically searched. The search was started from TS1-O+H_2O_2, and 617 MINs and 3058 LUP paths were obtained. Figure 5-2 shows the obtained reaction route network consists of 617 nodes and 1944 edges (loop paths and multiple edges connecting the same node pair were omitted). Colors of nodes and edges represents the relative electronic energies of corresponding structures in Figure 5-2(a) while color of nodes represent a type of the structure in Figure 5-2(b). In addition to conformers of the reactant TS1-O+H_2O_2 and the proposed intermediate TS1-O_2+H_2O, various intermediate structures were found. Especially, TS1-(OOH)(O) and TS1-(OOH)(OH) were considered in previous studies at the process of regenerating the reaction precursor after epoxidation.

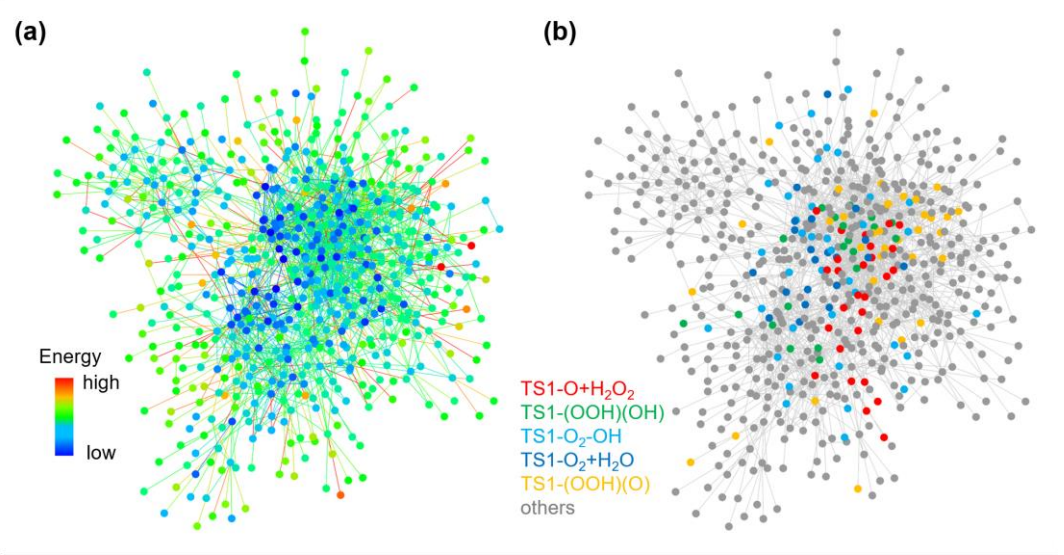

Figure 5-2. Reaction route network of (1) TS1-O+H_2O_2. Nodes and edges represent obtained MINs and paths connecting them, respectively. (a) Nodes and edges are colored based on their electronic energies. (b) Color of Nodes represents types of structures.

Next, the time evolution of the reaction route network was simulated by using the RCMC method. The initial population was set to the most stable reactant TS1-O+H_2O_2 (MIN121). The reaction temperature was set to T = 273.15 K referring to the experimental conditions. The resultant plots were summarized in Figure 5-3. Figure 5-3(a) shows the population change of kinetically major species. The reactant TS1-O+H_2O_2 is immediately consumed to form TS1-(OOH)(OH) at $t = 10^{-7}$ s. Then the population of TS1-O_2-OH is increased and that of TS1-(OOH)(OH) is decreased at $t = 10^{-6}$ s. TS1-O_2-OH is finally converted to TS1-O_2+H_2O at $t = 10^{-7}$ s. According to the previous study, TS1-O_2+H_2O is the resting state structure which is identified by ^{17}O NMR spectroscopy [19]. Figure 5-3(b) shows the population change of TS1-(OOH)(O) and minor species having the maximum population over 10^{-3}.

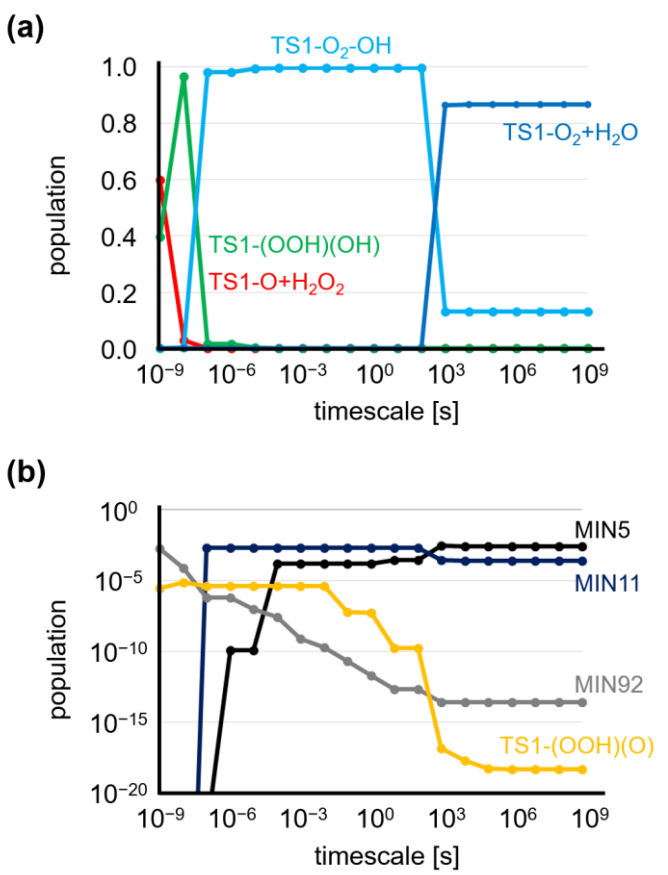

Figure 5-3. Population change of (1) TS1-O+H_2O_2 at T = 273.15 K. (a) for kinetically important structures, and (b) for TS1-(OOH)(O) and other minor structures having maximum population over 10^{-3}. The horizontal axis represents logarithm of timescale t when applying the RCMC method and the vertical axis corresponds to population of each structure type.

In addition, the most kinetically favorable path from reactant TS1-O+H_2O_2 was extracted. The RCMC method was recursively applied to the network at $t = 1.8 \times 10^{-6}$ s ~ 1.8×10^{4} s. The obtained energy profile was represented in Figure 5-4. TS1-O_2+H_2O is generated following to dissociative adsorption of H_2O_2 to form TS1-(OOH)(OH). Furthermore, it was indicated that TS1-O_2-OH is a resting state of the reaction. This is also understandable in Figure 5-3(a) that TS1-O_2-OH becomes major species at $t = 10^{-7} \sim 10^{2}$ s.

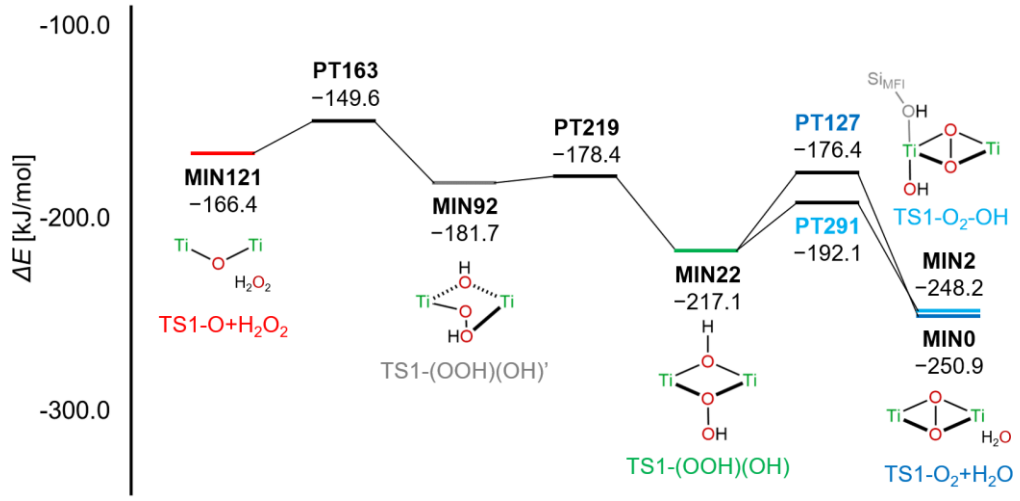

Figure 5-4. Energy profile of (1) TS1-O+H_2O_2. The kinetically most favorable route was extracted by applying the RCMC method to the network (see the text). The vertical axis shows the relative electronic energy refer to E_{tot}.

5.3.2 The most kinetically favorable epoxidation path

The same analyses as in (1) TS1-O+H_2O_2 were performed for all the other searches and summarized. The overview of the entire reaction mechanism was shown in Figure 5-5, and corresponding energy profiles were represented in Figure 5-6. Four types of epoxidation steps were found from the twelve networks. Each step has the different TS-1 precursor structures: (a) TS1-(OOH)(OH), (b) TS1-O_2-OH, (c) TS1-O_2, and (d) TS1-$(OOH)_2$. Note that the energy of the structure and path tops in Figure 5-6 were extracted from the most stable structure among the structures having same bond patterns, and the elementary step which has the lowest path top energy. In other words, energies in Figure 5-6 are not always same as the energy profile (most kinetically favorable route) for each reaction route network.

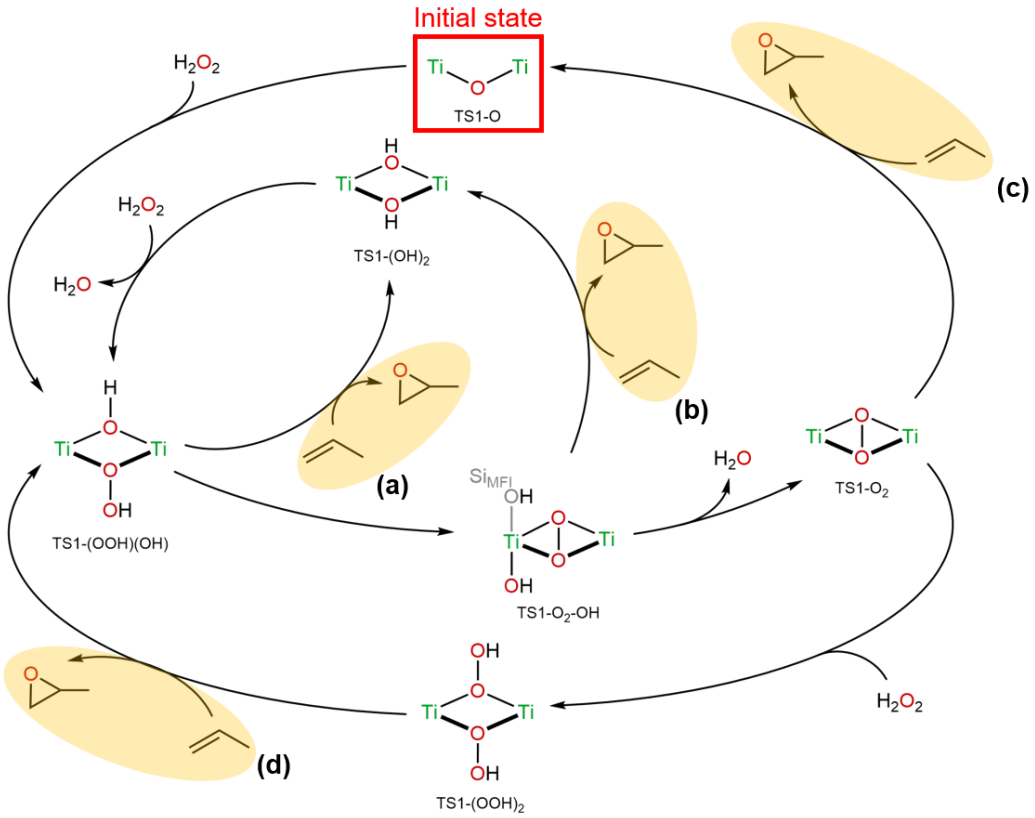

Figure 5-5. Overview of the reaction mechanism from the reaction path searches. “Initial state” means the starting structure of the cycle. The four types of epoxidation steps, (a), (b), (c) and (d), were colored.

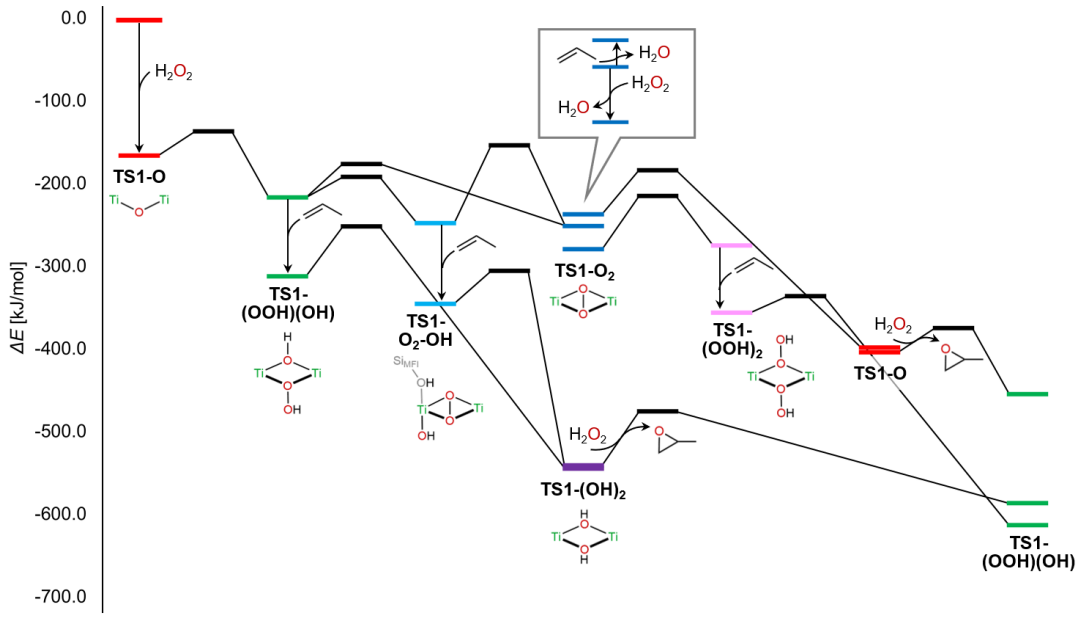

Figure 5-6. Energy profiles corresponding to the mechanism shown in Figure 5-5. The vertical axis shows the relative electronic energy refer to E_{tot}. Color of the states corresponds to the kind of TS-1 catalyst structure. The highest energy point of the elementary step (path top) was used instead of the transition state.

Comparing the four epoxidation routes, the most kinetically favorable epoxidation path was elucidated. Figure 5-7 shows each epoxidation path from the different TS-1 precursors. (a) via TS1-(OOH)(OH), (b) via TS1-O_2-OH and (c) via TS1-O_2 are intermediate of the reaction between TS1-O and one H_2O_2 molecule. (d) TS1-$(OOH)_2$ is referred as a precursor state in the previous study [19], and formed by TS1-O catalyst and two H_2O_2 molecules.

In the case of (a) via TS1-(OOH)(OH), the precursor was generated with the barrier 29.3 kJ/mol. Then epoxidation occurred with the barrier 60.5 kJ/mol, and TS1-$(OH)_2$ was formed. Finally, TS1-(OOH)(OH) was regenerated by the reaction between TS1-$(OH)_2$ and another H_2O_2 molecule. Assuming adsorption of propylene is barrierless or low barrier, this is the most favorable path. (b) via TS1-O_2-OH is similar to (a), only the difference is the precursor formation

step: TS1-(OOH)(OH) → TS1-O_2-OH. In the case of (c) via TS1-O_2, the precursor state TS1-O_2+H_2O was formed in the multistep reaction from TS1-O+H_2O_2. After H_2O desorption and propylene adsorption, epoxidation reaction proceeded to form the original catalyst structure TS1-O. The last step TS1-O+H_2O_2 → TS1-(OOH)(OH) is same as the first step. In the case of (d) via TS1-$(OOH)_2$, TS1-$(OOH)_2$ was endothermically generated from the reaction between TS1-O_2 and the second H_2O_2 molecule. Then epoxidation reaction TS1-$(OOH)_2$+propylene → TS1-(OOH)(OH)+epoxide occurred with the barrier 20.0 kJ/mol. The similar epoxidation reaction TS1-$(OOH)_2$+propylene → TS1-(OOH)(O)+epoxide was reported in the previous study [19] with the barrier 30.5 kJ/mol (7.3 kcal/mol), although the corresponding path was not obtained in this study. In summary, the most favorable precursor of the catalytic cycle is TS1-(OOH)(OH) because the structure prefer to occurring epoxidation reaction rather than forming TS1-O_2-OH, TS1-O_2, and TS1-$(OOH)_2$.

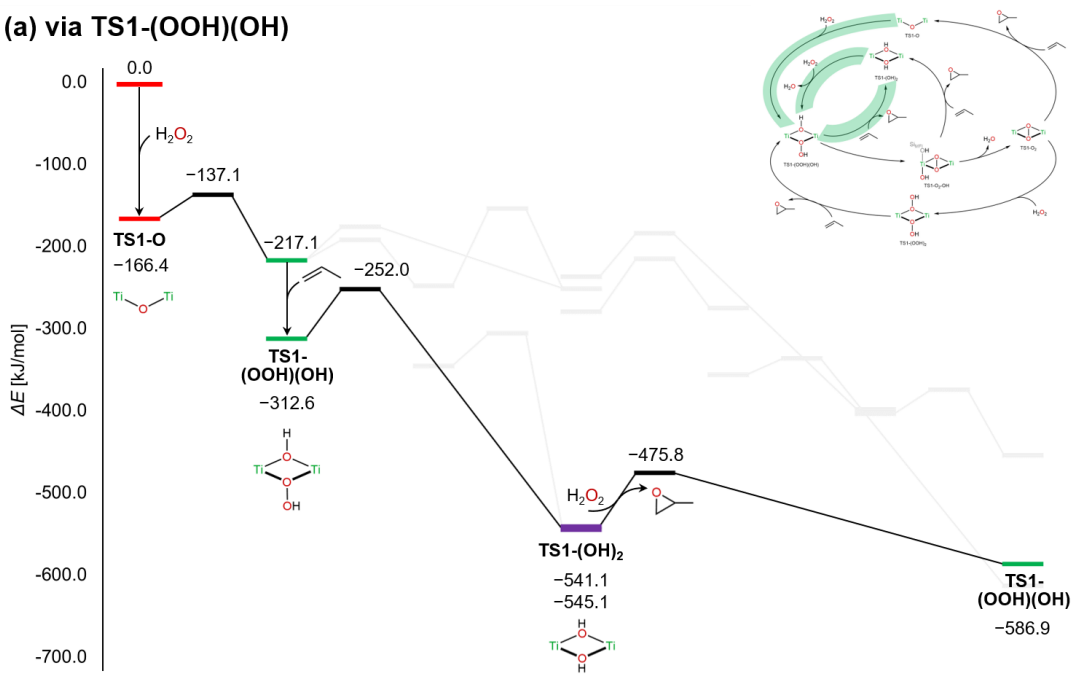
(a) via TS1-(OOH)(OH)
0.0
-100.0
-200.0
-300.0
-400.0
-500.0
-600.0
-700.0
ΔE [kJ/mol]
0.0
H2O2
−137.1
TS1-O
−166.4
−217.1
−252.0
TS1-(OOH)(OH)
−312.6
−475.8
H2O2
TS1-(OH)2
−541.1
−545.1
TS1-(OOH)(OH)
−586.9

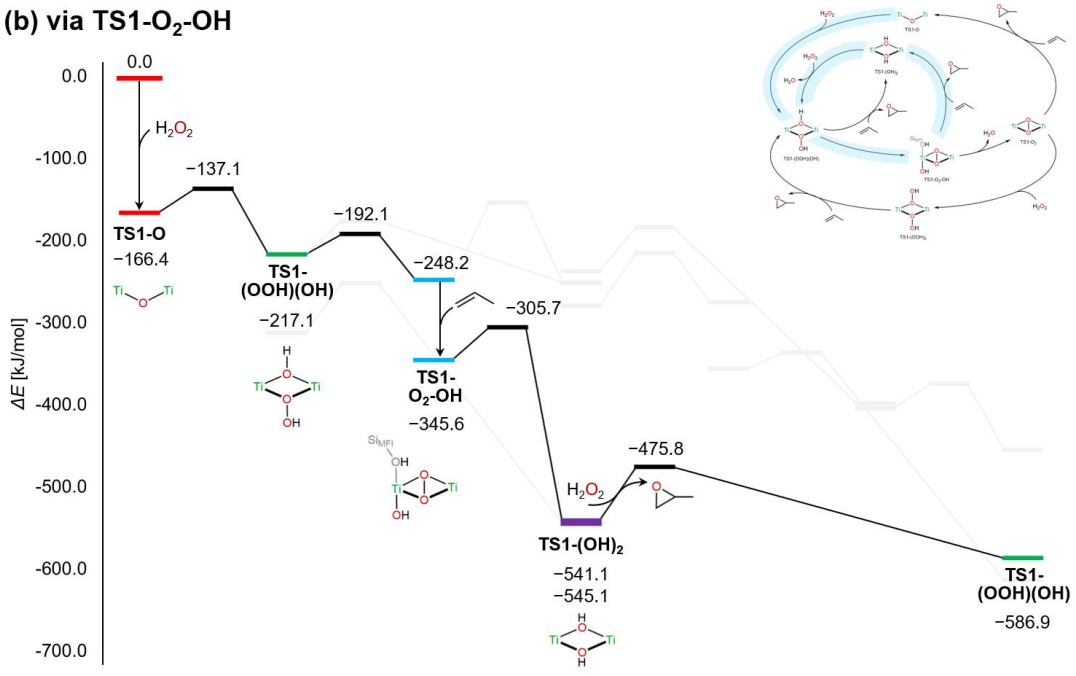
(b) via TS1-O2-OH
0.0
-100.0
-200.0
-300.0
-400.0
-500.0
-600.0
-700.0
ΔE [kJ/mol]
0.0
H2O2
−137.1
TS1-O
−166.4
−192.1
TS1-(OOH)(OH)
−217.1
−248.2
−305.7
TS1-O2-OH
−345.6
−475.8
H2O2
TS1-(OH)2
−541.1
−545.1
TS1-(OOH)(OH)
−586.9

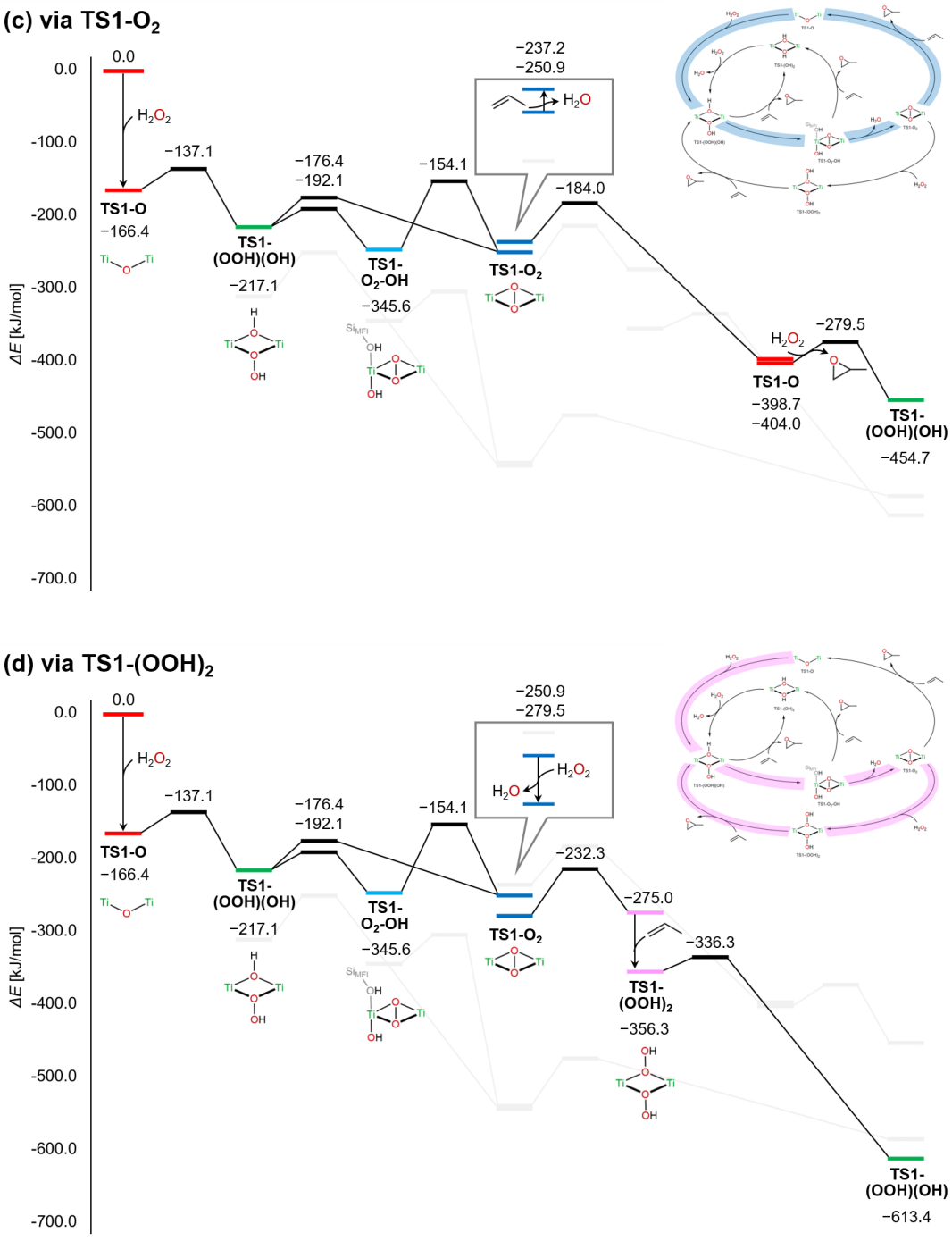

Figure 5-7. Energy profiles of four epoxidation paths. The vertical axis shows the relative electronic energy refer to E_{tot}. Color of the states corresponds to the kind of TS-1 catalyst structure. The highest energy point of the elementary step (path top) was used instead of the transition state. The upper right part shows epoxidation cycle of each path. (a) epoxidation path via TS1-(OOH)(OH). (b) epoxidation path via TS1-O_2-OH. (c) epoxidation path via TS1-O_2. (d) epoxidation path via TS1-$(OOH)_2$.

5.4 Conclusion

In this study, epoxidation reaction of propylene on TS-1 with H_2O_2 were studied by the combination of the reaction path search using the AFIR method and its kinetic analysis using the RCMC method. The searches were done by TS-1 cluster model and started from the multiple initial structures to consider multi-step reaction efficiently. Then the four types of epoxidation route were found in the networks. From the kinetic analyses, the new catalytic cycle involving TS1-(OOH)(OH) as the precursor of epoxidation was found while TS1-$(OOH)_2$ was proposed in the previous study. Furthermore, paths to generate byproducts and their kinetic contributions were investigated from the network targeting epoxidation steps. It was indicated that epoxidation proceeds selectively where byproducts formation paths were kinetically less favorable but most generated species were thermodynamically stable. To determine the mechanism, further consideration using DFT calculation is required.

The approach in this study can apply to any other reactions in porous materials or on surface oxides.

5.5 Supporting information: reaction route networks and kinetic analyses for the reaction of TS-1

In this section, the result of each reaction path search was summarized (see Table 5-1). See 5.3.1 for the result of (a) TS1-O+H_2O_2. A reaction route network with the number of obtained structures/paths (nodes/edges), population change of the network, and the most kinetically favorable path were represented. Here, the details of the kinetic analyses were described.

The time evolution of the reaction route network was simulated by using the RCMC method. The initial population was set to the most stable reactant in the network. The reaction temperature was set to T = 273.15 K referring to the experimental conditions [19]. To see the

population change with regards to the reaction timescale, kinetically major and/or minor species were elucidated.

In addition, the most kinetically favorable path from the most stable reactant was extracted. The RCMC method was recursively applied to the network at $t = 1.8 \times 10^{-6}$ s ~ 1.8×10^{4} s refer to the reaction condition of five hours. The reaction temperature was set to $T = 273.15$ K referring to the experimental conditions. The obtained energies are summarized as the energy profile by using the relative electronic energy ΔE with respect to E_{tot} of Eq. (1).

5.5.1 Reaction path search of (2) TS1-O+H_2O

In the previous experiment, H_2O_2 was introduced to the reactor as 30-wt% aqueous solution [19]. Thus, reaction of the original TS-1 catalyst (TS1-O) and one H_2O molecule were also searched. The search was started from TS1-O+H_2O, and 176 MINs and 1510 LUP paths were obtained. Figure S1-1 shows the obtained reaction route network consists of 176 nodes and 758 edges (loop paths and multiple edges connecting the same node pair were omitted). By comparing Figure S1 (a) and (b), the energies of reactant TS1-O+H_2O and intermediate TS1-$(OH)_2$ are lower than the other structures.

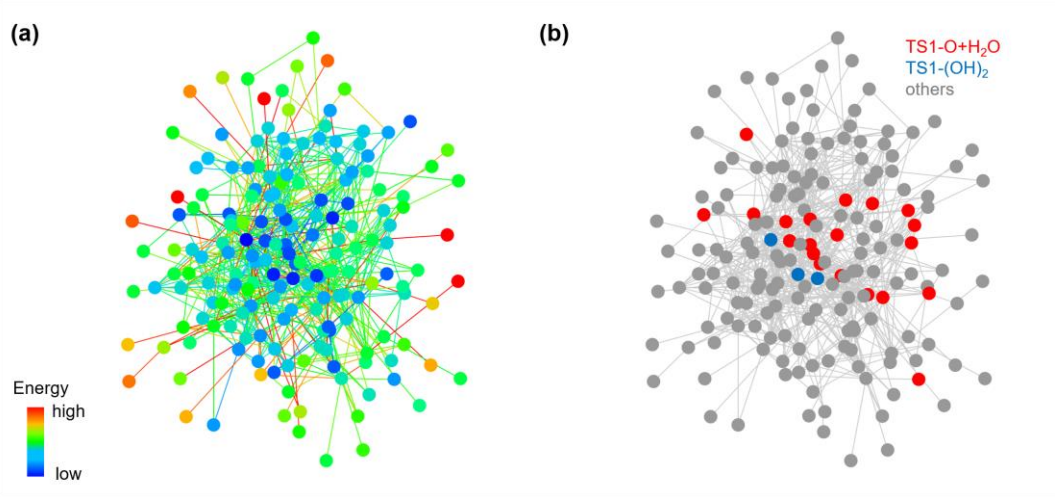

Figure S1. Reaction route network of (2) TS1-O+H_2O. Nodes and edges represent obtained MINs and paths connecting them, respectively. (a) Nodes and edges are colored based on their electronic energies. (b) Color of Nodes represents types of structures.

Next, the time evolution of the reaction route network from TS1-O+H_2O (MIN4) was simulated. Figure S2 shows the population change of kinetically major species having the maximum population over 10^{-1}. Then the population of TS1-$(OH)_2$ is increased and that of TS1-O+H_2O is decreased at $t = 10^{-4}$ s ~ 10^{-3} s. Therefore, TS1-O and H_2O is reacted at this timescale. Considering that the reaction between TS1-O and H_2O_2 is started from $t = 10^{-7}$ s (see Figure 5-3 (a)), the reaction of TS1-O and H_2O is considered to be less kinetically favorable than that of TS1-O and H_2O_2.

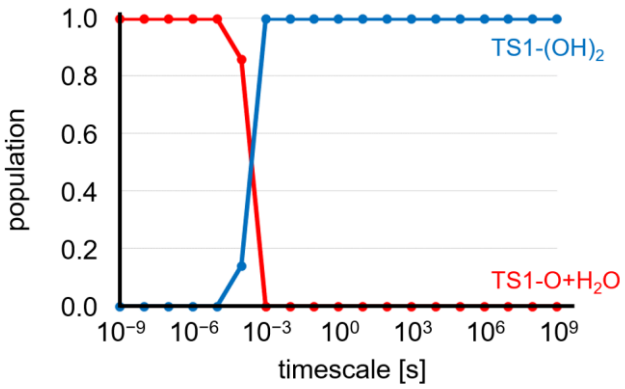

Figure S2. Population change of (2) TS1-O+H_2O at T = 273.15 K. Kinetically important structures having maximum population over 10^{-1} were shown. The horizontal axis represents logarithm of timescale t when applying the RCMC method and the vertical axis corresponds to population of each structure type.

In addition, the most kinetically favorable path from the reactant TS1-O+H_2O was shown in Figure S3. H_2O reacts with TS1-O to form intermediate TS1-$(OH)_2$ by a similar mechanism to TS1-O+H_2O_2 → TS1-(OOH)(OH).

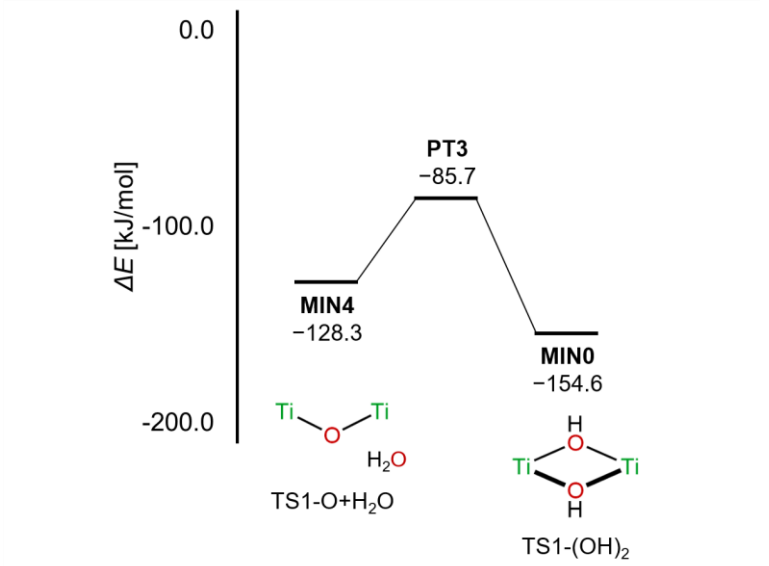

Figure S3. Energy profile of (2) TS1-O+H_2O. The kinetically most favorable route was extracted by applying the RCMC method to the network. The vertical axis shows the relative electronic energy refer to E_{tot}.

5.5.2 Reaction path search of (3) TS1-O+propylene

In this section, reaction of the original TS-1 catalyst (TS1-O) and one propylene molecule were systematically searched to elucidate the precursor structure of TS-1 catalyst for epoxidation reaction. The search was started from TS1-O+propylene, and 175 MINs and 1002 LUP paths were obtained. Figure S4 shows the obtained reaction route network consists of 175 nodes and 247 edges (loop paths and multiple edges connecting the same node pair were omitted). By comparing Figure S4 (a) and (b), the energies of reactant TS1-O+propylene is lower than the other structures. The conformer of TS1-O+propylene is the most stable structure in the network.

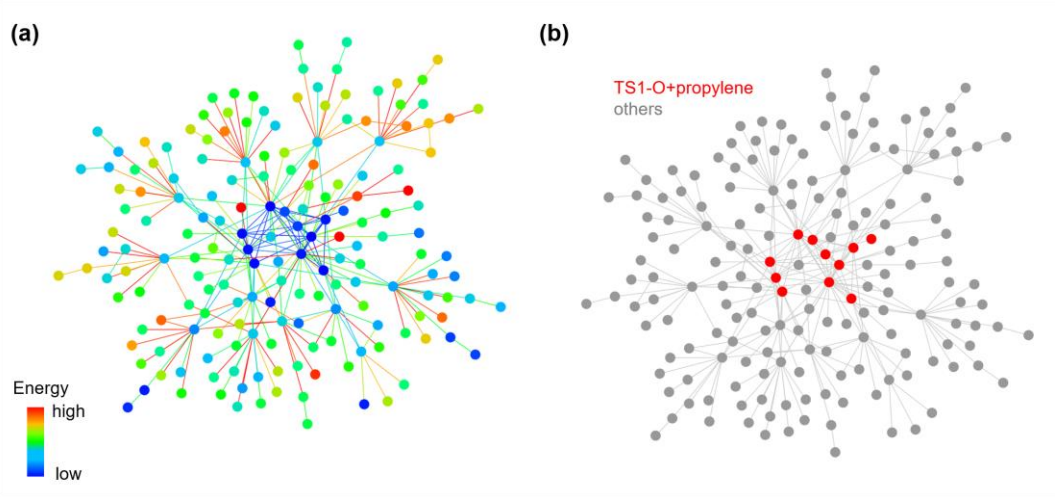

Figure S4. Reaction route network of (3) TS1-O+propylene. Nodes and edges represent obtained MINs and paths connecting them, respectively. (a) Nodes and edges are colored based on their electronic energies. (b) Color of Nodes represents types of structures.

Next, the time evolution of the reaction route network from the most stable reactant TS1-O+propylene (MIN0) was simulated. Figure S5 shows the population change of the reactant TS1-O+propylene. No reaction is occurred because the population of TS1-O+propylene is almost 1.0 at the all timescales. The population of other structures were less than 10^{-10}. From the result, TS1-O is not a precursor of epoxidation reaction.

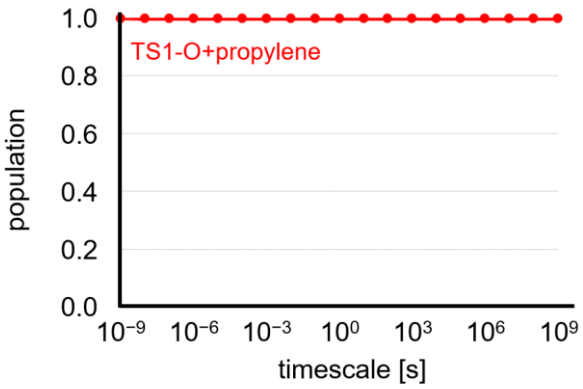

Figure S5. Population change of (3) TS1-O+propylene at T = 273.15 K. The horizontal axis represents logarithm of timescale t when applying the RCMC method and the vertical axis corresponds to population of each structure type.

5.5.3 Reaction path search of (4) TS1-O+2H_2O_2

According to the previous study, the precursor of epoxidation reaction is TS1-$(OOH)_2$ which is generated by TS-1 catalyst and two H_2O_2 molecules [19]. Therefore, reaction of the original TS-1 catalyst (TS1-O) and two H_2O_2 molecules were systematically searched. The search was started from TS1-O+2H_2O_2, and 2868 MINs and 5306 LUP paths were obtained. Figure S6 shows the obtained reaction route network consists of 2868 nodes and 4901 edges (loop paths and multiple edges connecting the same node pair were omitted). The obtained network includes not only the structures that is formed by the reaction of TS1-O and one H_2O_2 but also the mentioned structure TS1-$(OOH)_2$+H_2O.

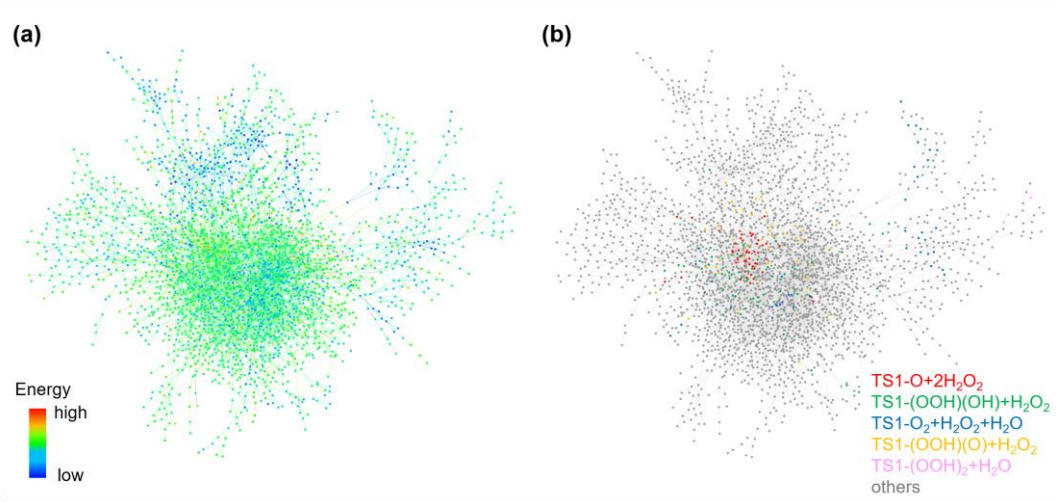

Figure S6. Reaction route network of (4) TS1-O+2H_2O_2. Nodes and edges represent obtained MINs and paths connecting them, respectively. (a) Nodes and edges are colored based on their electronic energies. (b) Color of Nodes represents types of structures.

Next, the time evolution of the reaction route network from the most stable reactant TS1-O+2H_2O_2 (MIN1203) was simulated. Figure S7(a) shows the population change of kinetically major species having the maximum population over 10^{-1}. First, two H_2O_2 molecules are subsequently reacted with TS1-O to form MIN114 (TS1-(OOH)(OH)-OOH) within 10^{-5} seconds. Then the population of MIN5 (TS1-(OOOH)(OH)+H_2O) is increased at $t = 10^0$ s ~ 10^2 s. Finally, the population of MIN5 is decreased and that of MIN2 (TS1-(O_3)(OH)+H_2O) is increased at $t = 10^2$ s ~ 10^3 s. On the other hand, Figure S7(b) shows the population change of TS1-(OOH)(O)+H_2O_2, TS1-(OOH)(OH)+ H_2O_2, TS1-O_2+H_2O_2+H_2O, and TS1-$(OOH)_2$+H_2O. As the case of (1) TS1-O+H_2O_2, the population of TS1-(OOH)(OH)+H_2O_2 is increased from $t = 10^{-8}$ s, and that of TS1-O_2+H_2O_2+H_2O is increased at $t > 10^{-8}$ s. However, the population of these structures are relatively small at each timescale. Besides, it is indicated that the reaction path to TS1-$(OOH)_2$+H_2O is considered to be less favorable kinetically because of small population.

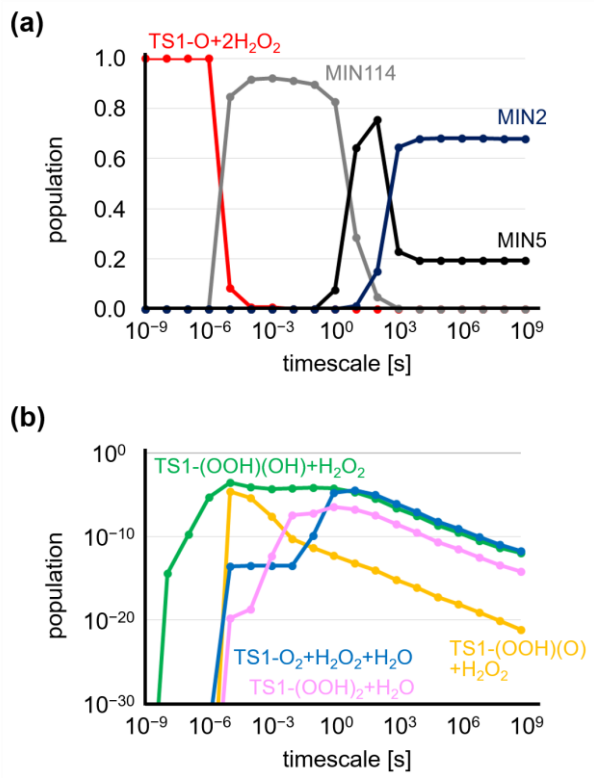

Figure S7. Population change of (4) TS1-O+2H_2O_2 at T = 273.15 K. (a) for kinetically important structures, and (b) for some minor structures. The horizontal axis represents logarithm of timescale t when applying the RCMC method and the vertical axis corresponds to population of each structure type.

In addition, the most kinetically favorable path from reactant TS1-O+2H_2O_2 was shown in Figure S8. Two H_2O_2 molecules are reacted and MIN2 is generated in multistep reaction. The passing structures are different from the case of one H_2O_2 molecule depicted in Figure 5-4.

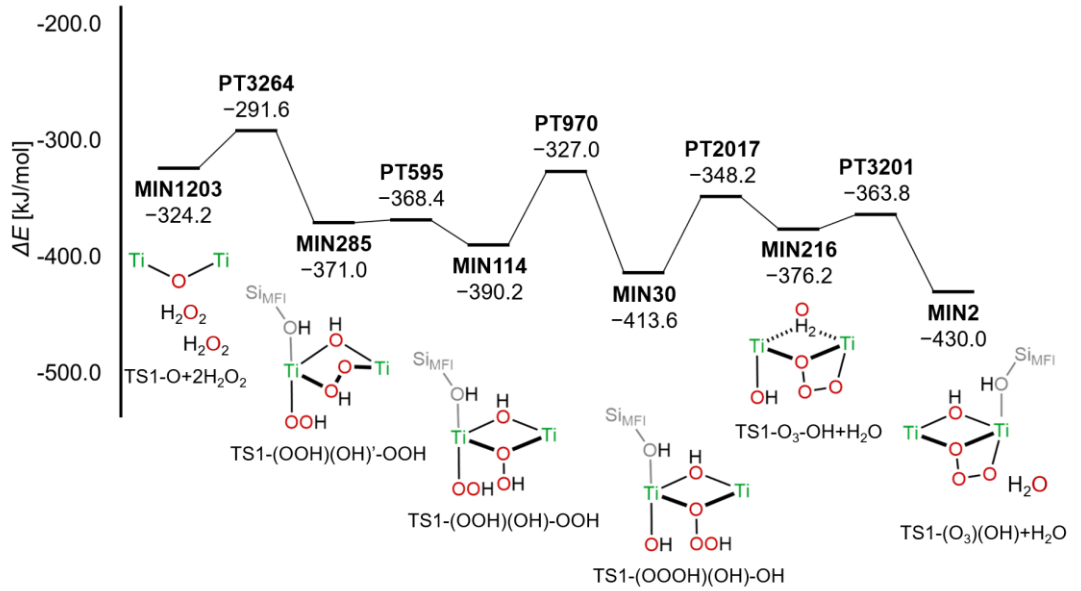

Figure S8. Energy profile of (4) TS1-O+2H_2O_2. The kinetically most favorable route was extracted by applying the RCMC method to the network. The vertical axis shows the relative electronic energy refer to E_{tot}.

5.5.4 Reaction path search of (5) TS1-O+H_2O_2+H_2O

As explained in the section 5.5.1, H_2O as well as H_2O_2 has possibility to react with TS1-O. In this section, reaction of the original TS-1 catalyst (TS1-O), one H_2O_2 molecule and one H_2O molecule were searched. The search was started from TS1-O+H_2O_2+H_2O, and 1669 MINs and 3543 LUP paths were obtained. Figure S9 shows the obtained reaction route network consists of 1669 nodes and 3064 edges (loop paths and multiple edges connecting the same node pair were omitted). Various structures in which only H_2O_2 reacted with TS1-O, only H_2O reacted with TS1-O, and both reacted were obtained.

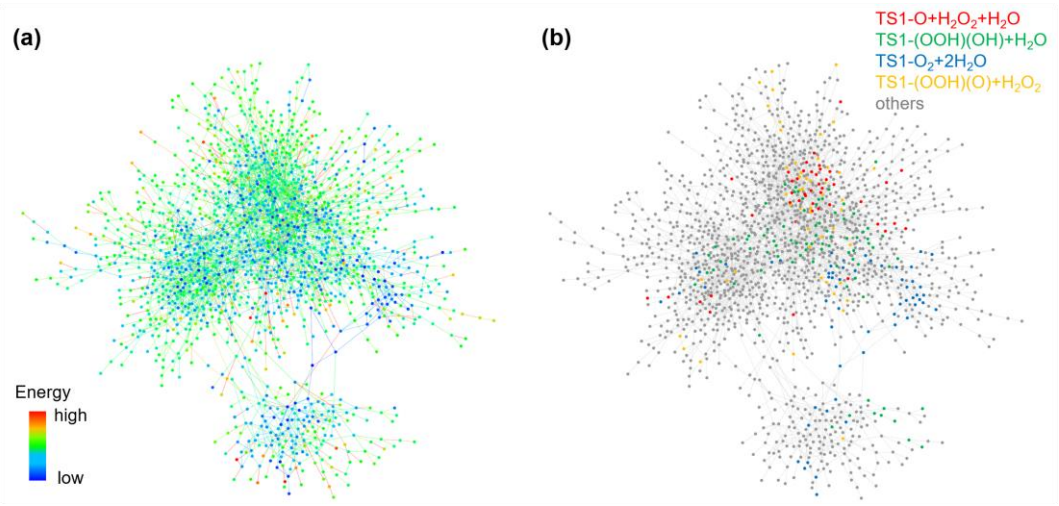

Figure S9. Reaction route network of (5) TS1-O+H_2O_2+H_2O. Nodes and edges represent obtained MINs and paths connecting them, respectively. (a) Nodes and edges are colored based on their electronic energies. (b) Color of Nodes represents types of structures.

Next, the time evolution of the reaction route network from the most stable reactant TS1-O+H_2O_2+H_2O (MIN489) was simulated. Figure S10(a) shows the population change of kinetically major species. At $t = 10^{-8}$ s ~ 10^{-6} s, the population of the reactant TS1-O+H_2O_2+H_2O is decreased and that of TS1-(OOH)(OH)+H_2O is increased. Then MIN0 (TS1-O_2-OH+H_2O) is formed at $t > 10^{-1}$ s. This is consistent to the result of (1) TS1-O+H_2O_2. In addition, Figure S10(b) shows the population change of TS1-(OOH)(O)+H_2O, TS1-O_2+2H_2O and minor species having the maximum population over 10^{-2}. The population of TS1-O_2+2H_2O, corresponding to TS1-O_2+H_2O of (1) TS1-O+H_2O_2, is still small at $t = 10^{9}$ s. From the results, H_2O_2 is considered to be more reactive than H_2O because MIN0, which has the maximum population at $t = 10^{9}$ s, is the structure with unreacted water.

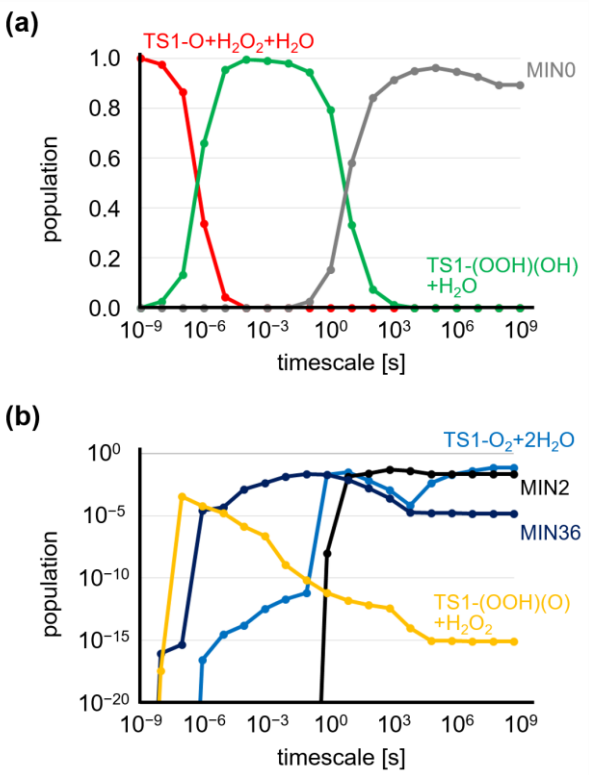

Figure S10. Population change of (5) TS1-O+H_2O_2+H_2O at T = 273.15 K. (a) for kinetically important structures, and (b) for TS1-(OOH)(O)+H_2O, TS1-O_2+2H_2O and minor structures having maximum population over 10^{-2}. The horizontal axis represents logarithm of timescale t when applying the RCMC method and the vertical axis corresponds to population of each structure type.

In addition, the most kinetically favorable path from reactant TS1-O+H_2O_2+H_2O was shown in Figure S11. Only H_2O_2 reacts with TS1-O and TS1-O_2-OH+H_2O is generated via multistep reactions similar to (1) TS1-O+H_2O_2 shown in Figure 5-4.

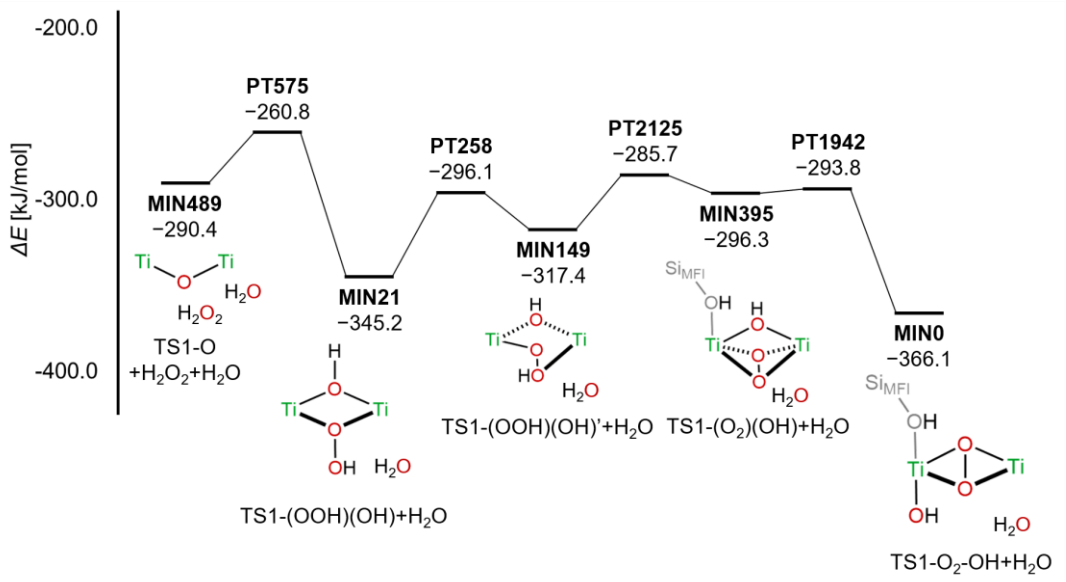

Figure S11. Energy profile of (5) TS1-O+H_2O_2+H_2O. The kinetically most favorable route was extracted by applying the RCMC method to the network. The vertical axis shows the relative electronic energy refer to E_{tot}.

5.5.5 Reaction path search of (6) TS1-(OOH)(OH)+propylene

According to Figure 5-3(a), TS1-(OOH)(OH) was formed from TS1-O+H_2O_2 within the short timescale. Thus, epoxidation path from TS1-(OOH)(OH) were systematically searched. The search was started from TS1-(OOH)(OH)+propylene, and 1942 MINs and 6330 LUP paths were obtained. Figure S12 shows the obtained reaction route network consists of 1942 nodes and 4410 edges (loop paths and multiple edges connecting the same node pair were omitted). Comparing Figure S12 (a) and (b), it is indicated that the energies of product epoxide and others were lower than those of reactant propylene. The network includes not only reactants and main products (epoxide) but also various intermediates and byproducts.

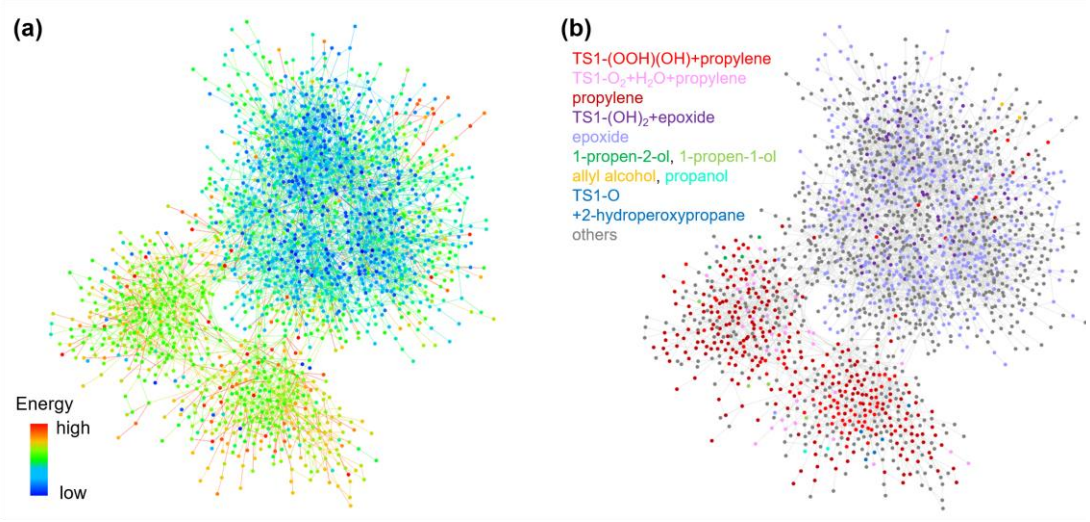

Figure S12. Reaction route network of (6) TS1-(OOH)(OH)+propylene. Nodes and edges represent obtained MINs and paths connecting them, respectively. (a) Nodes and edges are colored based on their electronic energies. (b) Color of Nodes represents types of structures. "epoxide" includes TS1-(OH)(O)+epoxide and TS1-O+H_2O+epoxide. "allyl alcohol" includes TS1-(OH)(O)+allyl alcohol and TS1-O+H_2O+allyl alcohol. "propylene" includes TS1-O+H_2O_2+propylene, and TS1-(OOH)(O)+propylene, TS1-O_2-OH+propylene, and TS1-(O_2)(OH)+propylene. "1-propen-2-ol" includes TS1-(OH)(O)+1-propen-2-ol and TS1-O+H_2O+1-propen-2-ol. "1-propen-1-ol" includes TS1-$(OH)_2$+1-propen-1-ol and TS1-(OH)(O)+ 1-propen-1-ol.

Next, the time evolution of the reaction route network from the most stable reactant TS1-(OOH)(OH)+propylene (MIN1274) was simulated. Figure S13(a) shows the population change of kinetically major species having the maximum population over 10^{-1}. In Figure S13(a), TS1-(OOH)(OH) likely to change into the other TS-1 catalyst structures such as TS1-O_2+H_2O. Then the population of the main product TS1-$(OH)_2$+epoxide was increased at $t \geq 10^2$ s. Figure S13(b) shows the population change of other byproducts. Note that epoxide, allyl alcohol, propylene, 1-propen-2-ol, 1-propen-1-ol means the sum of the population for the structures containing the corresponding product. The population of these byproducts is very small.

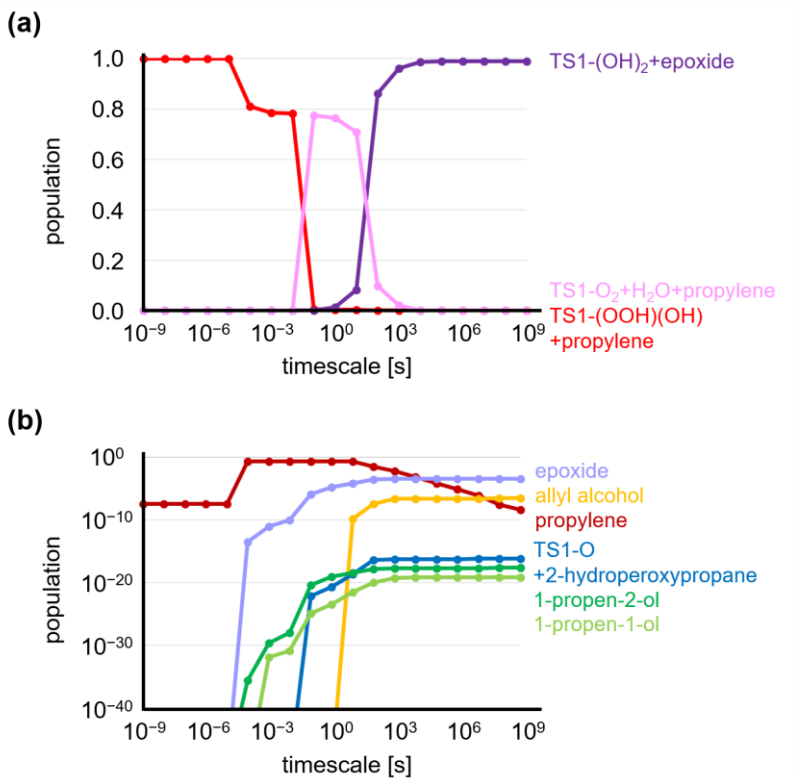

Figure S13. Population change of (6) TS1-(OOH)(OH)+propylene at T = 273.15 K. (a) for kinetically important structures, and (b) for some minor structures. The horizontal axis represents logarithm of timescale t when applying the RCMC method and the vertical axis corresponds to population of each structure type. The meanings of structural labels were same as that of Figure S12(b), and the sum of corresponding structures was plotted.

In addition, the most kinetically favorable path from reactant TS1-(OOH)(OH)+propylene was shown in Figure S14. The epoxidation step is TS1-O_2+H_2O+propylene → TS1-O+H_2O+epoxide with the barrier of 69.4 kJ/mol, while the energy barrier of the direct epoxidation step (TS1-(OOH)(OH)+propylene → TS1-$(OH)_2$+epoxide) is 60.6 kJ/mol (Figure 5-7(a)). Further investigation is required to understand the difference of extracted paths.

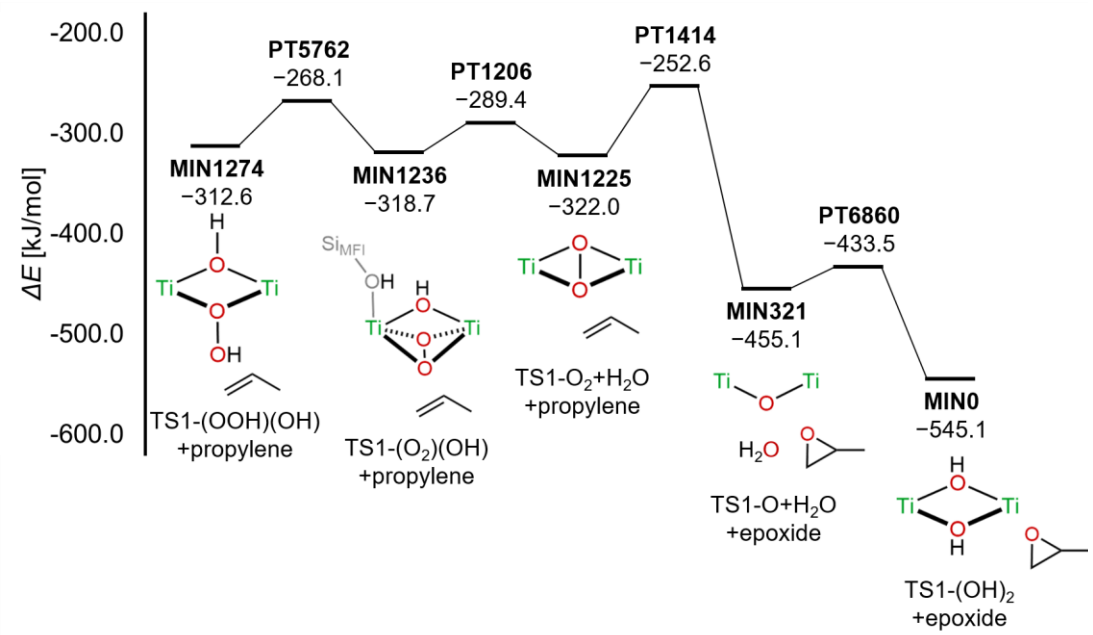

Figure S14. Energy profile of (6) TS1-(OOH)(OH)+propylene. The kinetically most favorable route was extracted by applying the RCMC method to the network. The vertical axis shows the relative electronic energy refer to E_{tot}.

The network includes various byproducts as well as main product TS1-$(OH)_2$+epoxide The reaction mechanism of these products is summarized in Figure S15. The shortest path to each byproduct is calculated by applying the Dijkstra method from the reactant TS1-(OOH)(OH)+propylene to each byproduct. Then these paths were grouped based on the passing structures. It is shown that 1-propen-1-ol, 2-hydroperoxypropane, allyl alcohol, and propanol are favored to generate from the reaction of TS1-(OOH)(OH), whereas 1-propen-2-ol and epoxide are favored to generate from the other TS-1 precursor structures.

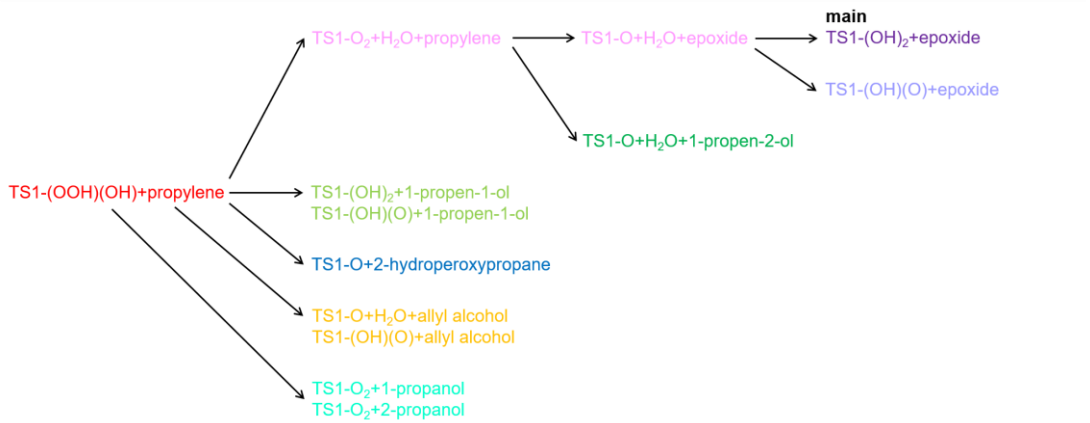

Figure S15. Products and byproducts of (6) TS1-(OOH)(OH)+propylene. Color of letters correspond to the color of nodes in Figure S12 and the color of datapoints in Figure S13.

5.5.6 Reaction path search of (7) TS1-O_2-OH+propylene

According to Figure 5-3(a) and 5-4, TS1-O_2-OH is a resting state of the reaction between TS1-O and H_2O_2. Thus, epoxidation path from TS1-O_2-OH were systematically searched. The search was started from TS1-O_2-OH+propylene, and 1775 MINs and 6246 LUP paths were obtained. Figure S16 shows the obtained reaction route network consists of 1775 nodes and 4191 edges (loop paths and multiple edges connecting the same node pair were omitted). Comparing Figure S16 (a) and (b), it is indicated that the energies of product epoxide and others were lower than those of reactant propylene. The network includes not only reactants and main products (epoxide) but also various intermediates and byproducts.

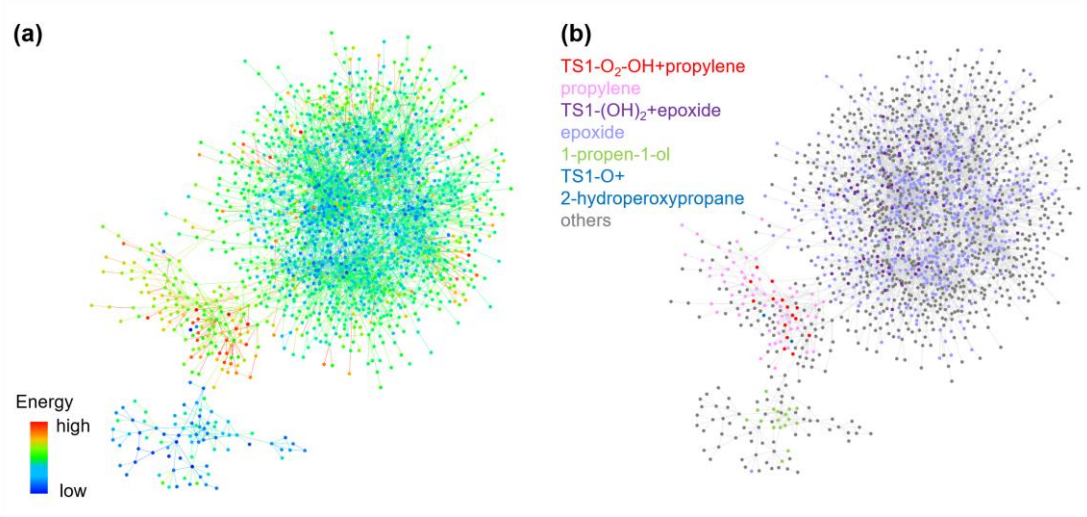

Figure S16. Reaction route network of (7) TS1-O_2-OH+propylene. Nodes and edges represent obtained MINs and paths connecting them, respectively. (a) Nodes and edges are colored based on their electronic energies. (b) Color of Nodes represents types of structures.

Next, the time evolution of the reaction route network from the most stable reactant TS1-O_2-OH+propylene (MIN1413) was simulated. Figure S17(a) shows the population change of kinetically major species having the maximum population over 10^{-1}. Selective reactions to TS1-$(OH)_2$+epoxide was proceeded. The population of other byproducts such as 1-propen-1-ol and 2-hydroperoxypropane were much smaller than that of main product TS1-$(OH)_2$+epoxide.

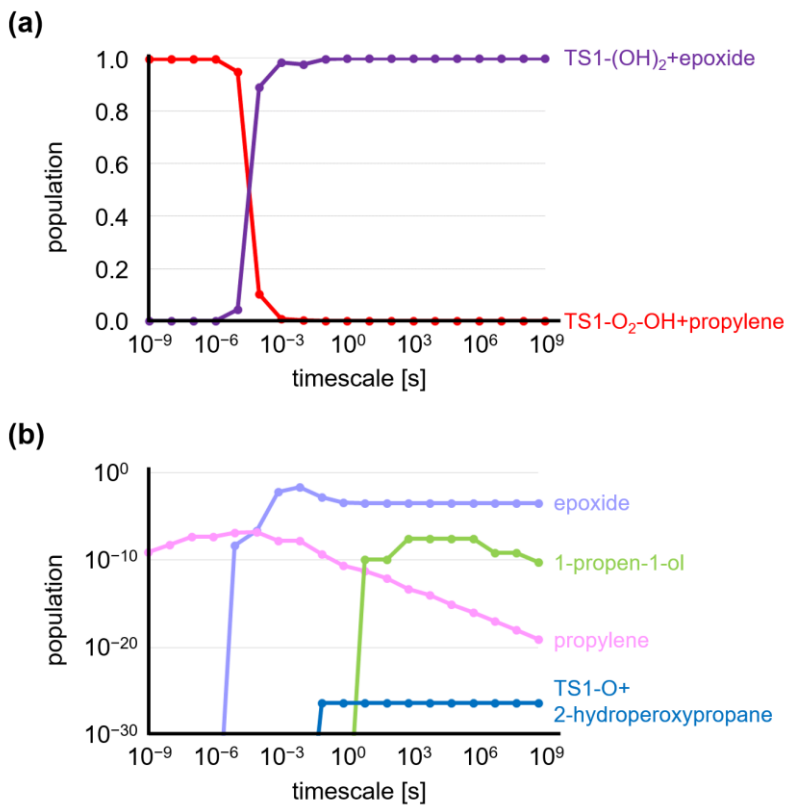

Figure S17. Population change of (7) TS1-O_2-OH+propylene at T = 273.15 K. (a) for kinetically important structures, and (b) for some minor structures. The horizontal axis represents logarithm of timescale t when applying the RCMC method and the vertical axis corresponds to population of each structure type. The meanings of structural labels were same as that of Figure S16(b), and the sum of corresponding structures was plotted.

In addition, the most kinetically favorable path from reactant TS1-O_2-OH+propylene was shown in Figure S18. The energy barrier of epoxidation step is 40.6 kJ/mol.

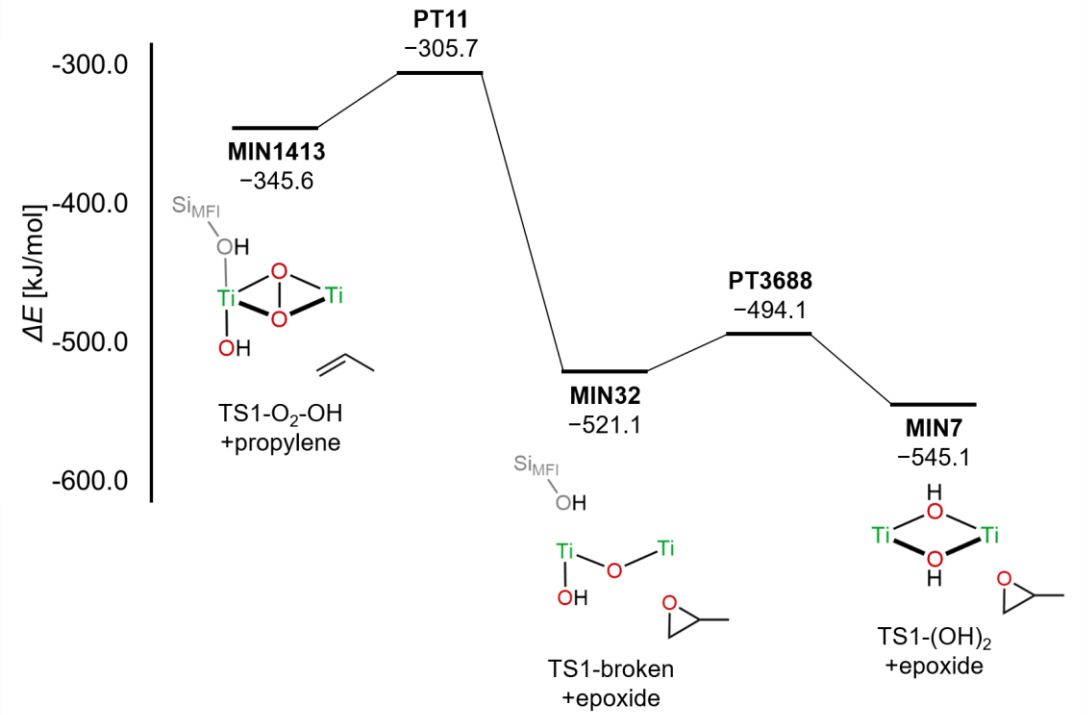

Figure S18. Energy profile of (7) TS1-O_2-OH+propylene. The kinetically most favorable route was extracted by applying the RCMC method to the network. The vertical axis shows the relative electronic energy refer to E_{tot}.

The network includes various byproducts as well as main product TS1-$(OH)_2$+epoxide The reaction mechanism of these products is summarized in Figure S1929. The shortest path to each byproduct is calculated by applying the Dijkstra method from the reactant TS1-(OOH)(OH)+propylene to each byproduct. Then these paths were grouped based on the passing structures. As seen in Figure S19, epoxide and 1-propen-1-ol can be directly formed.

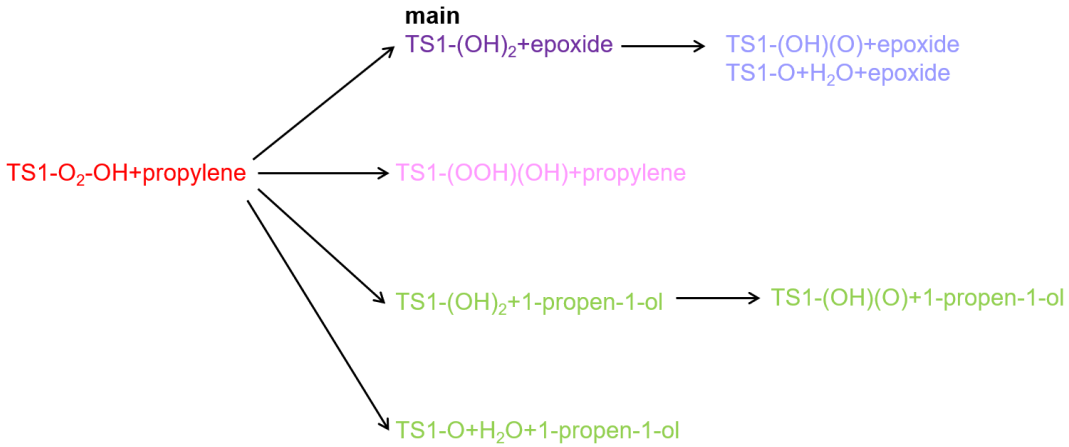

Figure S19. Products and byproducts of (7) TS1-O_2-OH+propylene. Color of letters correspond to the color of nodes in Figure S16 and the color of datapoints in Figure S17.

5.5.7 Reaction path search of (8) TS1-O_2+propylene

In this section, reaction of the intermediate TS1-O_2 and propylene molecule were searched. The initial structure was TS1-O_2+propylene, and 610 MINs and 3390 LUP paths were obtained. Figure S20 shows the obtained reaction route network consists of 610 nodes and 1375 edges (loop paths and multiple edges connecting the same node pair were omitted). As shown in Figure S20(b), the network includes TS1-O+epoxide. It is indicated that TS1-O_2 can be a precursor of epoxidation reaction. Furthermore, various byproducts were obtained: propylene epoxide, 1-propen-1-ol, 1-propen-2-ol, allyl alcohol, propionaldehyde (propanal), acetone, and acrolein. Note that acrolein is reported as a byproduct of epoxidation reaction of propylene by using Au-supported TS-1 catalyst with H_2O and O_2 in gas phase [37].

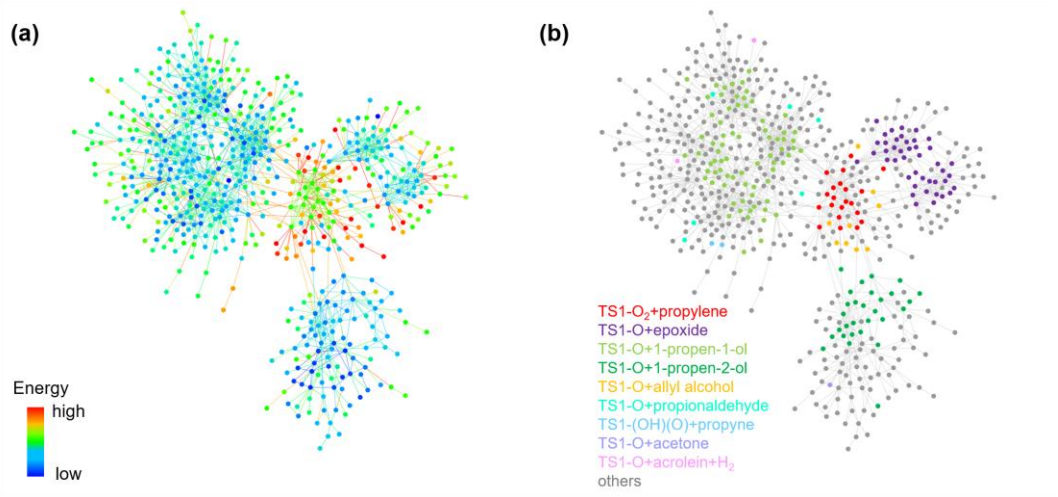

Figure S20. Reaction route network of (8) TS1-O_2+propylene. Nodes and edges represent obtained MINs and paths connecting them, respectively. (a) Nodes and edges are colored based on their electronic energies. (b) Color of Nodes represents types of structures.

Next, the time evolution of the reaction route network from the most stable reactant TS1-O_2+propylene (MIN464) was simulated by using the RCMC method. Figure S21(a) shows the population change of kinetically major species. The population of TS1-O_2+propylene is almost 1.0 at $t < 10^{-1}$ s, while that of TS1-O+epoxide becomes almost 1.0 at $t \geq 10^{-1}$ s. This means TS1-O+epoxide is main product, and the result is consistent to the previous study which showed the selective epoxidation reaction with the selectivity at most 96% [19]. Figure S21(b) shows the population change of other byproducts. The population of these byproducts is very small.

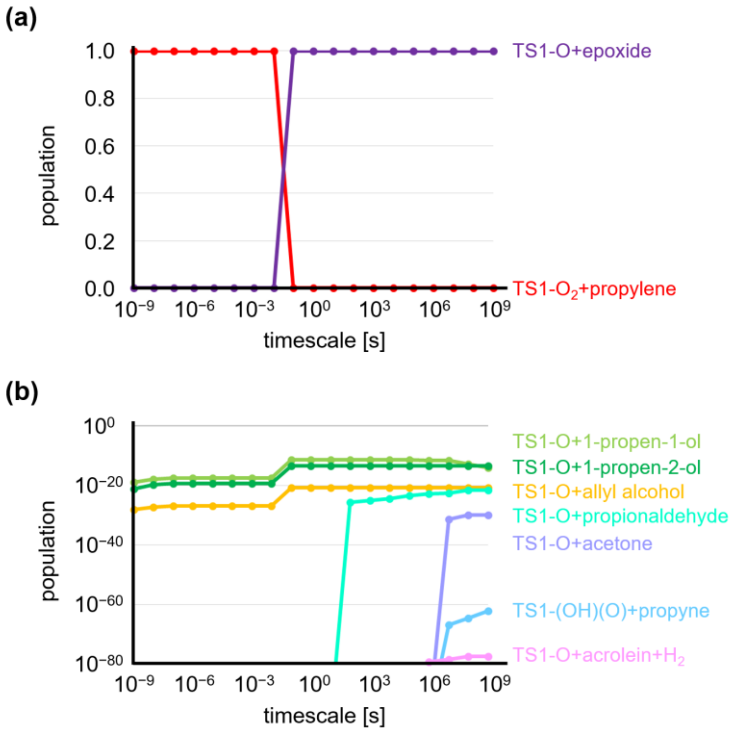

Figure S21. Population change of (8) TS1-O_2+propylene at T = 273.15 K. (a) for kinetically important structures, and (b) for minor byproducts. The horizontal axis represents logarithm of timescale t when applying the RCMC method and the vertical axis corresponds to population of each structure type.

In addition, the most kinetically favorable path from reactant TS1-O_2+propylene was shown in Figure S22. Propylene epoxide is directly generated from the reaction of TS1-O_2 and propylene. Thus, TS1-O_2 is a candidate of precursors of epoxidation reaction.

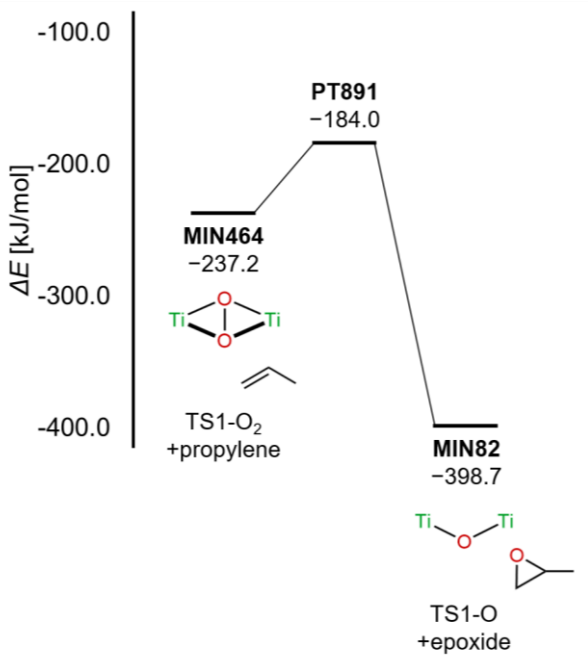

Figure S22. Energy profile of (8) TS1-O_2+propylene. The kinetically most favorable route was extracted by applying the RCMC method to the network. The vertical axis shows the relative electronic energy refer to E_{tot}.

The network includes various byproducts as well as main product TS1-O+epoxide The reaction mechanism of these products is summarized in Figure S23. The shortest path to each byproduct is calculated by applying the Dijkstra method from the reactant TS1-O_2+propylene to each byproduct. Then these paths were grouped based on the passing structures. For example, the shortest path to TS1-O+acetone goes through TS1-O+1-propen-2-ol. According to Figure S23, four products were directly formed: propylene epoxide, 1-propen-1-ol, 1-propen-2-ol, and allyl alcohol. The reaction barriers ($\Delta\Delta E$) and energies of these products (ΔE) were summarized in Table S1. The reaction barrier to TS1-O+epoxide is the lowest (53.2 kJ/mol). The other products are less kinetically favorable due to the reaction barriers while these byproducts are more thermodynamically stable than the reactant TS1-O_2+propylene (ΔE = −273.2 kJ/mol). Furthermore, the path top structures of corresponding LUP paths and product structures were

depicted in Figure S22. Although the structures are not actual but approximate transition states, there are differences to the reactive part of propylene molecule. O atom of TS1-O_2 reacts with double bond of the propylene for the case of epoxidation whereas with C atom of methylene group, middle C atom, and H atom of methyl group for the case of 1-propen-1-ol, 1-propen-2-ol, and allyl alcohol.

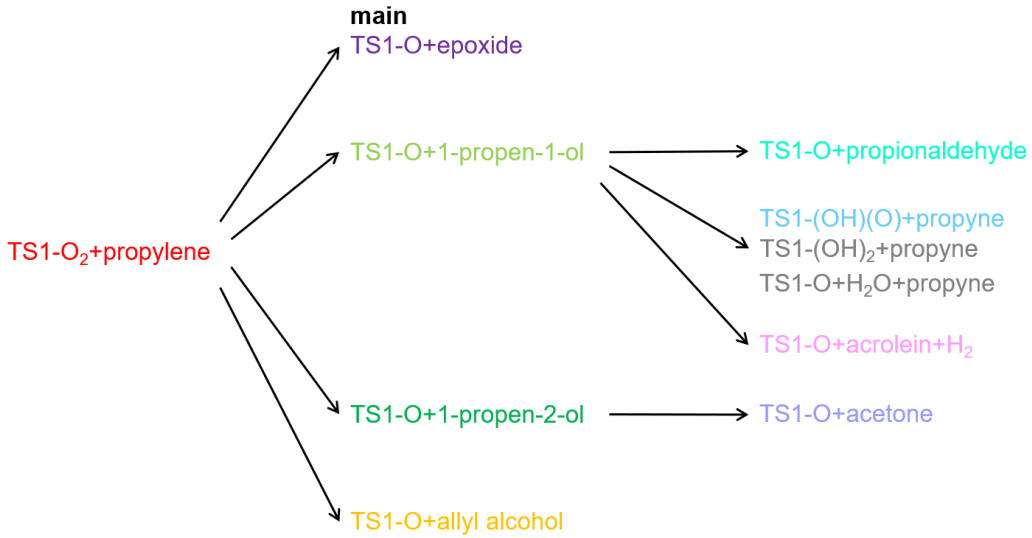

Figure S23. Products and byproducts of (8) TS1-O_2+propylene. Color of letters correspond to the color of nodes in Figure S20 and the color of datapoints in Figure S21.

Table S1 Reaction barriers from TS1-O_2+propylene

Product	$\Delta\Delta E$ [kJ/mol]	ΔE [kJ/mol]
TS1-O+epoxide	53.2	−398.7
TS1-O+1-propen-1-ol	112.8	−407.8
TS1-O+1-propen-2-ol	123.9	−418.7
TS1-O+allyl alcohol	170.8	−381.8

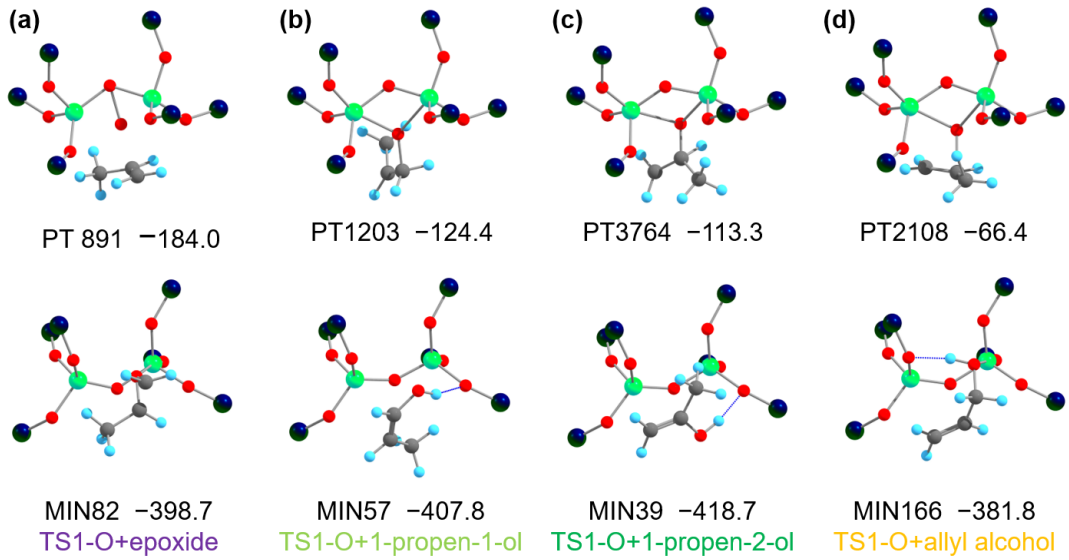

Figure S24. Path top and product structures from TS1-O_2+propylene to corresponding products. The vertical axis shows the relative electronic energy refer to E_{tot}. Only the atoms of reaction center were depicted.

5.5.8 Reaction path search of (9) TS1-O_2+H_2O+propylene

As discussed in 5.3.1, the intermediate TS1-O_2+H_2O was generated from the TS-1 catalyst and one H_2O_2 molecule. Therefore, reaction between the intermediate TS1-O_2+H_2O and propylene molecule were searched. The effect of generated water is considered in this section while the effect of the water is assumed to be ignored in the search of (8) TS1-O_2+propylene. The initial structure was TS1-O_2+H_2O+propylene, and 2422 MINs and 6432 LUP paths were obtained. Figure S25 shows the obtained reaction route network consists of 2422 nodes and 4959 edges (loop paths and multiple edges connecting the same node pair were omitted). There are structures contained the same products but had different catalyst structures. For example, propylene epoxide is included in TS1-$(OH)_2$+epoxide, TS1-(OH)(O)+epoxide, and TS1-O+H_2O+epoxide. The obtained network was very complicated because of the variety of catalyst structures as well as the variety of products. Furthermore, propylene glycol which is the reported byproduct in the previous

study [19] was included in the network (represented as TS1-O+propylene glycol).

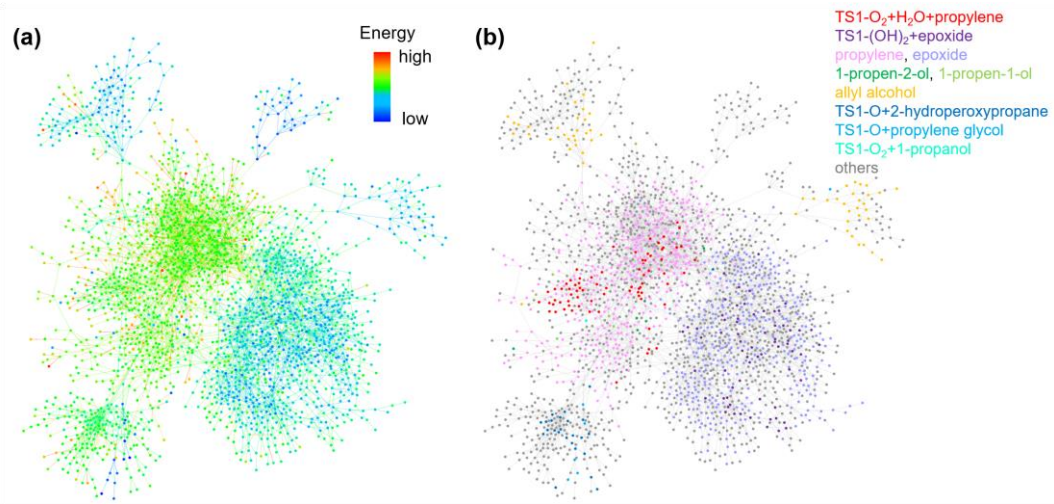

Figure S26. Reaction route network of (9) TS1-O_2+H_2O+propylene. Nodes and edges represent obtained MINs and paths connecting them, respectively. (a) Nodes and edges are colored based on their electronic energies. (b) Color of Nodes represents types of structures. "epoxide" includes TS1-(OH)(O)+epoxide and TS1-O+H_2O+epoxide. "allyl alcohol" includes TS1-$(OH)_2$+allyl alcohol, TS1-(OH)(O)+allyl alcohol, and TS1-O+H_2O+allyl alcohol. "propylene" includes TS1-O+H_2O_2+propylene, TS1-(OOH)(OH)+propylene, and TS1-(OOH)(O)+propylene. "1-propen-2-ol" includes TS1-(OH)(O)+1-propen-2-ol and TS1-O+H_2O+1-propen-2-ol. "1-propen-1-ol" includes TS1-$(OH)_2$+1-propen-1-ol, TS1-(OH)(O)+1-propen-1-ol, and TS1-O+H_2O+1-propen-1-ol.

Next, the time evolution of the reaction route network from the most stable reactant TS1-O_2+H_2O+propylene (MIN1221) was simulated. Figure S27(a) shows the population change of kinetically major species. The population of TS1-O_2+propylene is almost 1.0 at $t < 10^7$ s, while that of TS1-O+epoxide becomes almost 1.0 at $t \geq 10^7$ s. This means TS1-O+epoxide is main product, and the result is consistent to the previous study which showed the selective epoxidation reaction with the selectivity at most 96% [19]. However, the timescale of generating major product is different from the case of (8) TS1-O_2+propylene that shows epoxidation reaction is

completed within 10^{-1} s. Figure S27(b) shows the population change of other byproducts. Note that epoxides, allyl alcohol, propylene, 1-propen-2-ol, 1-propen-1-ol means the sum of the population for the structures containing the corresponding product. The population of these byproducts is very small.

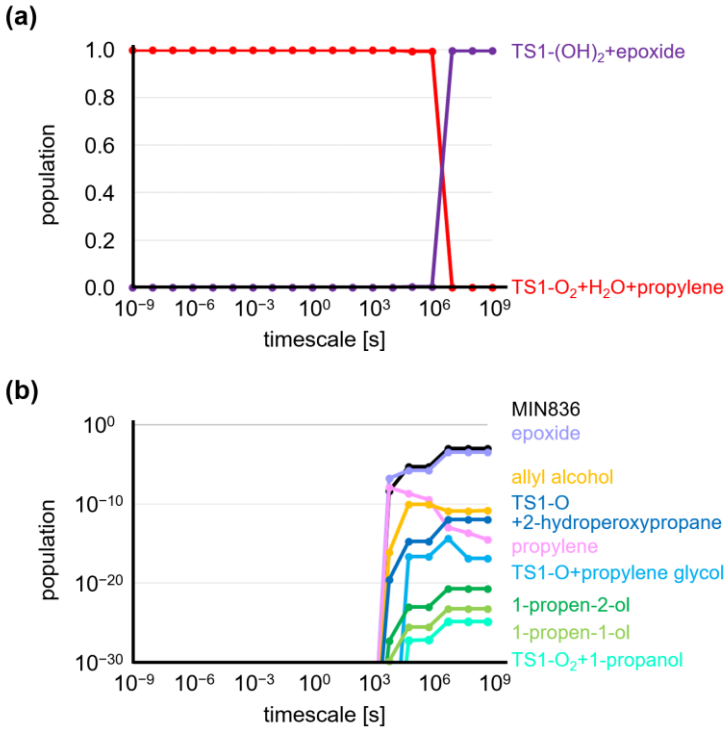

Figure S27. Population change of (9) TS1-O_2+H_2O+propylene at T = 273.15 K. (a) for kinetically important structures, and (b) for minor structures. The horizontal axis represents logarithm of timescale t when applying the RCMC method and the vertical axis corresponds to population of each structure type. The meanings of structural labels were same as that of Figure S26(b), and the sum of corresponding structures was plotted.

In addition, the most kinetically favorable path from reactant TS1-O_2+H_2O+propylene was shown in Figure S28. To see the kinetically favorable path, the precursor of epoxidation step is not TS1-O_2+H_2O+propylene but TS1-(OOH)(OH)+propylene. This means TS1-(OOH)(OH),

the intermediate of (1) TS1-O+H_2O_2, can be a precursor of epoxidation reaction. The reaction barrier of TS1-(OOH)(OH)+propylene → TS1-$(OH)_2$+epoxide is 43.7 kJ/mol whereas the barrier of TS1-O_2+H_2O+propylene → TS1-O+H_2O+epoxide (direct epoxidation path, PT937) is 36.6 kJ/mol. Further investigation is required to see the differences.

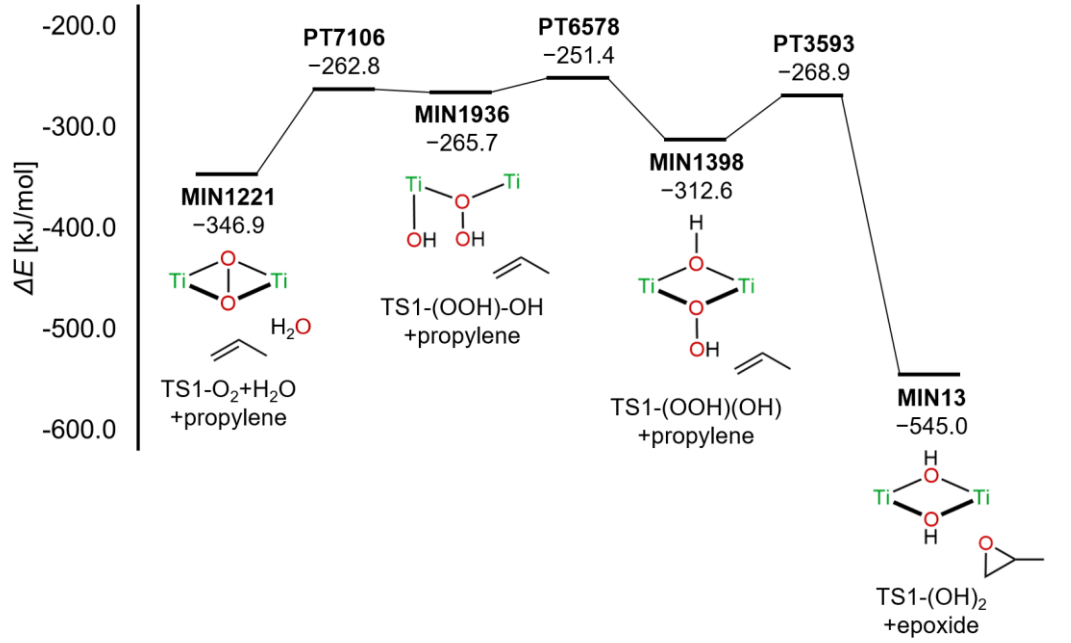

Figure S28. Energy profile of (9) TS1-O_2+H_2O+propylene. The kinetically most favorable route was extracted by applying the RCMC method to the network. The vertical axis shows the relative electronic energy refer to E_{tot}.

The network includes various byproducts as well as main product TS1-$(OH)_2$+epoxide The reaction mechanism of these products is summarized in Figure S29. The shortest path to each byproduct is calculated by applying the Dijkstra method from the reactant TS1-O_2+H_2O+propylene to each byproduct. Then these paths were grouped based on the passing structures. There are differences in the catalytic structures of the precursors in the path to the same products.

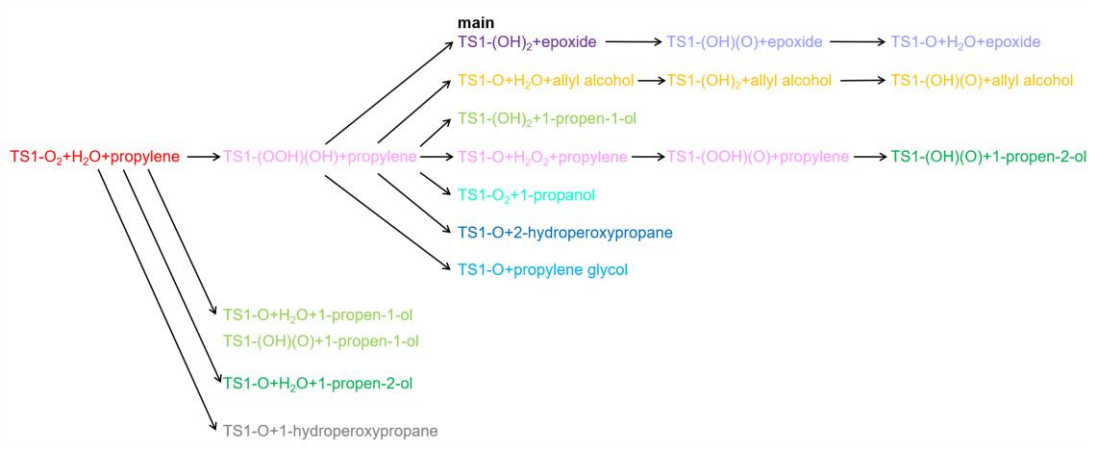

Figure S29. Products and byproducts of (9) TS1-O_2+H_2O+propylene. Color of letters correspond to the color of nodes in Figure S23 and the color of datapoints in Figure S24.

5.5.9 Reaction path search of (10) TS1-$(OH)_2$+H_2O_2

According to the result of (6) TS1-(OOH)(OH)+propylene and (7) TS1-O_2-OH+propylene, TS1-$(OH)_2$ was formed after epoxidation reaction. Therefore, reaction between TS1-$(OH)_2$ and H_2O_2 were systematically searched to see the catalyst regeneration steps. The search was started from TS1-$(OH)_2$+H_2O_2, and 1990 MINs and 4334 LUP paths were obtained. Figure S30 shows the obtained reaction route network consists of 1990 nodes and 3739 edges (loop paths and multiple edges connecting the same node pair were omitte

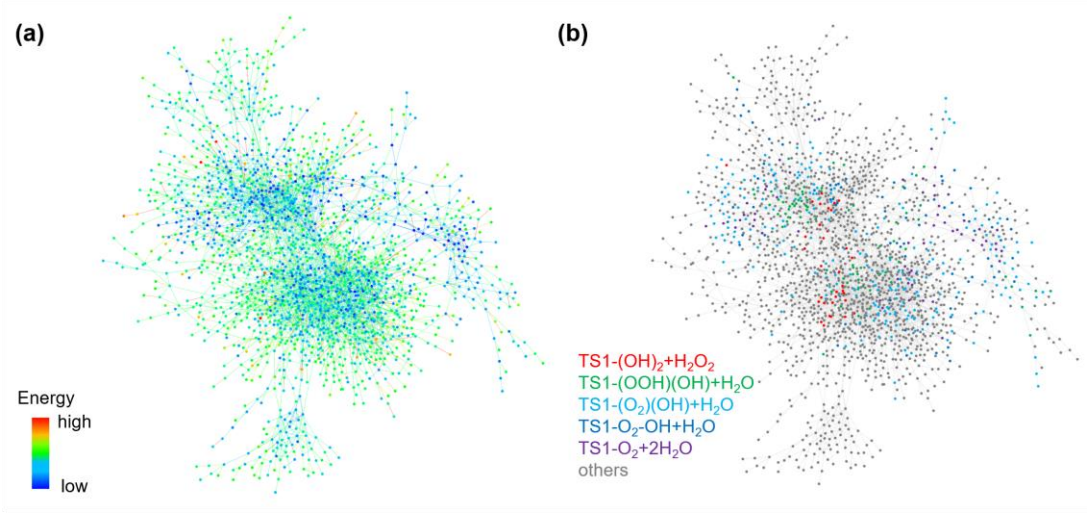

Figure S30. Reaction route network of (10) TS1-$(OH)_2$+H_2O_2. Nodes and edges represent obtained MINs and paths connecting them, respectively. (a) Nodes and edges are colored based on their electronic energies. (b) Color of Nodes represents types of structures.

Next, the time evolution of the reaction route network from the most stable reactant TS1-$(OH)_2$+H_2O_2 (MIN289) was simulated. Figure S31(a) shows the population change of kinetically major species having the maximum population over 0.5. TS1-$(OH)_2$ was reacted to another H_2O_2 molecule and TS1-O_2-OH+H_2O was formed. In Figure S32(b), the population change of the structures over 0.5. Although its kinetic impact is small, various TS-1 catalyst structures were found.

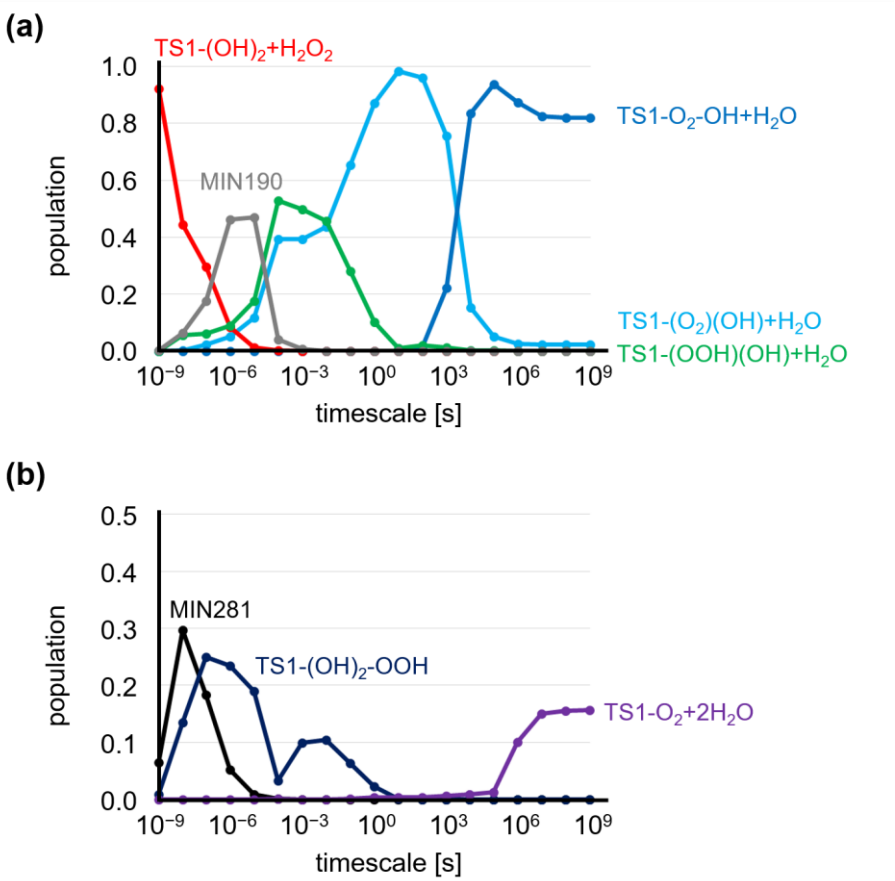

Figure S31. Population change of (10) TS1-$(OH)_2$+H_2O_2 at T = 273.15 K. (a) for kinetically important structures, and (b) for some minor structures. The horizontal axis represents logarithm of timescale t when applying the RCMC method and the vertical axis corresponds to population of each structure type.

In addition, the most kinetically favorable path from reactant TTS1-$(OH)_2$+H_2O_2 was shown in Figure S32. Dissociative adsorption was proceeded to TS1-O_2-OH+H_2O.

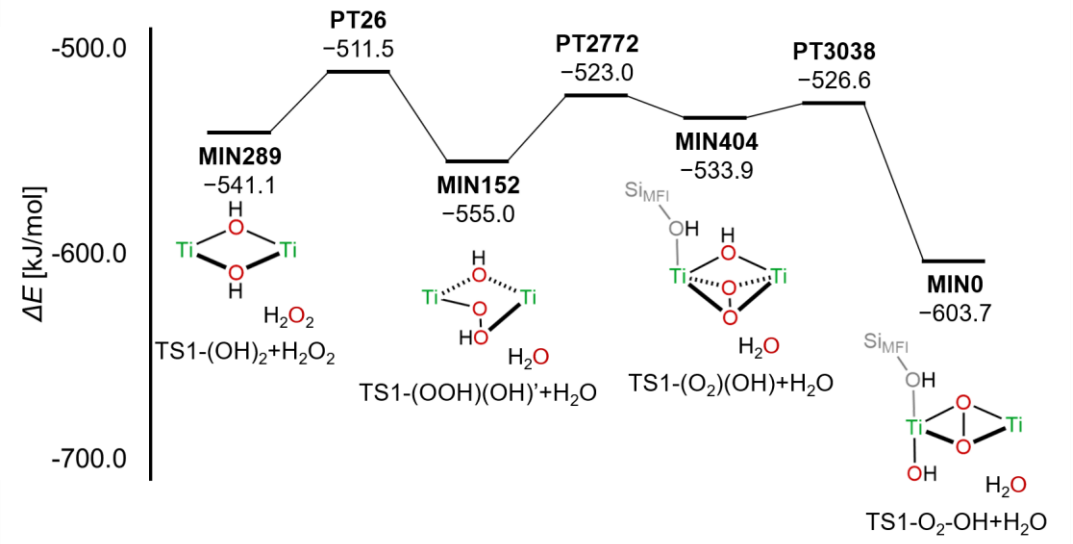

Figure S32. Energy profile of (10) TS1-$(OH)_2$+H_2O_2. The kinetically most favorable route was extracted by applying the RCMC method to the network. The vertical axis shows the relative electronic energy refer to E_{tot}.

5.5.10 Reaction path search of (11) TS1-O_2+H_2O_2

As discussed in 5.3.1, TS1-O reacts with the first H_2O_2 molecule to generate intermediate TS1-O_2+H_2O. In this section, reaction of the intermediate TS1-O_2 and the second H_2O_2 molecule were further studied. The search was started from TS1-O_2+ H_2O_2, and 1346 MINs and 3292 LUP paths were obtained. Figure S33 shows the obtained reaction route network consists of 1346 nodes and 2652 edges (loop paths and multiple edges connecting the same node pair were omitted). The obtained network includes TS1-$(OOH)_2$, which is the precursor of epoxidation reaction in the previous study [19].

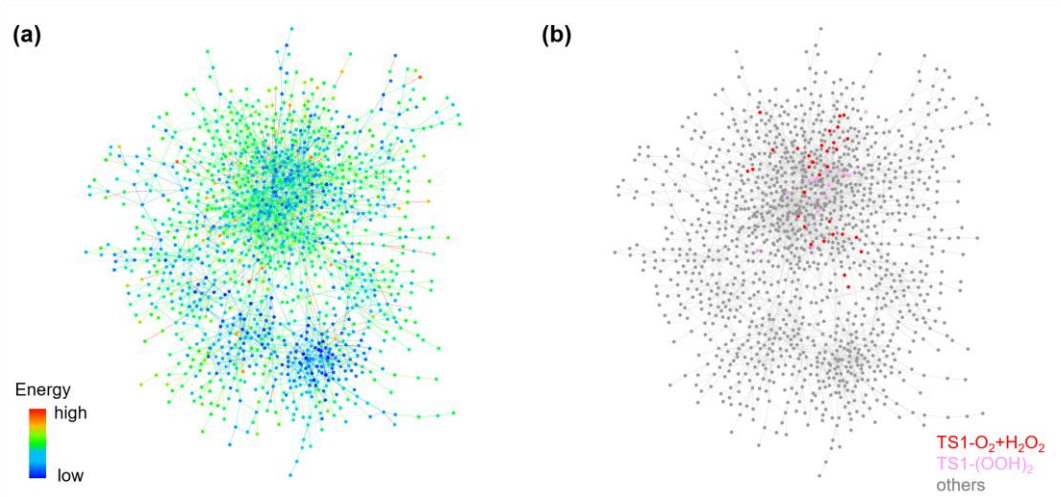

Figure S33. Reaction route network of (11) TS1-O_2+H_2O_2. Nodes and edges represent obtained MINs and paths connecting them, respectively. (a) Nodes and edges are colored based on their electronic energies. (b) Color of Nodes represents types of structures.

Next, the time evolution of the reaction route network from the most stable reactant TS1-O_2+ H_2O_2 (MIN56) was simulated. Figure S34(a) shows the population change of kinetically major species. The population of TS1-O_2+ H_2O_2 is gradually decreased at $t = 10^{-7}$ s ~ 10^{3} s. Then MIN51 (TS1-(O_2)(OOH)) is formed at the peak of $t = 10^{-1}$ s. Finally, the population of MIN9 (TS1-O_2-OOH) is increased at $t > 10^{-1}$ s. Figure S34(b) shows the population change of minor species having the maximum population over 10^{-3}. The population of mentioned structure TS1-$(OOH)_2$ becomes not so large. This means the reaction path to generate TS1-$(OOH)_2$ is kinetically less favorable, as is the case of (4) TS1-O+2H_2O_2.

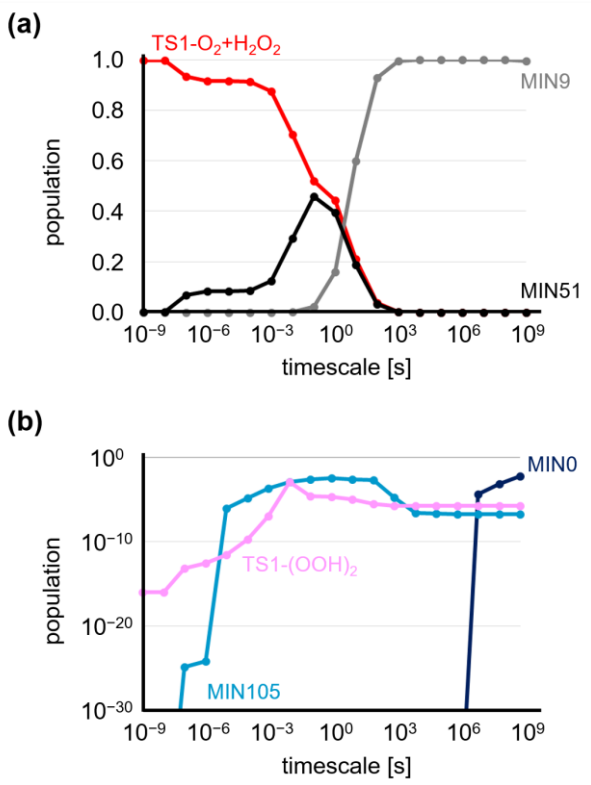

Figure S34. Population change of (11) TS1-O_2+H_2O_2 at T = 273.15 K. (a) for kinetically important structures, and (b) for minor structures having maximum population over 10^{-3}. The horizontal axis represents logarithm of timescale t when applying the RCMC method and the vertical axis corresponds to population of each structure type.

In addition, the most kinetically favorable path from reactant TS1-O_2+H_2O_2 was shown in Figure S35. TS1-$(OOH)_2$ is an intermediate of the reaction to TS1-O_2-OOH.

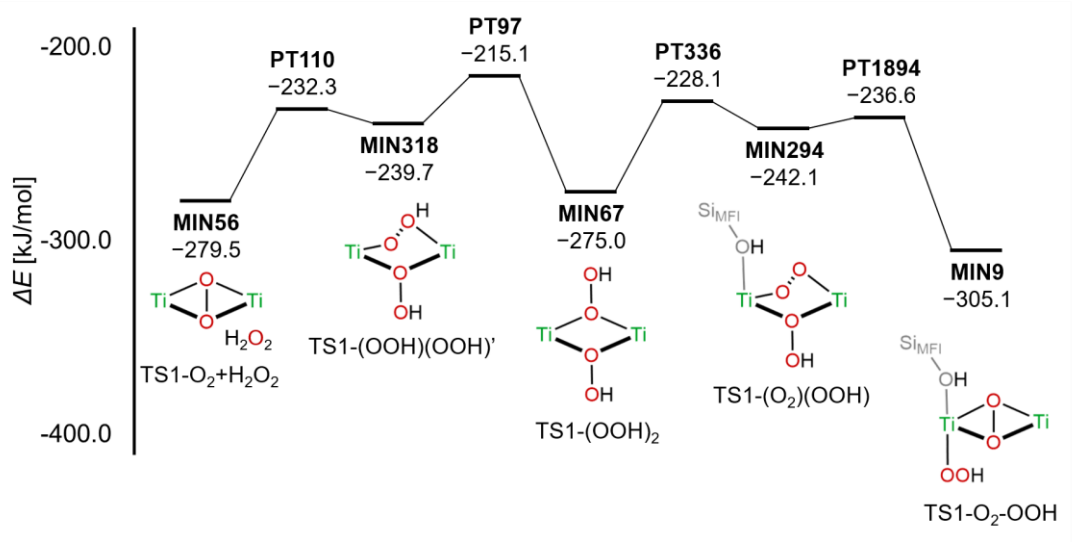

Figure S35. Energy profile of (11) TS1-O_2+H_2O_2. The kinetically most favorable route was extracted by applying the RCMC method to the network. The vertical axis shows the relative electronic energy refer to E_{tot}.

5.5.11 Reaction path search of (12) TS1-$(OOH)_2$+propylene

In the previous study, TS1-$(OOH)_2$ is assumed to be a precursor of epoxidation reaction [19]. Following this, reaction of TS1-$(OOH)_2$ and propylene was searched in this section. The initial structure was TS1-$(OOH)_2$+propylene, and 1385 MINs and 2815 LUP paths were obtained. Figure S36 shows the obtained reaction route network consists of 1385 nodes and 2373 edges (loop paths and multiple edges connecting the same node pair were omitted). There are structures contained the same products but had different catalyst structures. For example, propylene epoxide is included in TS1-O+H_2O_2+epoxide, TS1-(OOH)(OH)+epoxide, TS1-(OOH)(O)+epoxide, and TS1-O_2+H_2O+epoxide. The obtained network was very complicated because of the variety of catalyst structures as well as the variety of products. Furthermore, propylene glycol which is the reported byproduct in the previous study [19] was included in the network (represented as TS1-O_2+propylene glycol).

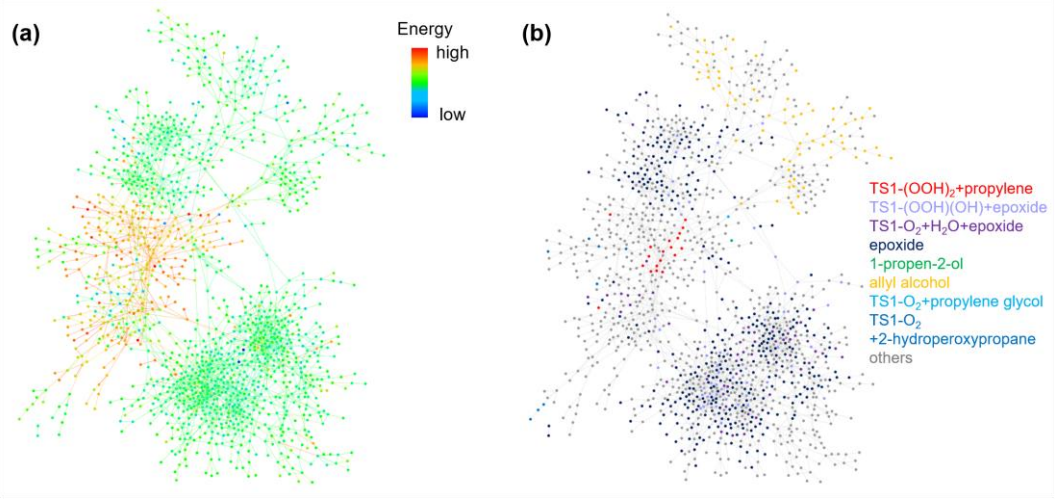

Figure S36. Reaction route network of (12) TS1-$(OOH)_2$+propylene. Nodes and edges represent obtained MINs and paths connecting them, respectively. (a) Nodes and edges are colored based on their electronic energies. (b) Color of Nodes represents types of structures. "epoxide" includes TS1-O+H_2O_2+epoxide and TS1-(OOH)(O)+epoxide. "allyl alcohol" includes TS1-O+H_2O_2+allyl alcohol, TS1-(OOH)(OH)+allyl alcohol, TS1-(OOH)(O)+allyl alcohol, and TS1-O_2+H_2O+allyl alcohol.

Next, the time evolution of the reaction route network from the most stable reactant TS1-$(OOH)_2$+propylene (MIN1186) was simulated. Figure S37(a) shows the population change of kinetically major species. The population of the reactant TS1-$(OOH)_2$+propylene is decreased at $t = 10^{-7}$ s and that of MIN1103 (TS1-O_2-OOH+propylene) is increased. Then the population of the product TS1-(OOH)(OH)+epoxide becomes major product at $t = 10^{-2}$ s. Finally, TS1-O_2+H_2O+epoxide becomes major product at $t = 10^{8}$ s by the structural change of TS-1 catalyst. These results are qualitatively consistent to the previous study which showed the selective epoxidation reaction with the selectivity at most 96% [19]. Figure S37(b) shows the population change of other byproducts. Note that epoxides, allyl alcohol, and 1-propen-2-ol means the sum of the population for the structures containing the corresponding product. The population of these

byproducts is very small.

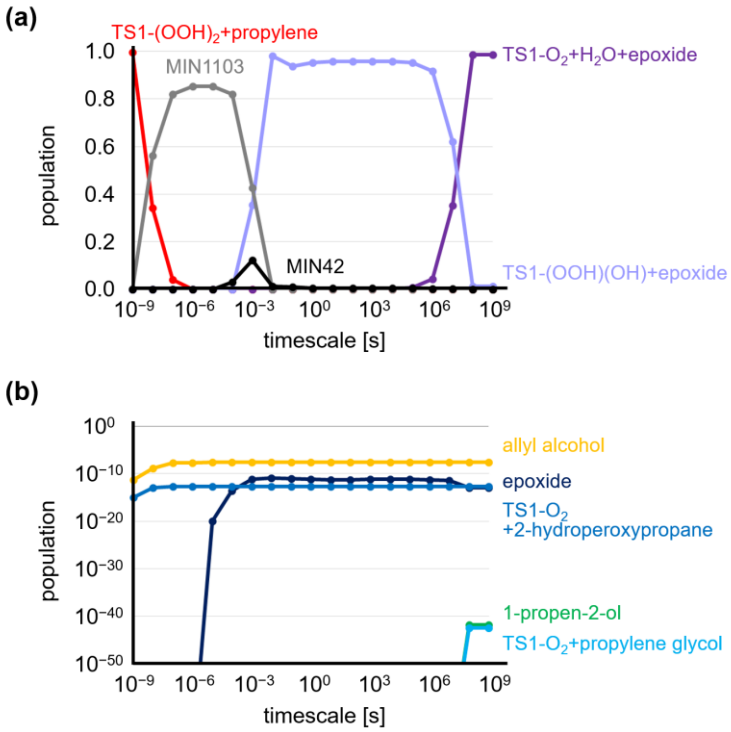

Figure S37. Population change of (12) TS1-$(OOH)_2$+propylene at T = 273.15 K. (a) for kinetically important structures, and (b) for minor byproducts. The horizontal axis represents logarithm of timescale t when applying the RCMC method and the vertical axis corresponds to population of each structure type. The meanings of structural labels were same as that of Figure S36(b), the sum of corresponding structures was plotted.

In addition, the most kinetically favorable path from reactant TS1-$(OOH)_2$+propylene was shown in Figure S38. To see the kinetically favorable path, the precursor of epoxidation step is not TS1-$(OOH)_2$+propylene but TS1-O_2-OOH+propylene. The reaction barrier of TS1-O_2-OOH+propylene → TS1-broken+epoxide is 48.4 kJ/mol. The reported path TS1-$(OOH)_2$+propylene → TS1-(OOH)(O)+propylene with the barrier of 30.5 kJ/mol [19] was not found in this study. Further investigation is required to see the differences.

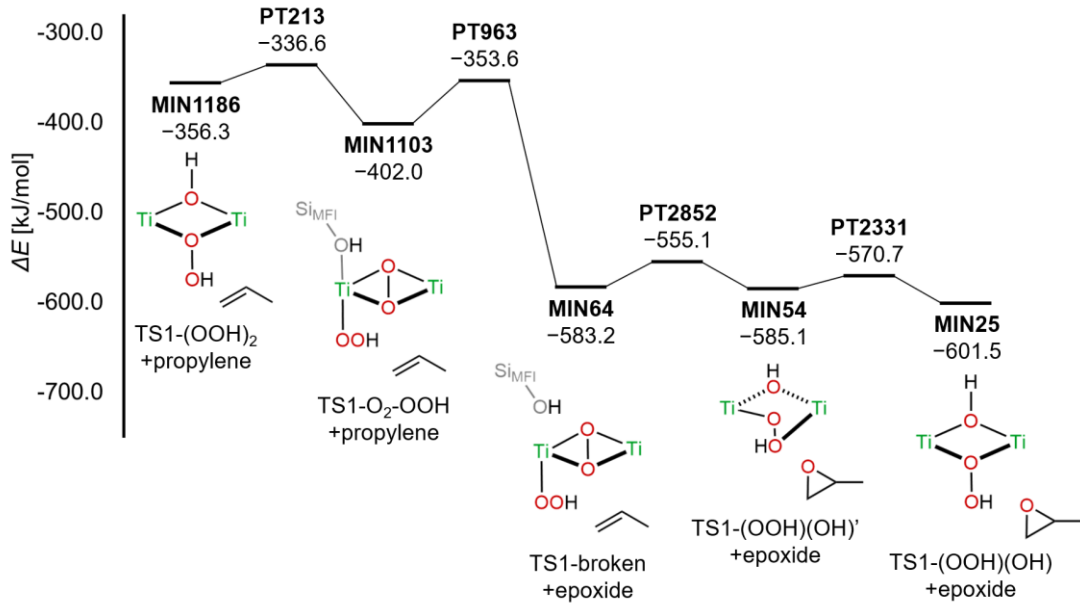

Figure S38. Energy profile of (12) TS1-$(OOH)_2$+propylene. The kinetically most favorable route was extracted by applying the RCMC method to the network. The vertical axis shows the relative electronic energy refer to E_{tot}.

The network includes various byproducts as well as main product TS1-(OOH)(OH)+epoxide or TS1-O+H_2O+epoxide. The reaction mechanism of these products is summarized in Figure S39. The shortest path to each byproduct is calculated by applying the Dijkstra method from the reactant TS1-$(OOH)_2$+propylene to each byproduct. Then these paths were grouped based on the passing structures. There are differences in the catalytic structures of the precursors in the path to the same products.

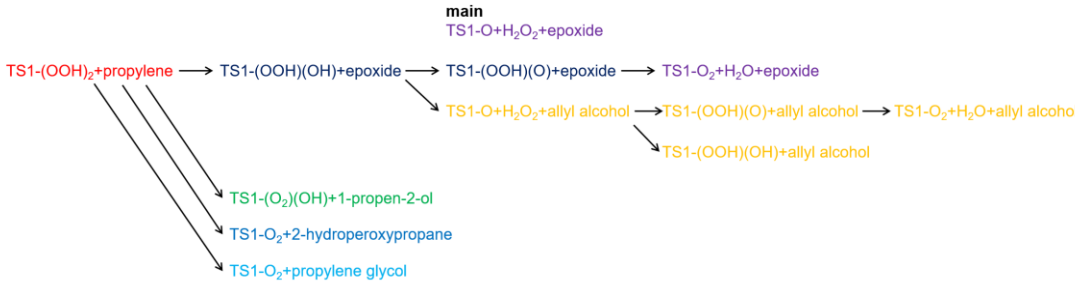

Figure S39. Products and byproducts of (12) TS1-$(OOH)_2$+propylene. Color of letters correspond to the color of nodes in Figure S36 and the color of datapoints in Figure S37.

References (Chapter 5)

[1] V. Russo, R. Tesser, E. Santacesaria and M. Di Serio, *Ind. Eng. Chem. Res.*, 2013, **52**, 1168–1178.

[2] S. L. Suib, J. Přech, J. Čejka, Y. Kuwahara, K. Mori and H. Yamashita, *Mater. Today*, 2020, **32**, 244–259.

[3] G. Bellussi, A. Carati, M. G. Clerici, G. Maddinelli and R. Millini, *J. Catal.*, 1992, **133**, 220–230.

[4] M. G. Clerici and P. Ingallina, *J. Catal.*, 1993, **140**, 71–83.

[5] F. Bonino, A. Damin, G. Ricchiardi, M. Ricci, G. Spanò, R. D'Aloisio, A. Zecchina, C. Lamberti, C. Prestipino and S. Bordiga, *J. Phys. Chem. C*, 2004, **108**, 3573–3583.

[6] D. H. Wells, Jr., W. N. Delgass and K. T. Thomson, *J. Am. Chem. Soc.*, 2004, **126**, 2956–2962.

[7] W. Panyaburapa, T. Nanok and J. Limtrakul, *J. Phys. Chem. C*, 2007, **111**, 3433–3441.

[8] C. E. Ramachandran, H. Do, Y. J. Kim, M. C. Kung, R. Q. Snurr and L. J. Broadbelt, *J. Catal.*, 2008, **253**, 148–158.

[9] S. B. Shin and D. Chadwick, *Ind. Eng. Chem. Res.*, 2010, **49**, 8125–8134.

[10] X. Nie, X. Ji, Y. Chen, X. Guo and C. Song, *Mol. Catal.*, 2017, **441**, 150–167.

[11] M. Li, X. Yan, M. Zhu, M. Wang and D. Zhou, *Catal. Sci., Technol.*, 2018, **8**, 4975–4984.

[12] M. Signorile, V. Crocella, A. Damin, B. Rossi, C. Lamberti, F. Bonino and S. Bordiga, *J. Phys. Chem. C*, 2018, **122**, 9021–9034.

[13] X. Liu, J. Liu, Y. Xia, D. Yin, R. K. Steven and L. Mao, *Catal. Comm.*, 2019, **126**, 40–43.

[14] M. Signorile, L. Braglia, V. Crocellà, P. Torelli, E. Groppo, G. Ricchiardi, S. Bordiga and F. Bonino, *Angew. Chem. Ind. Ed.*, 2020, **59**, 18145–18150.

[15] R. Millini, E. Previdi Massara, G. Perego and G. J. Bellussi, *J. Catal.*, 1992, **137**, 497.

[16] W. Lin and H. Frei, *J. Am. Chem. Soc.*, 2002, **124**, 9292–9298.

[17] L. Wang, G. Xiong, J. Su, P. Li and H. Guo, *J. Phys. Chem. C*, 2012, **116**, 9122–9131.

[18] X. Nie, X. Ren, X. Ji, Y. Chen, M. J. Janik, X. Guo and C. Song, *J. Phys. Chem. B*, 2019, **123**, 7410–7423.

[19] C. P. Gordon, H. Engler, A. S. Tragl, M. Plodinec, T. Lunkenbein, A. Berkessel, J. H. Teles, A.-N. Parvulescu and C. Copréret, *Nature*, 2020, **586**, 708–713.

[20] S. Maeda, Y. Harabuchi, M. Takagi, K. Saita, K. Suzuki, T. Ichino, Y. Sumiya, K. Sugiyama and Y. Ono, *J. Comput. Chem.*, 2018, **39**, 233–250.

[21] S. Maeda, K. Sugiyama, Y. Sumiya, M. Takagi and K. Saita, *Chem. Lett.*, 2018, **47**, 396–399.

[22] K. Sugiyama, Y. Sumiya, M. Takagi, K. Saita and S. Maeda, *Phys. Chem. Chem. Phys.*, 2019, **21**, 14366–14375.

[23] K. Sugiyama, K. Saita and S. Maeda, *J. Comput. Chem.*, 2021, **42**, 2163–2169.

[24] Y. Sumiya, Y. Nagahata, T. Komatsuzaki, T. Taketsugu and S. Maeda, *J. Phys. Chem. A*, 2015, **119**, 11641–11649.

[25] Y. Sumiya and S. Maeda, *Chem. Lett.*, 2020, **49**, 553–564.

[26] Ch. Baerlocher and L.B. McCusker, Database of Zeolite Structures: http://www.iza-structure.org/databases

[27] G. Kresse and J. Hafner, *Phys. Rev. B*, 1993, **47**, 558–561.

[28] G. Kresse and J. Hafner, *Phys. Rev. B*, 1994, **49**, 14251–14269.

[29] G. Kresse and J. Furthmüller, Comput. *Mater. Sci.*, 1996, 6, 15–50.

[30] Gaussian 16, Revision A.03, M. J. Frisch, G. W. Trucks, H. B. Schlegel, G. E. Scuseria, M. A. Robb, J. R. Cheeseman, G. Scalmani, V. Barone, G. A. Petersson, H. Nakatsuji, X. Li, M. Caricato, A. V. Marenich, J. Bloino, B. G. Janesko, R. Gomperts, B. Mennucci, H. P. Hratchian, J. V. Ortiz, A. F. Izmaylov, J. L. Sonnenberg, D. Williams-Young, F. Ding, F. Lipparini, F. Egidi, J. Goings, B. Peng, A. Petrone, T. Henderson, D. Ranasinghe, V. G. Zakrzewski, J. Gao, N. Rega, G. Zheng, W. Liang, M. Hada, M. Ehara, K. Toyota, R. Fukuda, J. Hasegawa, M. Ishida, T. Nakajima, Y. Honda, O. Kitao, H. Nakai, T. Vreven, K. Throssell, J. A. Montgomery, Jr., J. E. Peralta, F. Ogliaro, M. J. Bearpark, J. J. Heyd, E. N. Brothers, K. N. Kudin, V. N. Staroverov, T. A. Keith, R. Kobayashi, J. Normand, K. Raghavachari, A. P. Rendell, J. C. Burant, S. S. Iyengar, J. Tomasi, M. Cossi, J. M. Millam, M. Klene, C. Adamo, R. Cammi, J. W. Ochterski, R. L. Martin, K. Morokuma, O. Farkas, J. B. Foresman, and D. J. Fox, Gaussian, Inc., Wallingford CT, 2016.

[31] C. Bannwarth, S. Ehlert, S. Grimme, *J. Chem. Theory Comput.*, 2019, **15**, 1652.

[32] S. Grimme, J. Antony, S. Ehrlich and H. Krieg, *J. Chem. Phys.*, 2010, **132**, 154104 (19 pages).

[33] P. J. Hay and W. R. Wadt, *J. Chem. Phys.*, 1985, **82**, 270–283.

[34] P. J. Hay and W. R. Wadt, *J. Chem. Phys.*, 1985, **82**, 299–310.

[35] C. Choi and R. Elber, *J. Chem. Phys.*, 1991, **94**, 751–760.

[36] P. Y. Ayala and H. B. Schlegel, *J. Chem. Phys.*, 1997, **107**, 375–384.

[37] D. M. Perez Ferrandez, I. Herguedas Fernandez, M. P. G. Teley, M. H. J. M. de Croon, J. C. Schouten and T. A. Nijhuis, *J. Catal.*, 2015, **330**, 396–405.

Chapter 6. General Conclusion

In this study, the reaction path search by the AFIR method was applied to reactions on heterogeneous catalysts: metal surfaces like Cu(111) and Pt(111), and a porous materials TS-1. Then the systematic procedure to create reaction route networks of heterogeneous catalysts were established. In addition, reaction mechanisms were analyzed with considering paths of conformation changes (migration paths for surface reactions), side reaction paths to generate byproducts, and the influence of these paths to the kinetics, by applying the RCMC method to the networks.

In Chapter 2, a reaction of H_2O molecule on a Cu(111) surface was studied. A reaction route network was obtained by the reaction path search of the AFIR method. Although only four kinds adsorption states, i.e., H_2O, H+OH, H+H+O and H_2+O, were included, the network was very complicated than expected. This is because there are many conformers having the same adsorption states but different relative positions, and both migration paths and bond rearrangement paths. In addition, it was elucidated that the bottleneck step of the reaction is H_2O dissociation step to form H+OH by kinetic analysis of the time hierarchy of the network.

In Chapter 3, a reaction route network for CO oxidation on a Pt(111) surface was created. The network includes not only reactant CO+O_2, product CO_2(g)+O, and O_2 dissociated intermediate CO+2O but also short-lived intermediated such as OC-OO, CO_2+O, and CO_3. The two types of CO_2 generation paths were also included in the network: one is via O_2 dissociation and the other is via OC-OO complex. Then the kinetic analysis was applied to the network. The bottleneck step that CO_2 generation step from adsorbed CO molecule and O atom, CO+2O → CO_2(g)+O, is consistent with the results of previous studies. Besides, it is elucidated that many stable structures and transition states in the network were affected to the overall rate constants due to the entropic contributions of them.

In Chapter 4, methanol decomposition reaction on a Pt(111) surface was analyzed. A complex network consists of 290 MINs and 640 connecting paths were obtained. From the kinetic analysis of the network, the most kinetically favorable decomposition route, i.e., $CH_3OH \rightarrow CH_2OH+H \rightarrow HCOH+2H \rightarrow HCO+3H \rightarrow CO+4H$, was extracted. The kinetic contributions of the other intermediates and/or byproducts such as hydrocarbons and hydrogen were small.

In Chapter 5, epoxidation reaction of propylene on titanium silicate (TS-1) with hydrogen peroxides as an example to application to reactions on porous materials. The TS-1 cluster model considering structural changes of the catalyst was prepared. The reaction path search by the AFIR method was applied to each step in the proposed mechanism. The new catalytic cycle of epoxidation via TS1-(OOH)(OH) was proposed.

In this study, a systematic reaction path search and its analysis procedure for reactions on heterogeneous catalysts like metal surfaces or porous materials were developed. The framework of this study can apply to any other heterogeneous reactions because no assumption of the reaction mechanism is required. Thus, it is expected to use the method to predict reactions and/or to understand reaction selectivity and controlling yields when conducting experiments. On the other hand, the more complex reaction would require more computational costs. It is a future challenge that further optimization to apply the method for more complex heterogeneous reactions such as those involving surface reconstruction of surface-supported clusters.

Acknowledgement

All the studies in this thesis were carried out under Professor Satoshi Maeda, Department of Chemistry, Faculty of Science, Hokkaido University. I am very grateful for his careful guidance, giving me a lot of advice and answering my questions until I understood.

I would like to thank for my collaborators, Specially Appointed Assistant Professor Kenichiro Saita, Doctor Yosuke Sumiya, and Doctor Makito Takagi.

I also would like to thank for Professor Tetsuya Taketsugu, Professor Kenichi Shimizu, and Associate Professor Yu Harabuchi for serving my dissertation committee.

I am grateful for all members of Theoretical Chemistry Laboratory giving me fruitful discussion, practical advice, and technical supports. I also would like to thank you for Associate Professor Keisuke Takahashi and Assistant Professor Itsuki Miyazato for their advice and discussion to improve my study.

I wish to express my appreciation to the member of Quantum Chemistry Laboratory for teaching basics of quantum chemistry and programming as well as giving helpful advices and continuous communications.

Finally, I would like to thank to support by Ambitious Leader’s program of Hokkaido University.